Sigrid Skjelstad

Environmentally friendly substitute of phenolic resin in solid state sintered silicon carbide

August 2020

Master's thesis

2020

Master's thesis

Sigrid Skjelstad

NTNU
Norwegian University of
Science and Technology
Faculty of Natural Sciences
Department of Materials Science and Engineering

NTNU
Norwegian University of
Science and Technology

Environmentally friendly substitute of phenolic resin in solid state sintered silicon carbide

Sigrid Skjelstad

Submission date: August 2020
Supervisor: Kjell Wiik, IMA
Co-supervisor: Mari-Ann Einarsrud, IMA

Norwegian University of Science and Technology
Department of Materials Science and Engineering

Preface

The work presented in the master thesis has been conducted at the Department of Materials Science and Engineering at the Norwegian University of Science and Technology (NTNU). The work was done during the spring of 2020 and was a continuation of the specialisation project "Effect of the carbon source on sintering properties of SiC", by the same author. The work presented here is built on that work, and some of the general parts of literature is recognisable.

This work has been a collaboration between NTNU and Fiven Norge As in Lillesand, south in Norway, where production of the precursors and etching of sintered samples were performed. The rest of the work was done at the mentioned department.

During this work many people have offered me guidance and help. First of all I would like to give a huge thank you to my supervisor Kjell Wiik, for all the advise and insights he has provided, and for always taking the time when I needed it. Secondly, I would also like to thank my co-supervisors, Mari-Ann Einarsrud. I would also like to thank Vidar Johannessen and Stephen Rugholm from Fiven Norge AS for giving me the opportunity to work so closely with industry and for being so welcoming when I have visited the production site in Lillesand. Further I would like to thank everyone involved at the Department of Material Science and Engineering for help with instruments and training. A special thanks goes to Nikola Kanas and Johannes Ofstad for always being so willing and positive whenever I needed help. Lastly I would like to thank my fellow students and friends at campus for interesting weekly research meetings and good discussions during the course of this work, and to Martin Madsen who wrote his masters on the same topic and has been a great inspiration.

Abstract

Silicon carbide is a highly covalent ceramic that holds many outstanding properties. Because of the strong covalent bonds, densification is a challenge and sintering additives like carbon and boron are often used to obtain high densities after sintering. Carbon removes silica on the surface of the silicon carbide particles, which is necessary to start the sintering. Carbon is also thought to inhibit grain growth and therefore promote great properties in the sintered body.

Phenolic resin is the most used carbon source in the industry today, and was also the reference in this project. Phenolic resin works great as a sintering aid for silicon carbide, but it is carcinogenic and hazardous to the environment. The aim of this study was to investigate alternative carbon sources and see if they had the same qualities as a sintering aid while also being environmentally friendly. Modified starch and sucrose (normal table sugar) was used as alternative carbon sources. Precursors were made with the various carbons, and they were sintered using spark plasma sintering (SPS) with a heating rate of $100°Cmin^{-1}$. Bulk densities of 3.18, 3.16. and 3.15 gcm^{-3} was obtained for the precursor with resin, starch and sucrose respectively. Anisotropic grain growth was most prominent for the samples with sucrose as the carbon source, based on the results from images of etched surfaces and electron backscatter diffraction (EBSD). Raman spectroscopy was used to investigate the reactivity of the pyrolysed carbon sources, showing that there was an insignificant difference in reactivity between them.

Based on the experiments conducted in this study, it seems like both starch and sucrose could be good alternatives to phenolic resin from an environmental point of view and with regards to performance they have potential, but more research is needed.

Sammendrag

Silisiumkarbid er et meget kovalent materiale med mange enestående egenskaper. På grunn av de sterke, kovalente bindingene er det vanskelig å oppnå høye tettheter ved sintring og sintringsadditiver som karbon og bor må ofte tilsettes. Karbon fjerner silika på overflaten av silisiumkarbid-partiklene, noe som er nødvendig for å starte sintringen. Karbon skal også bidra til å hindre kornvekst og dermed forbedre egenskapene til den sintrede kroppen.

Fenolharpikser er den mest brukte karbonkilden i industrien i dag, og også referansen i denne oppgaven. Fenolharpikser fungerer utmerket som sintringsadditiv til silisiumkarbid, men er kreftfremkallende og miljøskadelig. Målet med denne oppgaven er å undersøke alternative karbonkilder for å se om disse har de samme egenskapene som fenolharpikser har, og samtidig være bedre for miljøet. Modifisert stivelse og sukrose (vanlig sukker) ble brukt som alternative karbonkilder. Silisiumkarbid-pulver med de forskjellige karbonkildene ble laget og sintret ved hjelp av "spark plasma sintering" (SPS) med en oppvarmingshastighet på $100°Cmin^{-1}$. Tettheter på 3.18, 3.16 og 3.15 gcm^{-3} ble oppnådd for silisiumkarbid-pulver med henholdsvis fenolharpiks, stivelse og sukrose som karbonkilde. Anisotropisk kornvekst var mest fremtredende hos prøvene med sukrose, basert på bilder av etsede overflater sammen med electron backscatter diffraction (EBSD). Raman spektroskopi ble brukt til å undersøke reaktiviteten til karbonkildene og resultatet var en ubetydelig forskjell.

Basert på eksperimentene gjort her kan både stivelse og sukrose være gode alternativer til fenolharpikser. De er definitivt mer miljøvennlige, og har potensial til å konkurrere i ytelse også, men mer forskning er nødvendig.

Table of Contents

TABLE OF CONTENTS

Chapter 1

Introduction

1.0.1   Background and motivation

Silicon carbide (SiC) can be found naturally in meteorites, in the form of green hexagonal plates [1]. It was first synthesized by E. G. Acheson, supposedly by coincidence while doing an experiment on the synthesis of diamond. This happened in 1891 while Acheson was T. Edison's assistant. Today, the Acheson process is the most common and cost efficient way to produce silicon carbide industrially, despite the very high energy consumption [2].

SiC is a highly covalent ceramic that owe its diverse applications to outstanding properties. High hardness together with low weight, low thermal expansion coefficient, chemical inertness and heat resistance are only some examples of the superior properties of SiC. With these properties, silicon carbide is used as armour for security and defence, as break discs in sports cars, as abrasives and in the space industry, to mention some. The main challenge with SiC, however, is consolidation which is another consequence of strong and stiff covalent bonds. To get silicon carbide powder transformed to a dense solid, a heat-treatment process called sintering is used. To sinter SiC to high densities, sintering additives are often used. If the sintering is performed pressure-less the additives are seen as a necessity, but when applying an external pressure together with high temperatures, high densities have been obtained without additives as well [3]. There are however other advantages of using sintering additive, for example is carbon thought to inhibit grain growth which will improve mechanical properties. Carbon and boron are the two most

used sintering additives and the general thought is that carbon inhibit grain growth and remove silica from the surface of the SiC - particles whilst boron has the effect to increase the densification mechanisms [4, 5]. Silica needs to be removed before sintering can start. Different carbon sources are used for this purpose and phenolic resin and carbon black are the two most used although they both have severe limitation. Carbon black does not obtain the highest densities, and that is most likely due to the distribution of carbon on the surface not being homogeneous. Phenolic resin, on the other hand, is typically predissolved in a solvent to provide a more homogeneous distribution of the carbon [6]. However, one major disadvantage with phenolic resins is that they release dissosiation products such as phenol, cresol and formaldehyde when they are thermally decomposed [6]. Compounds like that are hazardous to the environment and carcinogenic, but also expensive in terms of waste disposal and safety measures during production. One of the leading silicon carbide producers in the world, Fiven Norge AS, use phenolic resin as their carbon source today, but are interested in a substitute can have the same performance and simultaneously be less harmful to the environment and the people working with it.

1.0.2 Aim of work

The main goal of this study is to look at alternative carbon sources to use as a sintering aid for silicon carbide. Carbon is often needed to obtain high densities of silicon carbide. Today, the most used carbon source in phenolic resin. Phenolic resin provide high densities, but is harmful to the environment and to people working with it. Phenolic resin will be used as a reference and two potential carbon sources, modified starch and sucrose, will be compared to the reference.

The sintering method used in this study will be spark plasma sintering and the density will be measured using Archimedes' principle. There will be a great focus on different sintering techniques and their advantages. Characterisation will be performed on both carbon sources and sintered samples. The characterisation methods to be used here are:

- Thermogravimetric analysis (TGA)

- Scanning electron microscopy (SEM)

- Raman spectroscopy

- X-ray diffraction (XRD)

- Electron backscatter diffarction (EBSD)

This study is set to provide knowledge on why certain carbon sources works and others do not in the hope of finding one that can substitute resin in terms of performance and simultaneously be less harmfull to the environment

Chapter 2

Literature review

2.1 Silicon Carbide

Silicon carbide (SiC) is, as stated frequently in literature, one of the most interesting ceramic materials due to its relationship between superior properties and structure [7, 8]. The final properties varies with differences in microstructure that again is caused by different polytypes (structural modifications) [8]. High mechanical properties at a wide range of temperatures and distinctive electrical properties are two examples of outstanding properties that SiC holds, and that in combination with low density (3.21 g/cm^3) makes SiC the preferred material in many situations [9]. However, there are challenges related to SiC and the main one is consolidation, which has proven to be difficult without additives [10]. The possibility to modify polytype and microstructure to obtain specific properties give rise to many applications within several industries, and is a feature that makes silicon carbide a unique and interesting ceramic.

2.1.1 Structure

One feature that makes silicon carbide a very interesting and applicable ceramic is its polytypism, i.e formation of several different structures without changing the composition. This feature also makes understanding the structure of silicon carbide a relatively complex exercise [11, 12]. By looking at the short-range structure one can simply say that it is a diamond-like arrangement where alternating silicon and carbon atoms bond, creating a closely packed structure. More sophisticated, the structure can be explained as a

tetrahedral arrangement, either SiC_4 or CSi_4, that will arrange themselves differently, either parallell or anti-parallell, and give rise to various polytypes of silicon carbide [12]. These one - dimensional ordering sequences are different for each polytype, but the stoichiometry stays the same [13]. The most common and stable polytypes out of the about 200 discovered ones are 6H, 4H, 15R and 3C [11, 12] and these are often called the "basic" structures of silicon carbide [14]. Here, H, R and C means hexagonal, rhombohedral and cubic respectively, and the first number denotes how many layers are needed in order to obtain periodicity. Sometimes 3C is denoted $\beta - SiC$ while all the hexagonal structures are named $\alpha - SiC$. $\beta - SiC$ has zinc blende (cubic) structure while $\alpha - SiC$ has a combination of zinc blende and wurtzite (hexagonal) structure [2]. There are only three possible positions for bilayers in the lattice of cubic SiC while maintaining the tetrahedral bonds, hence only one polytype with cubic structure is possible [15]. If the three different layers are arbitrarily denoted A, B and C, then the structure is, as mentioned before, zinc blende with the stacking sequence of ABCABC... [15]. A stacking sequence of ABABAB... gives hexagonal symmetry and the only purely hexagonal polytype is 2H-SiC. 4H-SiC have as many hexagonal bonds as cubic while 6H-SiC has two-thirds cubic bonds and the rest hexagonal. Despite the fact that $\alpha - SiC$ has both cubic and hexagonal components, the overall structure is thought to be hexagonal [15].

There is a lack of understanding and knowledge regarding the transformation from one polytype to another for SiC. Some polytypes are known to be more stable at certain temperatures, but the reasoning behind is yet to be understood and is the main reason why the transformations are also not understood. Jepps et al. [13] tried to present an overview of the mechanisms and kinetics behind the polytype transformations for SiC and came to some interesting conclusions. The most common and spoke about transformation with regards to SiC is the one from $\beta - SiC$ (cubic) to $\alpha - SiC$ (hexagonal). With the transformation in structure comes a change in properties. The mentioned transformation often leads to a microstructure consisting of more large and elongated grains rather than equiaxed grains which again can lead to lower densities and a degradation of mechanical properties [13]. The transition from cubic to hexagonal structure is the most common one and also the most relevant one for this study. The reason for this transformation being the most common one is that 3C often is the first polytype formed, but it is only

stable at lower temperatures, below 1600 °C, and will therefore transform to a stable polytype at elevated temperatures (i.e. a hexagonal structure). Cubic structures are thought to be most stable at low temperatures, while hexagonal structures are stable at higher temperatures [1]. There are however examples of other transformations happening and even transformations being reversed. It has been observed that 6H can go to 3C in presence of high pressures of nitrogen gas. This is an example of impurities having a great influence on the stability of the polytypes at variable temperatures [13, 14]. The transition of polytypes will be discussed in terms of sintering techniques and heating rates in Section 2.3.2.

An overview of properties and features of some of the "basic" structures of silicon carbide are found in Table 2.1.1.

Table 2.1.1: Overview of the most common structures of silicon carbide [14, 16, 17, 18, 19]

| Property	SiC polytype		
	6H	4H	3C
Crystal structure	Wurtzite/zink blende	Wurtzite/zink blende	Zink blende
Space group	$C_{6v}^4(P6_3mc)$	$C_{6v}^4(P6_3mc)$	$T_d^2(F43m)$
Lattice parameter a [Å]	3.0806	3.0730	4.3596
Lattice parameter c [Å]	15.1173	10.0530	-
% of hexagonality	33	50	0
Temperature range where polytype is stable [$°C$]	2100 -	1600 - 2100	1400 - 1600

Figure 2.1.1 illustrates two of the most common structures of SiC. Image a) shows 6H, which is a hexagonal structure with 6 layers in the repeating unit. Image b) is 3C, which denotes cubic structure with 3 layers in the repeating unit.

(a) 6H   **(b)** 3C
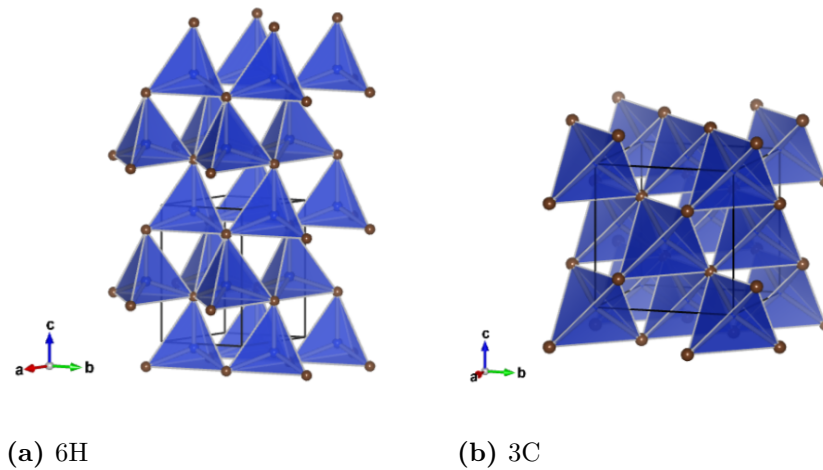
Figure 2.1.1: The two most common structures of SiC. The blue spheres represent silicon
atoms and the brown spheres represent carbon atoms. The structures are
generated using VESTA [20].

Electron Backscatter Diffraction

Electron backscatter diffraction (EBSD), or orientation imaging microscopy (OIM), was
discovered by Shoji Nishikawa and Seishi Kikuchi in 1928 [21]. The diffraction patterns
found by using EBSD is therefore also commonly known as Kikuchi patterns. EBSD
is a technique mostly used to make spatially specific measurements of crystallographic
orientation [22]. The technique can be used on most inorganic crystalline materials like
metals, minerals, semiconductors and ceramics [21]. EBSD can reveal more than just
grain orientation, and grain size, grain boundary character, texture and phase identity
are some examples of other purposes of using EBSD. A schematic of the EBSD setup
can be found in Figure 2.1.2. A flat and highly polished sample is placed in a specific
angle to the incident electron beam. This angle is normally decided by the tilt on the
SEM stage, which is often set to 70 °. The acceleration voltage is typically in the range
of 10-30 kV and the incident beam current in the range of 1-50 nA. The interaction
between the primary beam and the crystal lattice leads to low energy loss backscattered
electrons being channeled. These electrons are subject to path differences that lead to
constructive and destructive interference that again give rise to diffraction patterns if a
phosphor screen is placed close to the tilted sample [21].
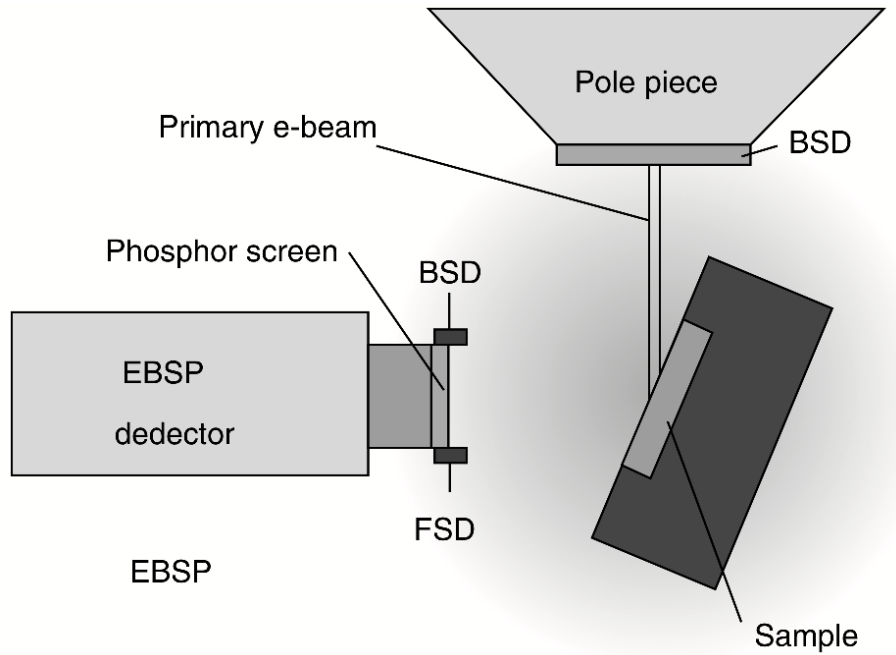
Figure 2.1.2: Schematic of a typical EBSD setup [21].

The spatial resolution of the EBSD pattern is governed by the SEM electron optics, so for high quality patterns, a high performance SEM is required [21]. The EBSD detector is usually attachable to the SEM instrument. How the EBSD pattern look depend on several factors like the lattice parameters of the crystal under the electron beam and the orientation of the crystal in space [21]. After obtaining the online patterns, an offline indexing and calibration is done using a specialized software. This software will detect Kikuchi patterns by the use of an optimized Hough transform [23]. With some materials it is harder to get good EBSD patterns, and hence it can be difficult to index the patterns. A measure of the greatness of the pattern indexing is the so called confidence index (CI) [24]. The CI is a number between 0 and 1 denoting that the match is between 0 - 100%. A CI value above 0.5 is considered to be good [23]. After indexing, the software can display the the EBSD pattern in several ways; as a phase map (for composition) or inverse pole figure (for orientation). An example of an inverse pole figure (IPF) of silicon carbide can be found in Figure 2.1.3. Here, the silicon carbide has been hot pressed for an hour at 1600°C followed by an hour at 2050°C. There was observed larger and more elongated grains at enhanced sintering temperatures [25].
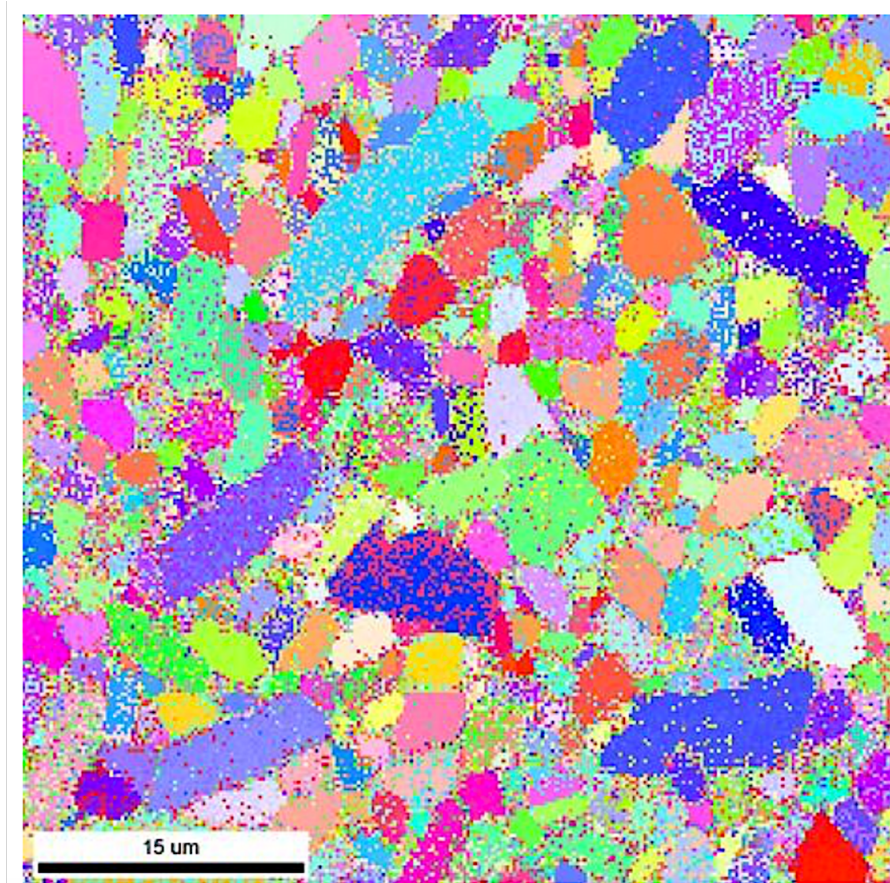
Figure 2.1.3: EBSD pattern of a silicon carbide sample that has been hot pressed. The colours change with direction of the grain; red represent the [0001] direction out of the plane, while blue is [10$\bar{1}$0] and green [2$\bar{1}\bar{1}$0], the latter two directions being in-plane [25]

2.1.2 Properties

Silicon carbide is a widely used ceramic, as will be addressed in Section 2.1.3 below, and that is due to its superior properties. One of the reasons for the high interest in silicon carbide is the ability to change properties with polytype and as discussed in the previous chapter, Chapter 2.1.1, there are ways to control the transformations between the different polytypes. Table 2.1.2 shows some important properties for SiC. As mentioned, different polytypes have different properties and in Table 2.1.2 certain properties are listed for both 6H and 3C for comparability reasons. Where polytype is not specified in literature, the property is listed under 6H. All properties are measured at room temperature and the elastic modulus is measured using load deflection with a thickness of 10 mm for an undoped substrate.

10

Table 2.1.2: Properties of silicon carbide. Properties only given for SiC in literature, with no specification of polytype, are listed under 6H [19, 1].

Property	SiC	
	6H	3C
Elastic modulus [GPa]	448	
Density [gcm^{-3}]	3,211	3,166
Thermal conductivity [$Wcm^{-1}K^{-1}$]	3,6	3,2
Thermal expansion coefficient	$3,8 \cdot 10^{-6}$	
Poisson's ratio	0,17	
Hardness		
Fracture toughness [$MPa \cdot m^{1/2}$]	3,0-3,5	
Lattice parameters [Å]	a = 3,0806 c = 15,1173	a = 4,3596

Some of the features of silicon carbide, and the reason for its many applications, are its high hardness, heat resistance, corrosion resistance, oxidation resistance and low density [13].

The hardness of silicon carbide is highly related to the strong covalent bonds. $\alpha - SiC$ has the same structure as BeO, but BeO has ionic bonds instead of covalent which results in a significantly higher hardness and strength for SiC [1]. However, for SiC to have high hardness, the density needs to be high. Denobel et al. studied the effect of density on the resulting hardness and found that the relationship was strong. Investigating additive-free SPSed SiC with densities ranging from 80-95% and one highly dense sample with minimal additives, the results showed that the hardness increased with around 7 GPa when the density was increased from 80% to 95%. The hardness was measured using Knoop and Vickers indentation tests [26].

SiC also has a high thermal conductivity compared to other ceramics. This is due to the fact that carbon and silicon are similar in atomic weight and size leading to lattice vibrations moving relatively easy through the structure compared to structures where the differences between the elements are bigger, like in UO_2 and ThO_2 [1]. UO_2, as a

comparison, has less than one tenth the thermal conductivity of SiC, while materials like MgO and Al_2O_3 are somewhere in between. Compared to pure silicon, silicon carbide has superior properties with over 3.3 times as high thermal conductivity, around 10 times as high electric field breakdown strength and 3 times as wide bandgap [15].

SiC has a low thermal expansion coefficient, meaning the dimensions do not change much when subjected to elevated temperatures [1]. Relative to most metals and even some ceramics, SiC has a very low Poisson's ratio of 0.17 which implies that when a tensile load is applied in one direction, the thickness of the material in the perpendicular direction is relatively stable [1].
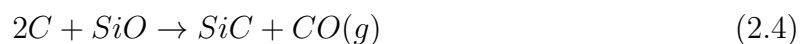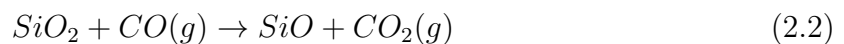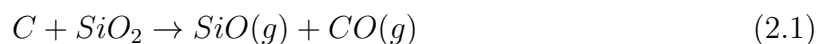
2.1.3 Applications

Because of its many great properties, silicon carbide is a widely used ceramic, and more so over the last few decades [2]. The reason for the limiting use of silicon carbide previously has been the low sinterability, but with pioneering work done by Prochazka to form dense SiC microstructures using pressureless solid state sintering, a new world of applications has opened [2, 27]. SiC is especially suitable for applications in high temperature environments. With a decomposition temperature of around 2400 °C, SiC can be used at extreme temperatures and some examples are interior in furnaces and heating elements [13, 2]. Another example of high temperature uses are semiconductors for high-temperature applications, where traditional circuit technologies using silicon can only operate up until around 250°C [15]. For applications in aerospace like turbine engines, nuclear power instrumentation or satellites, operating temperatures from 350°C to 500°C is required [15]. Apart from high-temperature applications, silicon carbide is also superior when it comes to high-power, high-frequency and high-radiation environments with regards to the properties discussed in Section 2.1.2. The combination of high strength and very low density which results in a high specific strength, is the reason why SiC is one of the materials that have been used as armor by the U.S Military since the 1960s [27]. Abrasives are also often made out of SiC due to the high hardness [2].

2.1.4 Production

As mentioned in previous sections, it is said that silicon carbide was discovered by accident when E. G. Acheson was synthesizing diamond in 1891 [2]. The most common process for making SiC today is named after Acheson and is thus called the Acheson process. Beginning with a simple electric furnace of his own design he made the first SiC, before upgrading to a more efficient electric furnace that contributed to a profitable business [28]. This business started with the use for SiC in jewelry making due to its abrasive qualities, being the far superior material for this use at that time. The demand grew tremendously and Acheson built the first commercial plant in 1896, trying to meet this demand. A few years later, almost all the SiC in the world was produced following Achesons' concept.

A simple explanation of the process is that silica or quartz sand is mixed with powdered coke and placed around a graphite core in a furnace [28]. A current is sent through the graphite core heating up the surrounding reactants to around 2200°C [1]. At this temperature the coke and silica react exothermically and this reaction continues until the core is all SiC (low impurity green hexagonal SiC crystals). The unreacted silica and silicon carbide further away from the core is treated with subsequent additions of carbon to further synthesize silicon carbide [1]. The following four sub-reactions explain the path from SiO_2 and coke (C) to SiC and CO [28].

$$C + SiO_2 \rightarrow SiO(g) + CO(g) \tag{2.1}$$

$$SiO_2 + CO(g) \rightarrow SiO + CO_2(g) \tag{2.2}$$

$$C + CO_2(g) \rightarrow 2CO(g) \tag{2.3}$$

$$2C + SiO \rightarrow SiC + CO(g) \tag{2.4}$$

The Acheson process is highly inefficient with only 10 - 15 % of the energy being converted to the finished product [29]. Regardless, this process is still very cost-effective and is

therefore the most used process for SiC synthesis worldwide [1]. Another advantage of this process is the simultaneously production of high purity SiC for electrical applications and lower-grade SiC for lower quality requirements such as abrasives.

2.2 Carbon Sources

The carbon sources of relevance in this study are phenolic resin, starch and sucrose together with carbon black that is included as a second reference. Out of the four, sucrose is the most familiar being a major commodity in world trade and consumed by people world wide [30].

Phenolic resins are a product of the reaction between phenols and aldehydes with phenol and formaldehyde being the two main components in commercial phenolic resin production [31]. Phenols belong to the family of aromatic compounds with a hydroxyl group bonded directly on the aromatic nucleus. Phenol, which is easily inhaled, is classified as highly toxic and is also considered a carcinogen [31]. Formaldehyde is also considered a highly hazardous chemical.

Sucrose is commonly known to most people as sugar and has the molecular formula $C_{12}H_{22}O_{11}$ [32]. Sucrose is often used as a precursor for producing hard carbon by pyrolysis for several reasons like availability, low cost and high chemical purity [33] Starch is also a known specie that comes in many forms and compositions. The starch is normally modified when used commercially. That is done by treating the starch with acid without substantially changing the granular form [34].

Below, the thermogravimetric properties of some of the relevant carbon sources are discussed. In a later section, Section 2.2.3, the pyrolysis properties of some alternative carbon sources will be evaluated.

2.2.1 TGA

The purpose of thermo gravimetric analysis (TGA) is to look at mass change over a temperature range. Venugopal et al. performed TGA on different carbon sources, and the results from the analysis can be seen in Figure 2.2.1. Only liquid phenolic resin and

sucrose are of interest in this project.
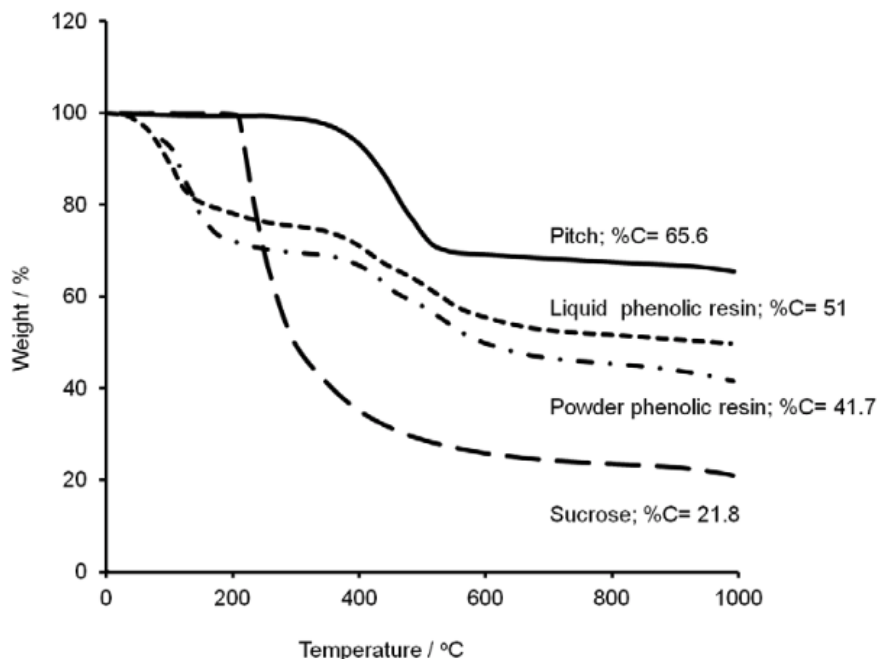
Figure 2.2.1: TGA results for various carbon sources obtained by Venugopal et al. [35]. All samples were heated up to 1000°C with a heating rate of $5°Cmin^{-1}$ and in an argon atmosphere.

The carbon sources were heated up to 1000°C in an inert argon atmosphere. The heating rate was $5°Cmin^{-1}$ and the weight changes were compared, as observed in Figure 2.2.1. The liquid phenolic resin had a mass drop in the beginning where it lost water before it cured at around 145°C [35]. After that there was a constant weight loss where only degassing of CO and CO_2 happened followed by another weight drop at around 400°C resulting from degradation of the resin and evaporation of several volatiles namely phenol and cresol [35]. The residual carbon after pyrolysis was measured to 51,0 % C. Sucrose was the carbon source with the largest weight loss out of the ones investigated in this study with only 21,8 % C after pyrolysis. Sucrose was stable until around 200°C before dehydration, dehydrogenation and volatilisation of CO and CO_2 was observed and hence resulted in a drastic weight drop [33].

Many materials carbonize when pyrolysed under an inert atmosphere with a fixed heating rate [36]. The normal steps of carbonisation is that oxygenated functional groups are released followed by CH groups. If the material is heated to higher temperatures, graphitization will occur.

2.2.2   Raman

Raman spectroscopy is a widely used non-destructive tool for characterisation of crystalline, nanocrystalline, and amorphous solids [37, 19]. Raman spectroscopy is especially useful in characterisation of carbon materials as they exhibit strong raman scattering. Raman spectroscopy observes vibrational and rotational modes in a system [38]. All carbons have some common features seen in their Raman spectra and the G and D peaks are examples of such features as can be seen in Figure 2.2.2 [39]. a-C denotes amorphous carbon and various deposition methods have been used to increase the degree of sp^3 bonding, like sputtering and plasma enhanced chemical vapour deposition (PECVD). The latter deposition method have a surprisingly low degree of sp^3 bonds and rather a larger content of hydrogen, and is denoted as ta-C (hydrogenated tetrahedral amorphous carbon) in Figure 2.2.2. The D peak represent the disorder (or diamond-like) band and the G peak the graphitic (or graphite-like) band [40, 41]. The D peak and G peak have centers at around 1360 cm^{-1} and 1560 cm^{-1} respectively [38]. For highly oriented pyrolytic graphite only the G band will appear in the Raman spectra whilst for more disordered carbons, there will be a D band appearing around 1350 cm^{-1}. The D peak arise from breathing modes of sp^2 atoms in rings, while the G peak arise from bond stretching of all pairs of sp^2 atoms in both rings and chains [38]. What peaks appear, at what position they appear, their area ratio (A_D/A_G) and full width at half medium (FWHM) are all parameters that can give information about the structure of the material [41]. Both the relative peak size of the D and G peak and full widths at half maximum (FWHM) indicate the degree of disorder in the material [40]. Broader peaks corresponds to more disorder in the material [39]. The intensity ratio (or area ratio) between the D and G peak, I_D/I_G, increase with increasing disorder in the material and can therefore indicate the degree of grapitisation [42, 43]. From Figure 2.2.2 it is clear to that the peaks get broader the more amorphous the material, and for the bottom three peaks it is hard to distinguish between the D and the G peak. This also illustrates the importance of deconvoluting the peaks to look at the difference between the area of the D peak and the G peak and that the fitting used for that purpose will influence the result strongly. Fitting of these curves are discussed in more detail below.
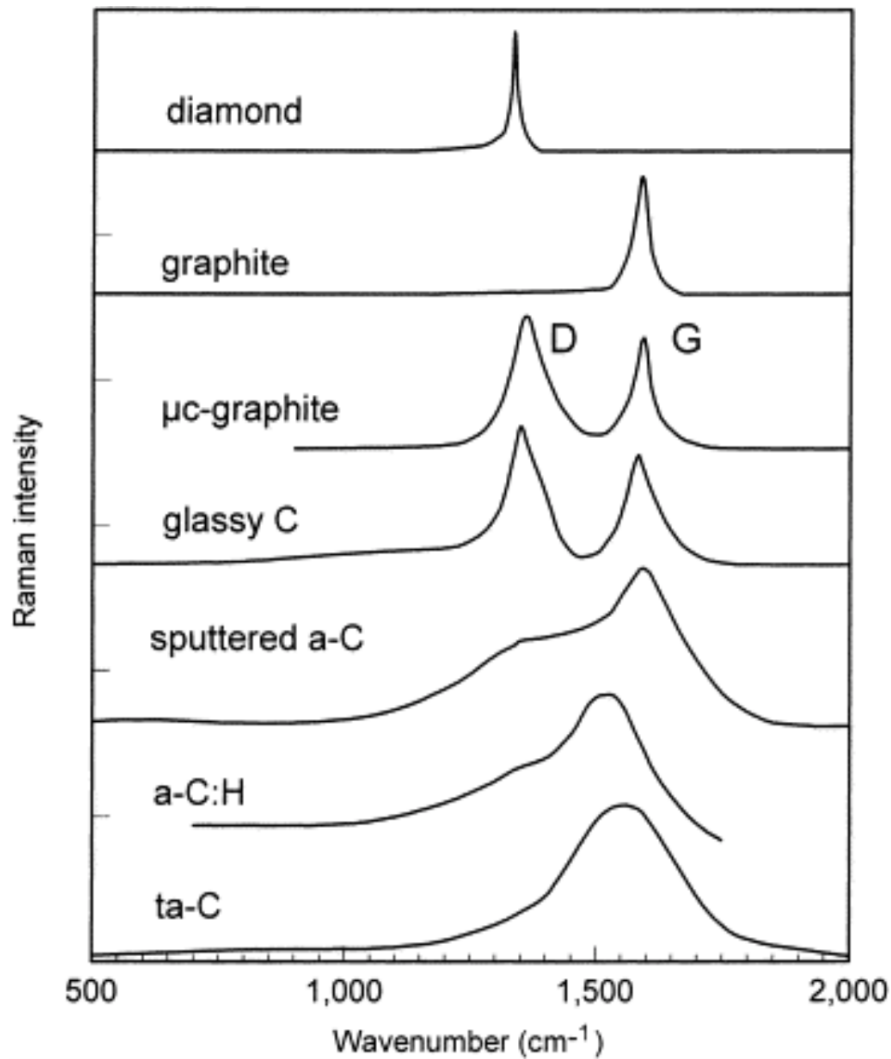
Figure 2.2.2: Typical raman spectra for some carbon materials. The top two peaks show the raman spectra of pure diamond structure materials and pure graphite structure materials [39]

.

A combination of Lorentzian-shaped and Gaussian-shaped bands are often used when successfully fitting Raman spectra [40], although there is a lack of consistency in literature. Figure 2.2.3 show an example of a fitting done on a Raman spectre of aromatic-rich soot, where three lorentzian curves and two gauss curves have been used [40]. Deconvolution reveals the presence of several peaks, and will therefore give a more reasonable result when analysing.
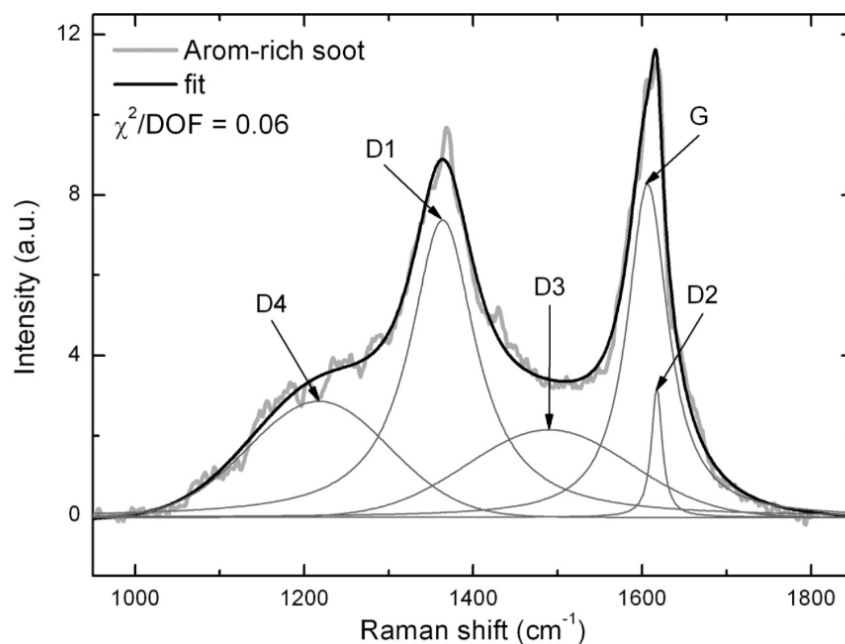
Figure 2.2.3: An example of deconvolution of a carbon material (here aromatic-rich soot). G, D1 and D2 band profiles are fitted with Lorentzian curves while D3 and D4 is a Gaussian fit [40].

The G band (ideal graphitic lattice, E_{2g} symmetry) and the D1 band (disordered graphitic lattice, A_{1g} symmetry) are mentioned previously, and are the main peaks of focus in this project. D1 is attributed to graphene layer edges while D2 is related to surface graphene layers with E_{2g} symmetry. The D3 band comes from amorphous carbon while D4 is disordered graphitic lattice with the same symmetry as D1 [40].

Petrus et al. performed Raman spectroscopy on various carbon sources as part of an investigation around their abilities to work as a good sintering aid [9]. The results obtained are presented in Figure 2.2.4.
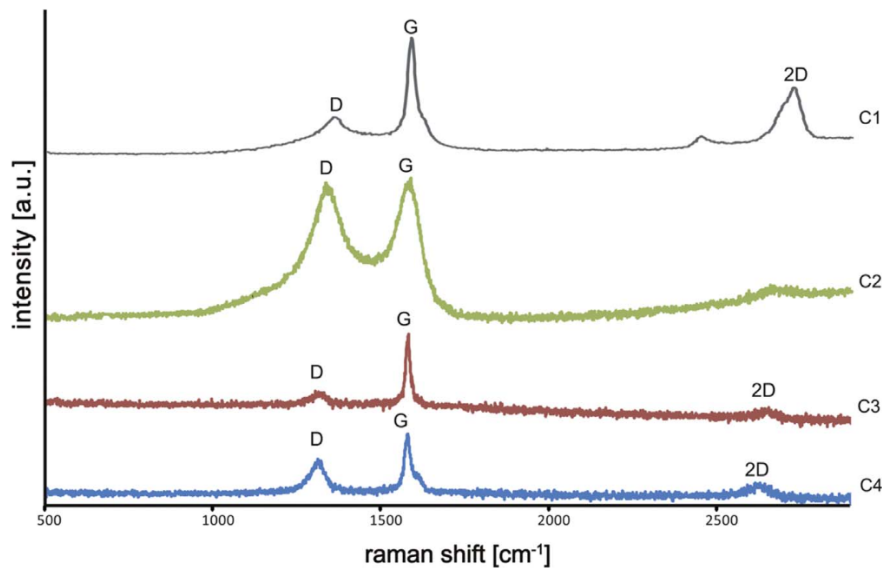
Figure 2.2.4: Raman spectra of various carbon sources, C1 being commercial multilayer graphene, C2 commercial carbon black, C3 highly oriented pyrolytic graphite and C4 commercial synthetic graphite. The scans were performed with a laser with a wavelength of 532 nm [9].

2.2.3 Alternative carbon sources

Inigaki et al. investigated carbon materials prepared from aromatic polyimides (polymers consisting of imide monomers) [44]. One polyimide examined was PMDA/ODA which is made from pyromellitic dianhydride (PMDA) and 4,4 - oxydiamine (ODA). Commercially, this product is called Kapton [44]. Advantages of using aromatic polyimides as carbon precursor to produce carbon materials are wide range of well-defined molecular structures, simple carbonisation behavior and high carbon yields. Disadvantages are cost and limited solvents that can be used [44].

As seen in Figure 2.2.5, the carbonisation of a Kapton film proceeds in two steps. The first step is an abrupt weight decrease within a short temperature range of 500 - 650 °C and simultaneously, evolution of large amounts of CO and CO_2 gases. As a consequence of the pyrolysis, there can be observed a pronounced shrinkage along the film at this temperature range [44]. In the second step of the pyrolysis, a smaller weight loss is observed. This is due to the evolution of small amounts of methane, hydrogen and nitrogen at a temperature range from 800 °C to 1000 °C [44]. The residual carbon after pyrolysis for the Kapton film is about 60 mass% [44].

19
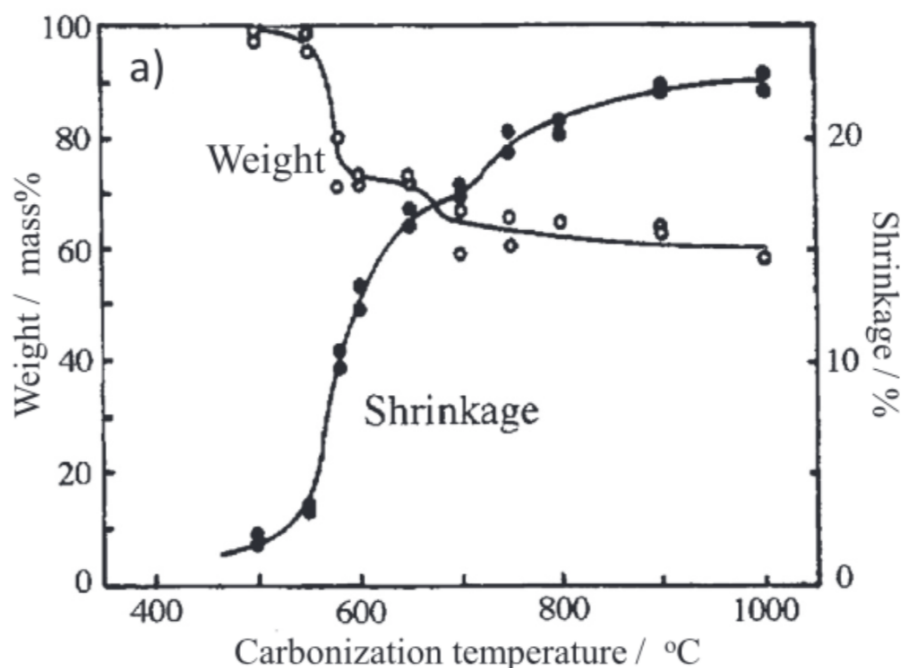
Figure 2.2.5: Weight loss and shrinkage of a Kapton film under various carbonisation
temperatures [44].

The molecular structure of the polyimide have a strong influence on the structure of
the residual carbon after pyrolysis, which is as mentioned, one of the advantages with
using polyimides as precursors [44]. By comparing Kapton (PMDA/ODA) with Upilex
(BPDA/ODA) one can look at these structural differences. Upilex is a commercial name
of another polyimide with a different atomic arrangement in the repeating unit. Planarity
of the repeating unit is presumed to govern the degree of graphitisation of the residual
carbon. From Figure 2.2.6 it is clear that Kapton is more planar than Upilex, giving rise
to a residual carbon with a higher degree of graphitisation [44].
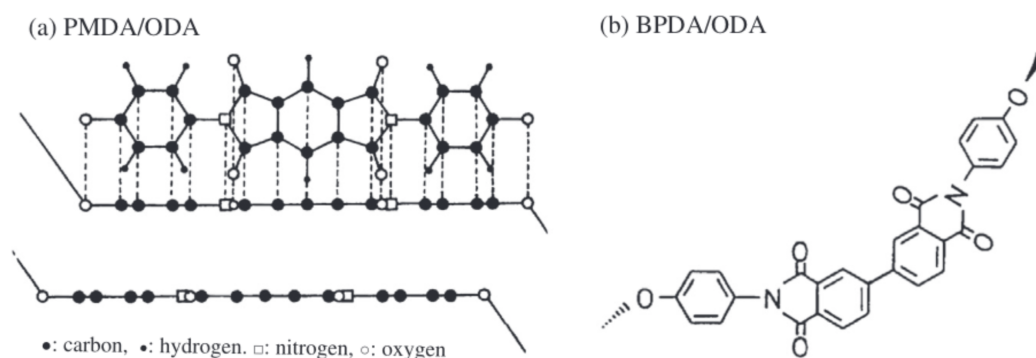
Figure 2.2.6: Atomic arrangement in the repeating unit of a) Kapton (PMDA/ODA) and
b) Upilex (BPDA/ODA) [44].

Stefanidis et al. investigated the pyrolysis properties of lignocellulosic biomass [45]. Lignocellulosic biomass is composed three main components, namely; cellulose, hemicellulose and lignin [46]. The composition of the three depend on the biomass type [45]. In this study Xylan was used as a replacement for hemicellulose, being easier to find commercially. Xylan is known as an adequate substitute and is widely used in literature for this purpose. At a dry basis cellulose, xylan and lignin have a carbon content of 42wt.%, 42wt.% and 63wt. respectively [45]. By performing a TG analysis on the components it was found that cellulose decomposed between 280-360 °C, a narrow temperature range. The reason for the well defined decomposition temperature range is believed to be the homogeneous unbranched structure that is highly crytalline. Total solid residue for cellulose at 800 °C was 7.4 wt.%. Xylan, another polysaccharide, behaved differently and decomposed at lower temperatures between 200 °C and 320 °C. Xylan has amorphous structure and many branched units, hence the lower decomposition temperature range. The residual solid content at 800 °C was 25 wt.% for Xylan, significantly higher than for cellulose. Lignin, on the other hand, decomposed at a fairly wide temperature range from 140 °C to 600 °C and had a solid residue of 41.2 wt.% at 800 °C, by far the highest of the three. The structure of lignin contain of a network of aromatic molecules that are highly cross-linked. Because of the high degree of cross-linking, the molecules are difficult to decompose and thus have a high thermal stability [45]. Lignin is known to be the most difficult component in biomass due to its structure [46]. After thermal pyrolysis of lignin, the main product derived was phenols. [45].

2.3 Sintering

Solid state sintering can easily be explained as a process to consolidate and form a material in solid form by applying heat and/or pressure without melting the material [1]. In a more sophisticated way, sintering is a process of elimination of interparticle pores in a granular material by atomic force driven by capillary forces [47]. Consolidation is achieved by the use of thermal activation energy of mass transport processes, a process driven merely by reduction of surface energies and grain boundary energies [48]. It is the preferred way to manufacture ceramics in the industry. However, there are some well-known challenges related to sintering with the main one being uncontrollable grain growth.

2.3.1 General sintering

For sintering to occur there are two factors that must be present; a mechanism for material transport and sufficient energy to activate and obtain that mechanism [1]. The most common mechanism for sintering is diffusion and a temperature increase often initiates the beginning of diffusion. Reduction in surface free energy is the driving force for sintering and this can be accomplished by either densification of the body or coarsening of the microstructure [49]. Figure 2.3.1 illustrates the diffusion path for both densification and coarsening of two ideal spherical particles. These two mechanisms are competing and the coarsening process will decrease the driving force for densification. If the densification mechanism is dominating, a dense body is obtained, but if the coarsening mechanism is dominating, a porous body is obtained. The problem of getting coarsening rather than consolidation is more common in highly covalent ceramics like SiC and Si_3N_4 [49]. When the powder of interest does not melt, but consolidate through atomic diffusion in solid state, the sintering is called solid-state sintering and is what will be the focus of this study. However, one way to avoid grain growth during sintering is to use an additive that form a liquid state during sintering, hence use so-called liquid-phase sintering [49].
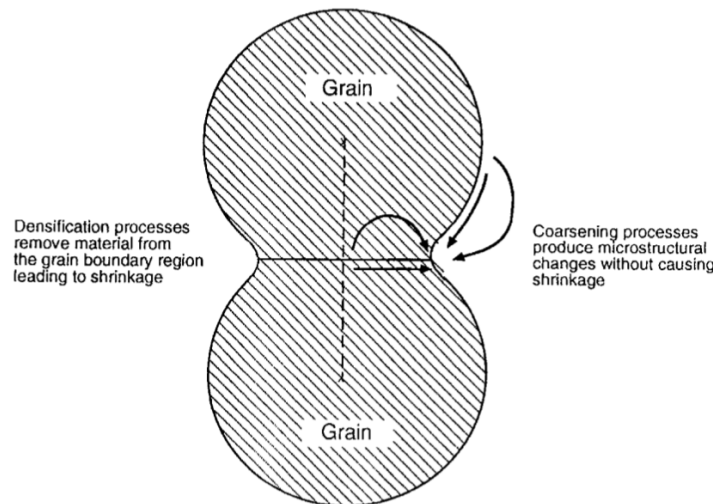
Figure 2.3.1: Illustration of the competing mechanisms of densification and coarsening [49].

An overview of different sintering mechanisms and whether they are densifying or not are presented in Table 2.3.1. Densification is enhanced by applying a pressure, which is a core advantage of SPS, discussed in Section 2.3.2. Other factors that can be varied

to obtain higher densities are temperature, particle size and atmosphere, which are also factors easily controlled using the SPS technique [49].

Table 2.3.1: Sintering mechanisms, source of matter and their ability to densify during sintering [50].

| Mechanism	Source of matter	Densifying	Non-densifying
Surface diffusion	Surface		X
Lattice diffusion	Surface		X
Vapour transport	Surface		X
Grain boundary diffusion	Grain boundary	X	
Lattice diffusion	Grain boundary	X	
Plastic flow	Dislocations	X	

Sintering is often seen as a process of several stages according to physical changes and porosity decreasing. This is a simplified visualization, but sufficient to understand the basic mechanisms occuring during sintering [1]. The first stage is called the initial stage and involve rearrangement of particles and neck formation at contact points between the particles. In order to obtain as many contact points as possible, adjacent particles rotate or move slightly. In the contact points, where the surface energy is highest and material transport can happen, bonding will occur. The pore geometry will enter the next stage when the bonds have grown sufficiently relative to the particle diameter and the surface has begun to smooth out.

The second stage of sintering, the intermediate stage, is where the neck between particles grow and the centre of particles move closer resulting in a decrease in porosity and an increase in density. During the intermediate stage there will be grain growth to accommodate further neck growth and thus reduce the porosity. The intermediate stage is where most of the shrinkage occurs during sintering and increase in density is highest [51]. The second sintering stage will continue until there are no more pore channels interconnected and all the pores are isolated.

The third stage of sintering involve the final removal of porosity together with grain growth and is called the final stage. Removal of porosity in the final stage happens by vacancy diffusion along grain boundaries [1]. Grain growth is an important mechanism

in stage three and the ability to control grain growth is crucial for obtaining dense results and usable mechanical properties. If grain growth is too rapid there is a chance that the pores will be isolated inside the grains as a result of grain boundaries moving faster than the pores, hence is controlling the grain growth of high importance for removal of porosity [49].

Chen et al. suggested an alternative route to conventional sintering where the sintering happens over two steps and high densities are obtained without compromising with grain growth [47]. Figure 2.3.2 show the sintering process for Y_2O_3 with a grain size of 60nm where densities close to theoretical density was obtained. By exploiting the difference in kinetics between grain boundary migration and grain boundary diffusion, the suppression of grain growth is achieved [47]
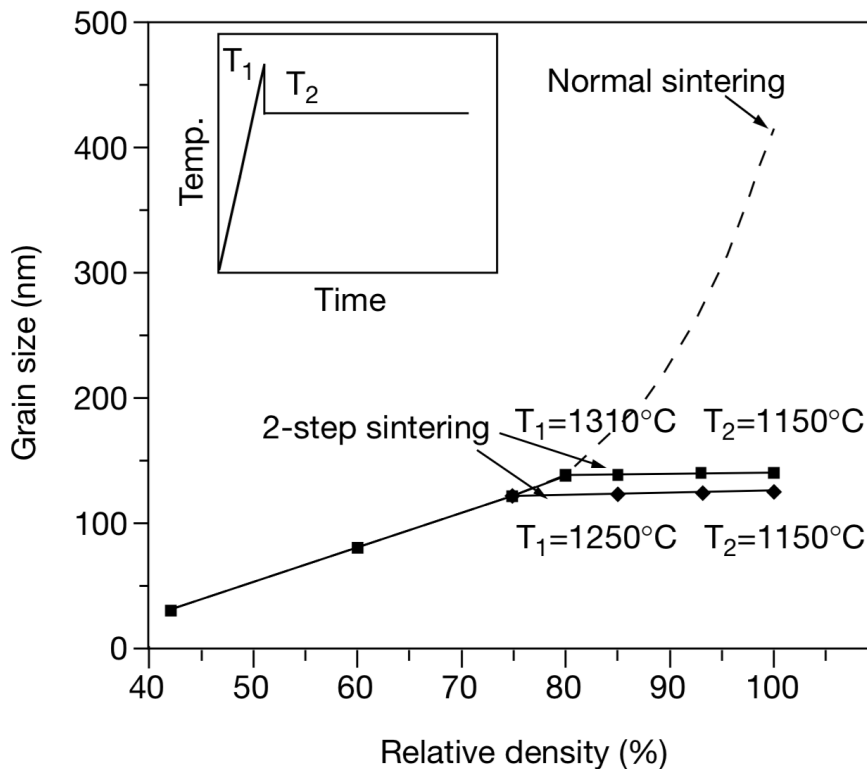
Figure 2.3.2: Illustration of how a 2-step sintering program can result in high theoretical densities and simultaneously avoid grain growth.[47]

There are several sintering methods that can be used to obtain the preferred result. All methods have positive and negative effects. Here, only one method will be discussed in detail, namely spark plasma sintering (SPS) as that is the only method used in this project. There will however be an extensive comparison between SPS and hot pressing

(HP) as HP is more commonly used in industry today.

2.3.2 SPS

Spark plasma sintering (SPS) is a recent development in sintering technology that utilizes axial pressure with a pulsed electrical current passing through the die with the powder body. With these features, very high densities are obtained. This new development within sintering has shown interesting results and have therefore drawn massive research interest to it over the last decades [48, 52, 53]. SPS is often referred to as pulsed electric current sintering (PECS), field-activated sintering technique or current-activated pressure-assisted densification, all identifications that describe the technique better [48].

Powders subjected to SPS have been proven to have enhanced sinterability due to increased particle surface activation and increased diffusion rates in contact zones with the applied pulse current [52]. Rapid heating is one of the sintering promotion factors of SPS that will result in obtaining the desired temperature faster in regions where bulk diffusion is dominant, as opposed to surface diffusion, which is more significant at lower temperatures [52, 54]. A schematic of a spark plasma sintering setup can be seen in Figure 2.3.3. The powder sample is loaded into a graphite die, with the necessary graphite paper and graphite wool inside and around it, and pressed together with one graphite punch on each side. The use of graphite for the die and punches limits the applied external pressure to 100 MPa [48]. The sintering environment inside the chamber can vary, but common environments are vacuum, argon, hydrogen and air. The sintering process starts by applying a pulsed current. The current is applied in pulses with a sequence of current followed by a sequence with no current, a so-called on-off DC pulse. A typical pulse of current can last for about 1-300 ms [52, 48]. When a sufficient activation level is reached, densification starts and it is amplified by an external pressure, which is either constant during the sintering or gradually increased [52]. The applied voltage is typically around 30 V and the current around 600-1000 A. Sintering time and temperature is dependent on the type of material and the wanted density. The sintering program is typically set beforehand and runs automatically during sintering. It is also possible to manually control the sintering by controlling the pulsed current and pressure as sintering is ongoing. The contact points between the particles are where the current normally

travels, thus that is the path with the least resistance. Because of oxide layers on the surface of the particles, small capacitors are formed across the contact points between the particles and electrical discharges are created here [52]. These electrical discharges may generate a spark/plasma which can be explained as ionized gas among the powder particles. This plasma environment creates modifications in the composition and that again will enhance removal of oxide layers and surface impurities and favor densification [52].
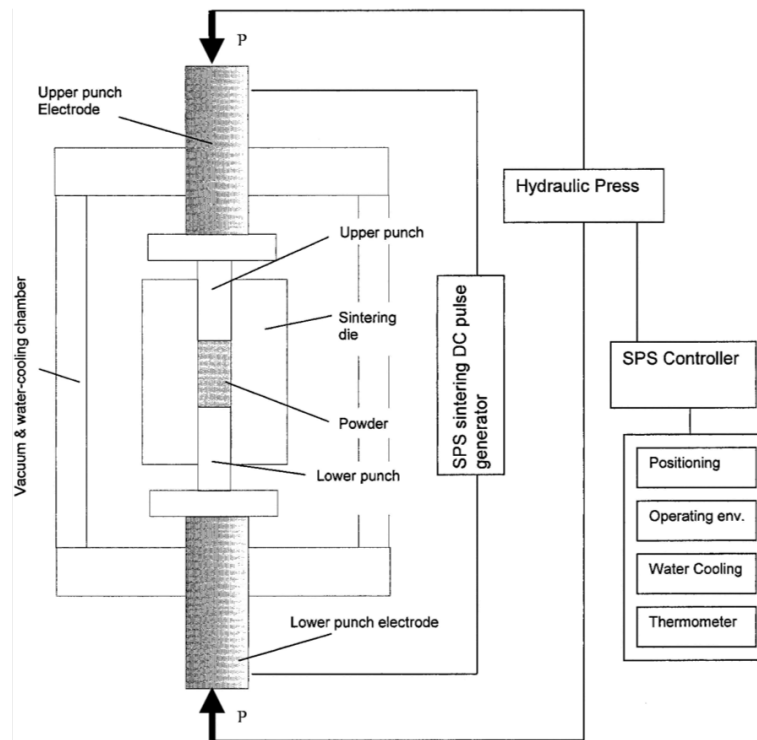
Figure 2.3.3: Schematic of a spark plasma sintering setup illustrating how the technique works [52].

SPS is used in industry in cases where it is very difficult to obtain high densities and where high performance materials are needed. A great advantage of SPS is the simultaneous monitoring of temperature, dimensional changes and gas pressure, making it possible to control and observe sintering better [52]. Compared to conventional sintering methods like hot pressing (HP), SPS can apply a higher heating rate and thus obtain high densities faster and at lower temperatures [48]. An additional benefit from the heating used for SPS is that it is uniform for the entire sample, compared to HP where thermal conductivity of the material is of more importance. SPS is therefore an excellent sintering technique when the material is for example a ceramic with a lower thermal conductivity [54]. Shorter

sintering time and lower temperatures means that there is a potential for massive energy savings by using SPS rather than HP. Energy savings is one great advantage of shorter time and lower temperature, but also compositional and microstructural changes like less material loss due to vaporization, undesirable phase transformation and suppression of grain growth are positive [48]. Some improvements of material properties reported after using SPS are cleaner grain boundaries, increase in superelasticity, improved mechanical and optical properties and better thermoelectric properties [48]. There are however some opposing theories about the consequences of using SPS. Zhou et al. densified a nanometer SiC powder doped with 2.04 wt% Al_4C_3 and 0.4 wt% B_4C using the SPS technique with various sintering parameters [55]. Common for all experiments was a sintering temperature of 1600°C and a sintering pressure of 47MPa. Both holding time and heating rate was varied and the results were compared. All of the samples, regardsless of holding time and heating rate, reached a density close to the theoretical density. It was found that rapid densification, i.e. rapid heating, led to significant changes in microstructure compared to a slower densification. The most noticeable change was growth of large elongated grains (anisotropic grain growth). The grain size increased with increasing heating rate. Polytype transformation is also evident when increasing the heating rate. Faster heating rate promotes the formation of 6H polytype while slower heating rate was more accompanied by formation of 4H [55]. The transformation from cubic to hexagonal structure ($\beta \to \alpha$ transformation) also enhance anisotropic grain growth [56]. Stacking faults have also been seen to occur simultaneously with polytype transformation, and one possible reason is the large energy difference between the different polytypes [57].

The mechanical properties of silicon carbide after sintering is of high importance, and the sintering techniques can, like mentioned, have a big influence on the final properties. It is interesting to compare hot pressing to spark plasma sintering because the two techniques are the most similar. Tamari et al. did a comparison of the two sintering techniques with regards to density, strength and hardness [54]. They used a silicon carbide powder with alumina and yttria as sintering additives. The sintering conditions, both for SPS and HP, was a pressure of 30MPa and a holding time of 5 minutes. The heating rate for SPS and HP was around $200°Cmin^{-1}$ and $70°Cmin^{-1}$ respectively. The authors found that there was a relatively large difference between the two techniques when it came to density, especially at lower sintering temperatures, and that the bending strength was

significantly higher for SPS samples. These results are presented in Figure 2.3.4 below. Hardness was also measured using Vickers and the results showed the same trend as density, which are two highly relatable properties. In the case of hot-pressing, 200°C more was needed in order to get densities around 98% of theoretical density, compared to using SPS.The bending strength does not follow the same trend as density and even with same densities, the samples subjected to hot pressing had a significantly lower strength [54]. Hayun et al. also reported a great advantage using SPS when sintering silicon carbide, and stated that SPS is highly competitive with HP [53].

(a) Theoretical density   **(b)** Bending strength
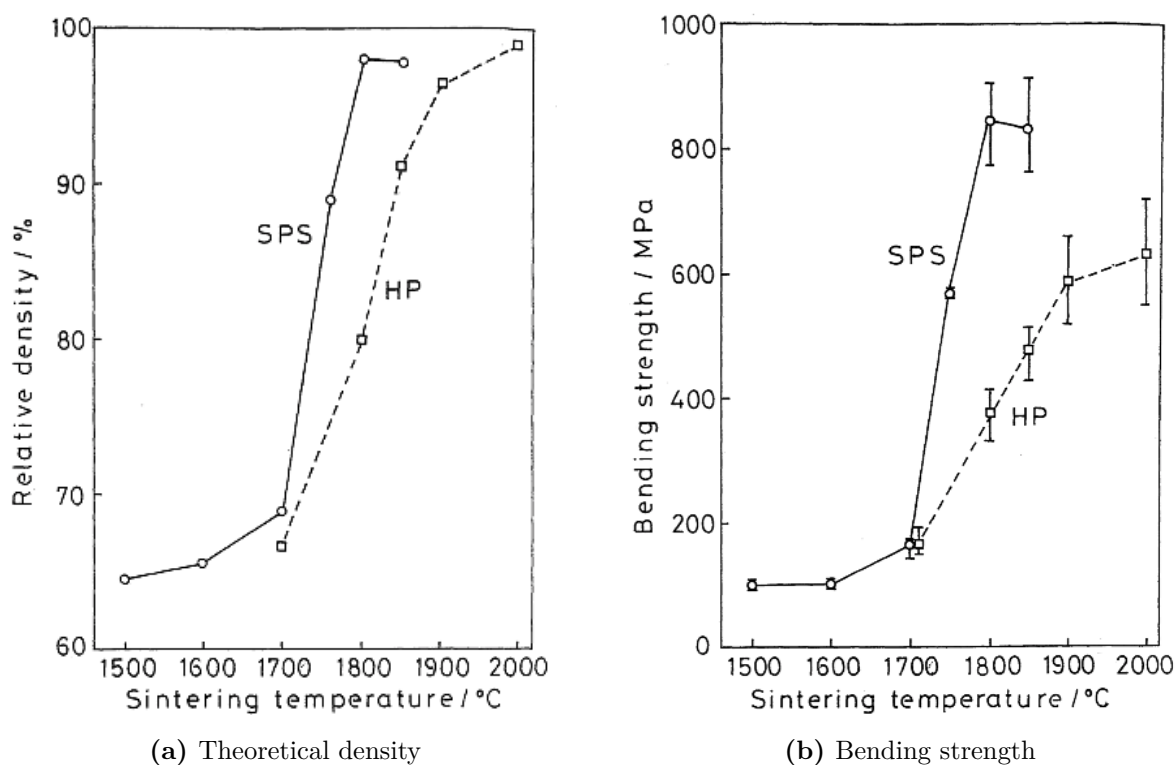
Figure 2.3.4: A comparison of a) theoretical density and b) bending strength at different sintering temperatures when using SPS and HP as sintering techniques [54].

There are both advantages and disadvantages regarding the use of SPS. The need for further research on the field is evident and despite the achievable properties, there are many limitations for industrial scalability, i.e. equipment complexity, product size and shape and cost [52, 7].

2.3.3 Sintering of SiC

Silicon carbide has, as described in Section 2.1.2, properties that beat most other materials. Properties such as high hardness, low thermal expansion coefficient and high resistance to thermal shock arises from the strong and stiff covalent bonds between silicon and carbon in the structure [9, 10]. On the other hand, these strong covalent bonds inhibit solid-state sintering and the lack of ionic bonds often result in slow bulk diffusion being rate-controlling during consolidation [58, 10]. Stobierski et al. stated that both boron and carbon are necessary sintering additives in obtaining dense SiC [5]. It has been experimentally observed that a few percent of carbon and boron is optimal in order to obtain densities close to theoretical densities of SiC using a pressure-less sintering technique [3, 5, 4]. SiC has been sintered without any additives as well, but then theoretical density was only achieved using a hot-press method with a temperature of 2500 °C and a pressure of 50 MPa [59]. SPS is normally the sintering technique used when sintering without additives due to the increased need for external sintering drivers [53]. There are examples of additive-free sintering with lower temperatures where silicon carbide is freeze granulated and heat treated prior to sintering (using SPS) [60]. Here, high densities and great properties were obtained [60]. However, there are still some challenges with not using sintering additives. Even though it is possible to obtain high densities of SiC without using additives, the energy required to do so makes it inconvenient and expensive. In addition to that, there are two main reasons for using sintering additives in SiC; enhancing the densification rate and slowing down grain growth kinetics [56]. Maitre et al. observed the advantages of free carbon and boron present even when consolidation SiC with SPS [56]. Here, the addition of carbon and boron had a positive effect on minimizing the grain growth.

There are no explicit explanation of the mechanisms behind the effects of carbon and boron as sintering aids for silicon carbide, but the general thought is that carbon will inhibit processes that do not favour dense sintered bodies, while boron will activate processes that promotes dense sintered bodies [4]. Boron can be introduced as elemental boron or as B_4C [3]. There are several opposing theories as to what happens when boron is used as a sintering aid, and what makes boron an important additive when sintering SiC. Prochazka, a pioneer on the field, stated that densification happens by

solid-state sintering [3]. An opposing theory by Stobierski et al. claims that boron form a liquid phase (boron - silicon - carbon phase) inside the sintered material which activates the sintering by enhancing the capillary forces in the densification process [4]. The optimal boron concentration is in the range of 0.2–0.5 wt.% according to Stobierski et al. [4]. Skarpeid suggested that a higher boron concentration, 0.7 wt% was optimal if considering both density and mechanical properties [50]. Within this range boron had a good effect and no discontinuous growth of SiC - grains were observed. Only very small concentration of boron was needed to observe the liquid phase and its effects, but with greater amounts the liquid phase increased. The liquid phase formed is not stable and by lowering the temperature, precipitates are formed which is not wanted, hence the upper limit for optimal boron concentration [4]. Prochazka, with the solid-state sintering theory, also found that very small amounts of boron was needed (several tenths of a percent) in order to get close to theoretical density [3]. Ogbuji is very critical to the theory about boron forming a liquid phase during sintering and specifies that this is only possible at very high sintering temperatures (over 2000°C), if even possible at all [61]. Prochazka believes that boron increases the solid-state diffusion by near grain boundary vacancy formation [3]. Maitre et al. suggested that free boron could form further point defects in the SiC lattice as a result of improved densification kinetics [56]. Another effect seen by Maitre et al. was that borosilicate glass would form by dissolution of B_4C in a silica rich melt causing anisotropic grain growth rather than densification [56]. This goes to show that there is a fine balance between getting positive or negative effects from using sintering additives.

Rijswijk et al. presents several ways that carbon can have a positive effect on the sinterability of SiC [58]. The most common explanation is that carbon removes silica (SiO_2) from the surface of SiC which is necessary for achieving a dense sintered body [3]. This is discussed in more detail in the following section, Section **??**.

There are also several other possible additives used in literature as sintering aids for silicon carbide. Tanaka et al. used AlB_2 instead of elemental boron and obtained densities around 98% of theoretical density using lower temperatures than conventional sintering with carbon and boron as additives [57]. Al_4C_3 has also been used with great outcomes, as it forms a liquid phase during sintering [62]. Other examples of sintering additives

used are Mg, MgO, $AlO_3 - Y_2O_3$ and $Al_2O_3 - Y_2O_3 - CaO$, all of which the purpose is to achieve high densities at lower temperatures [10].

2.4 Carbon as a sintering aid

Prochazka et al. were the first to demonstrate the effects of carbon as an aid when sintering silicon carbide. They showed that SiC can be densified to approximately 98% of theoretical density with additions of carbon and boron. Years later, Stobierski et al. explained the effects by stating that carbon reacts with silica on the surface of SiC particles and hence reduce the effects of mass transport mechanisms that are not beneficial for densification. Boron was, by the same authors, explained to have an increasing effect on the diffusion rate by forming a liquid phase with silicon and carbon.

2.4.1 Removal of silica

On the surface of SiC there is always a thin layer of native silica that will react with present carbon according to Reaction (2.5) and create CO gas and secondary SiC or according to Reaction (2.6) and create SiO and CO instead [58].

$$SiO_2 + 3C \rightarrow SiC + 2CO \tag{2.5}$$

$$SiO_2 + C \rightarrow SiO + CO \tag{2.6}$$

It is crucial that the carbon is well-distributed in order to react with the surface-forming silica and thus be an effective sintering aid [58].

Both reactions above are spontaneous at relatively low temperatures. Another possible reaction, Reaction (2.7) with $\Delta G = 0$ at 1870°C, would take place at higher temperatures.

$$2SiO_2 + SiC \rightarrow 3SiO + CO \tag{2.7}$$

Here, silica will react with silicon carbide itself and create SiO and CO gas. SiO is a very volatile specie and will therefore promote vapor transport which has been shown to

have a negative effect on sintering by inhibiting densification and causing coarsening [58]. Reaction (2.7) is therefore not a wanted reaction and elemental carbon is important in order to promote Reaction (2.5) instead. Another possible reaction that can happen at even higher temperatures, with $\Delta G = 0$ at 1950°C, is Reaction (2.8).

$$SiC + SiO \rightarrow 2Si + CO \tag{2.8}$$

This reaction is very efficient at temperatures that are normal for sintering SiC. The formation of silicon might lead to silicon transport through surface diffusion [58]. The presence of excess carbon can prevent having condensed silicon by the grain boundaries.

Prochazka et al. have shown that, in the absence of carbon, vapor transport strongly inhibits densification and leads to coarsening. However, the presence of elemental carbon could promote the reaction in Equation (2.5), and also convert SiO to SiC and CO, and Si to SiC, thereby preventing this type of vapor transport.

2.4.2 Particle size of carbon

Contarini et al. looked at the relationship between milling time of SiC slurry and dispersion of carbon, and how the dispersion of carbon in the green body would affect the density of sintered material [63]. The carbon sources used in this study was carbon black and graphite and the milling time was varied between 1h, 4h and 16h. X-ray photoelectron spectroscopy (XPS) was performed on the green bodies to investigate the size of the carbon particles as an increase in surface area will cause a higher C-C XPS peak (carbon-carbide peak). Results indicated that there is an increase in intensity with increasing milling time and the increase is more significant when using graphite rather than carbon black. In other words, carbon black seems to be quite well distributed even at short milling times. This is assumed to be because of the smaller particle size of carbon black before milling compared to graphite.

The authors also concluded that there is a strong correlation between the intensity of the C-C peak and the resulting density after sintering. Her as well, carbon black showed better qualities than graphite, reason being carbon black is largely amorphous thus have a higher reactivity [63].

Celik et al. looked at the particle size of the carbon black used as a sintering aid on the resulting density qualities. According to Figure 2.4.2, the smaller the particle size of carbon black the denser the result. The reason for the decrease in density with larger carbon particles is that there are less carbon particle to react with silica on the surface of the silicon carbide particles. Hence, the more particles that can react with silica the higher density is obtained.
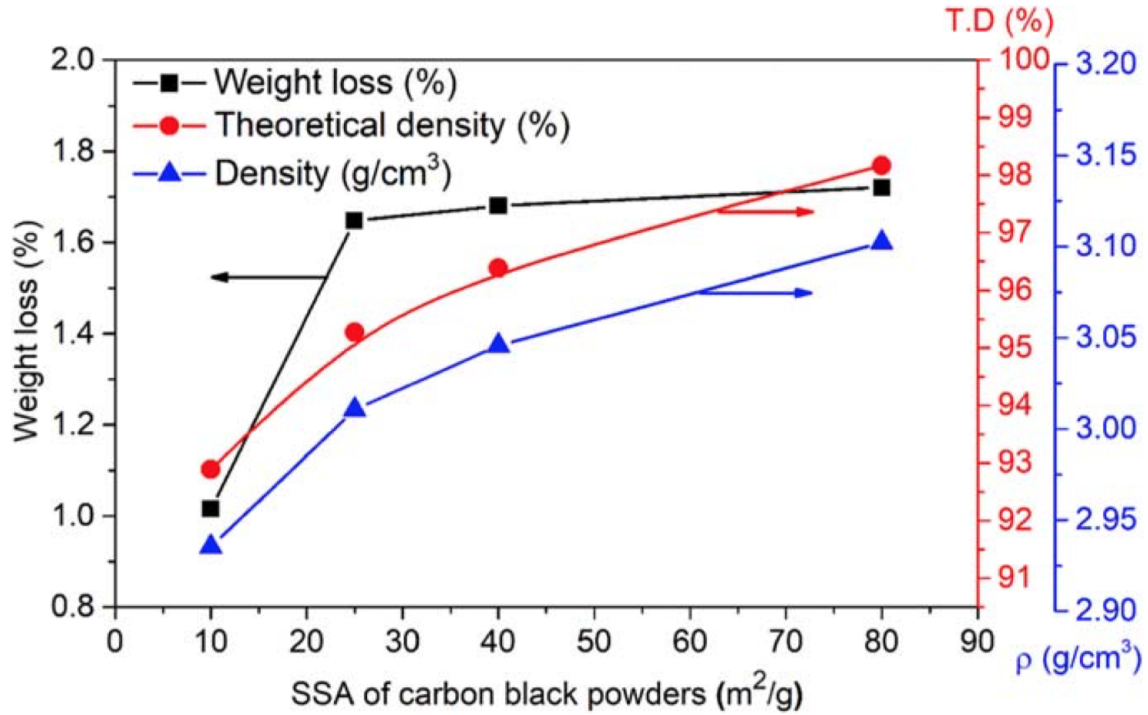
Figure 2.4.1: Correlation between specific surface area (SSA) of carbon source, here carbon black, and densification properties of the sintered body [64]

In a study performed by Venugopal et al., the only variable in the different precursor powders was the carbon source, hence could differences in size and/or structure for the final HfB_2 - powders be linked directly back to the type of carbon used [35].

Generally, it was found that the structure of the final particles produced were directly correlated to the structure and level of agglomeration of the carbon source used [35]. Liquid phenolic resin and sucrose have a sheet like carbon structure after pyrolysis which give rise to small particles in the final powder.

If a carbon source had a high degree of agglomeration it resulted in higher degree of agglomeration in the final powder and hence coarser particles.

Another observation made by Venugopal et al. was that the amounts of carbon present had an effect on the final powder size. With excess carbon present, the carbon matrix would prevent ceramic particles from coalescing and thus growing. This would leave quite a severe carbon impurity. Using the stoichiometric carbon amounts would result in larger particles but less carbon impurities [35].

The study showed that the structure of the residual carbon from different carbon sources vary and have a huge impact on the size of the resulting powder synthesized. The particle size of the powder will again have a great impact on the sintering abilities and thus the need to use sintering aids. Petrus et al. argues that regardless of the amount of carbon added being the same, the various forms of carbon have a big influence on sintering properties and final microstructure [9].

2.4.3   Carbon dispersion

Celik et al. investigated the localisation of carbon in SiC granulates where carbon black was used as the carbon source [64]. The SiC granulates were made by spray drying and the assumption that there is an heterogeneous distribution of carbon in the granules were investigated. EDX mapping was performed on a fracture surface of a SiC granule to identify and reveal the distribution of carbon, as can be seen in Figure 2.4.2. The authors observed a remarkably higher concentration of carbon at the outer boundary of the granulates in 1 μm depth.
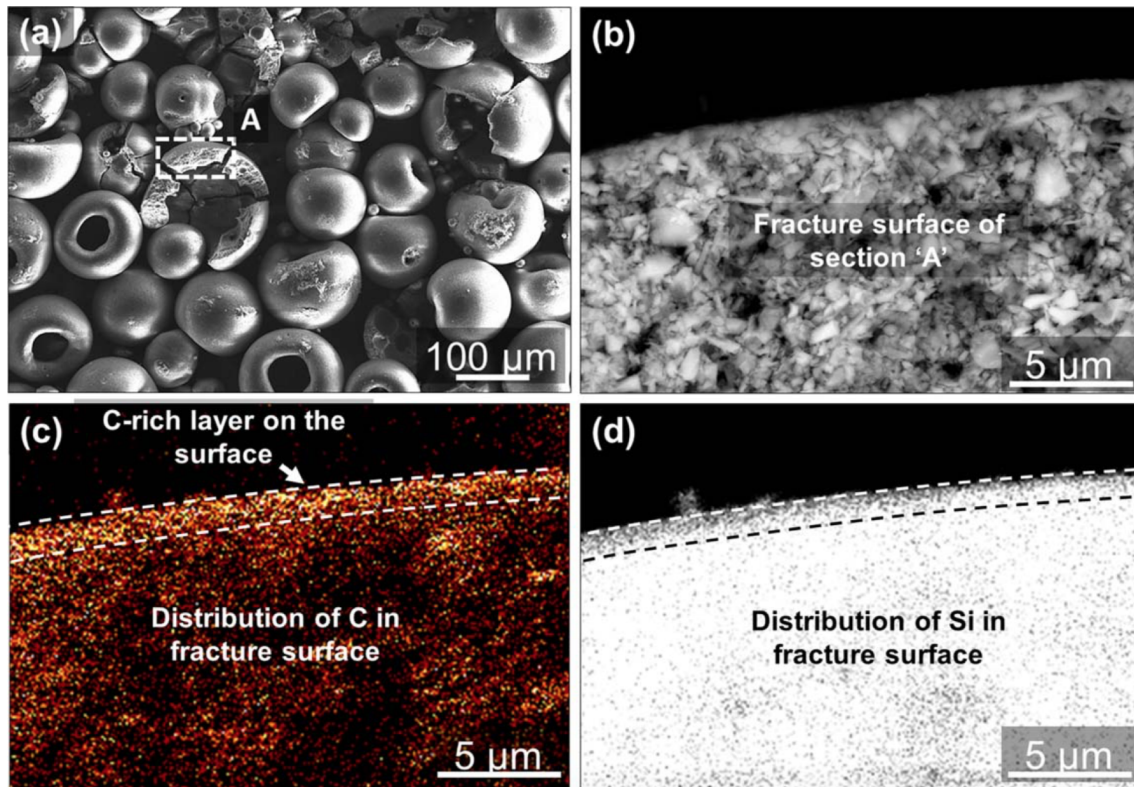
Figure 2.4.2: a) SEM image of spray dried SiC granulates, b) high magnification of the area A in a), c) EDX map of carbon in b), d) EDX map of SiC in b) [64]

When looking at the microstructure with an in-lens detector of SEM, found in Figure 2.4.3, the authors discovered some black curved spots that is assumed to be carbon segregation. The shape of the carbon and the amount in each sample gives the base for the assumption. The brightest, slightly elongated grains are SiC. The boron additive, in the form of B_4C, is not visible in the images due to the low concentration. Carbon, however, are marked in the images as these darker, curved-like structures. The shape of the carbon is a result from the localisation of carbon black particles on the outer surface of the granulates after spray drying. The particle size of carbon black added increases from a) to d) with respective specific surface area of 80, 40, 25 and 10 m^2g^{-1}. It is clear to see that the occurrence of the curve-like shaped carbon increases with increasing particle size of the added carbon source.
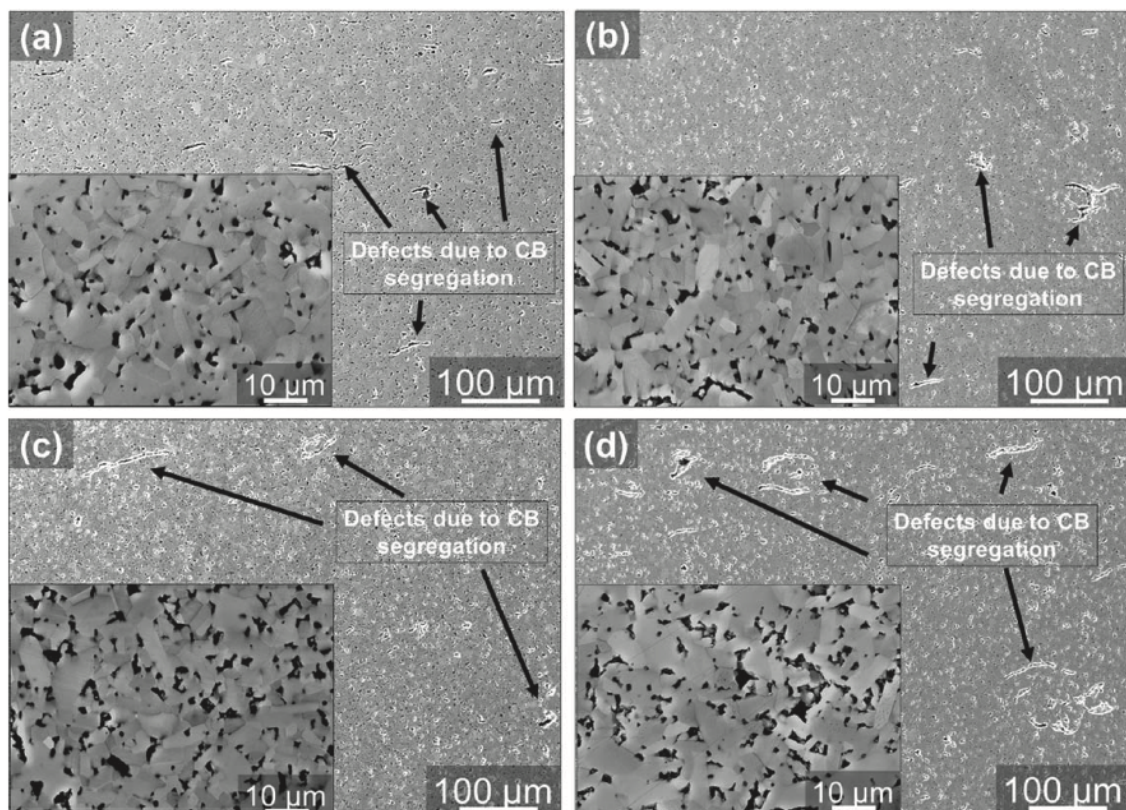
Figure 2.4.3: a) SEM image of spray dried SiC granulates, b) high magnification of the area A in a), c) EDX map of carbon in b), d) EDX map of SiC in b) [64]

Chapter 3

Experimental

3.1 Powders and apparatus

The silicon carbide powders were all produced by Fiven Norge AS. The pure carbon sources were also provided by them, but they were manufactured elsewhere. The detailed composition of the silicon carbide powders and the carbon sources are confidential, but an overview of what is known can be found in Table 3.1.1 and 3.1.2.

Table 3.1.1: A list of carbon sources used in this research project. Both the resin and the starch came in liquid form, however, the water in resin had evaporated before this project started so the residual carbon is calculated from solid state.

Trade name	Distributor	Residual carbon after pyrolysis [wt%]	Notation
Phenolic resin	Zschimmer & Schwarz	56.4	Resin
Modified starch	Momentive	34.7	Starch
Table sugar	Grocery store	19.1	Sucrose
Carbon black	-	100	Carbon black

Table 3.1.2: A list of the precursor powders used in this research project. The silicon carbide powder with starch and sucrose as carbon source do not have a trade name as they are not commercial products. Other additives like binders and pH regulators are also added.

Trade name	Silicon carbide source	Carbon Source	Residual carbon [wt%]	Notation
Densitec 15HR	Sintex 15	Resin	1.0	SiCRe
-	Sintex 15	Starch	1.0	SiCSt
-	Sintex 15	Sucrose	1.2	SiCSu

3.2 Procedures

The procedures used in this study is presented in this chapter and an overview of the work done is presented as a flowchart found in Figure 3.2.2. Table 3.2.1 show a list of the apparatus together with the specific model used for the procedures.
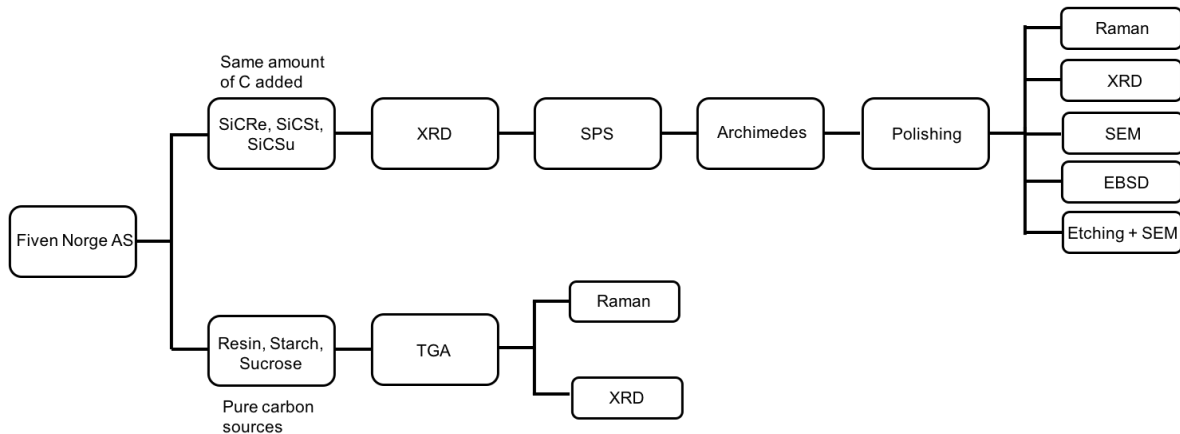
Figure 3.2.1: Flow chart illustration of the course of the work done for this project. A set of experiment were performed on precursor powders whilst another set of experiments were conducted on pure carbon sources.

Table 3.2.1: A list of the apparatus used in this study with the associated model and application.

| Apparatus	Model	Application
Thermogravimetric analysis (TGA)	Netzsch STA 449	Measure mass loss over a temperature range
Spark plasma sitering (SPS)	SPS 825 Dr. Sinter	Sinter with applied pressure
Archimedes' prinsiple	Mettler Toledo	Measure density
Raman spectroscopy	Alpha 300R WITec	Measure degree of graphitisation
XRD	D8 Advance DaVinci	Study phase composition
SEM	Zeiss Supra FESEM 55	Study microstructure and fracture surface
EBSD	NORDIF UF - 420	Study microstructure and grain orientation
Polishing	Struers Tegrapol - 31	Surface preparation

3.2.1 Powder preparation

The powders used in this research project was provided by Fiven Norge AS. The production of the powders were done at their pilot facilities in Lillesand, in the south of Norway [65]. Pure silicon carbide is produced according to the Acheson process prior to crushing and milling to obtain a powder of wanted size. This results in a *SiC* powder that is sold commercially by Fiven Norge AS by the name Sintex. Sintex products have a number behind denoting the specific surface area of the powder. Sintex products can be mixed with different additives to obtain a "ready to press" (RTP) powder. These additives can typically be carbon, boron, binding agents, dispersion agents and pH regulators. Fiven Norge AS calls their commercial RTP products Densitec. By adding different components with variable amounts to the Sintex powder, a variety of Densitec powders are obtained. Depending on the amounts of additives, some Densitec powders are made for hot pressing and some are not. Less additives requires a stronger driving force in order to sinter to high

densities, hence there are less additives in a hot press powder. For this research project three different powders were produced. The reference was simply just a commercially produced Densitec15 powder made for hot pressing with phenolic resin as the carbon source, called SiCRe for simplicity. The other two powders were made in small batches solely for the purpose of this research project and are not commercial products today. One powder has modified starch as the carbon source and the other has pure sucrose as the carbon source, denoted SiCSt and SiCSu respectively for this project.

Sintex 15 was used in this study, hence the specific surface area of the SiC particles are $15m^2/g$. Both amounts of water and additives were chosen carefully to fulfill the requirements of solid load and residual carbon after pyrolysis. The water based slurry was then put in a sealed container with steel balls for better mixing and placed on a planetary ball mill over night to ensure homogeneous mixing. Spray drying was done in a pilot-scale spray dryer with an inlet and outlet temperature of 200 °C and 130 °C, respectively. The temperatures were set to obtain a certain water content in the resulting agglomerates. The feed-speed was regulated by a pump to obtain granulates with a size of around 100 μm

An overview of the main processes for producing the spray dried agglomerates are illustrated in a flow chart in Figure 3.2.2.
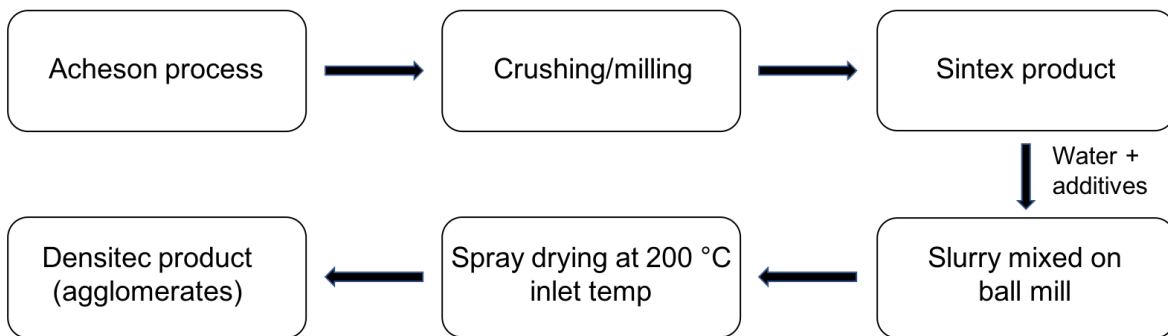
Figure 3.2.2: Main steps in preparation of powders used in this study. These processes were done by Fiven Norge AS.

The amounts of carbon source added was corrected to obtain the same carbon residue after pyrolysis, hence the same carbon residue presence at around 1500 $°C$ where sintering starts. This was done to eliminate one variable that can affect the densification of SiC and make it easier to investigate differences with using alternative carbon sources. Like

mentioned, three different precursor powders are investigated in this study, namely SiRe, SiCSt and SiCSu. Compared to the specialisation project leading to this study there are two main differences with the precursor powders investigated here; a) powders are made for hot pressing and b) pure sucrose is added as a carbon source and not a mix of sucrose and starch.

3.2.2 Thermogravimeteric analysis (TGA)

Thermogravimetric analysis was performed on all the carbon sources to observe mass change over time with increasing temperature. First, a background was loaded in the thermogravimetric analyzer (Netzsch STA 449 F1 Jupiter), before the actual carbon sources were analyzed one by one. The background was an empty alumina crucible with an alumina lid. The analysis was done in an argon atmosphere and the chamber was flushed with argon three times (vacuum was obtained between every flush) before the temperature program was started. The four different carbon sources tested, resin, starch, sucrose and carbon black, were all heated up to 1500°C with a heating rate of 10°C per minute and held at that temperature for one hour. Prior to that holding time, the carbon sources were held at 180°C for two hours to make sure they were dry for the further heating process, as starch and resin were in liquid form originally. This was the reason for using a lid with a tiny hole on the crucible, to ensure that the liquids would not leave the crucible. A schematic of the setup can be found in Figure 3.2.3.
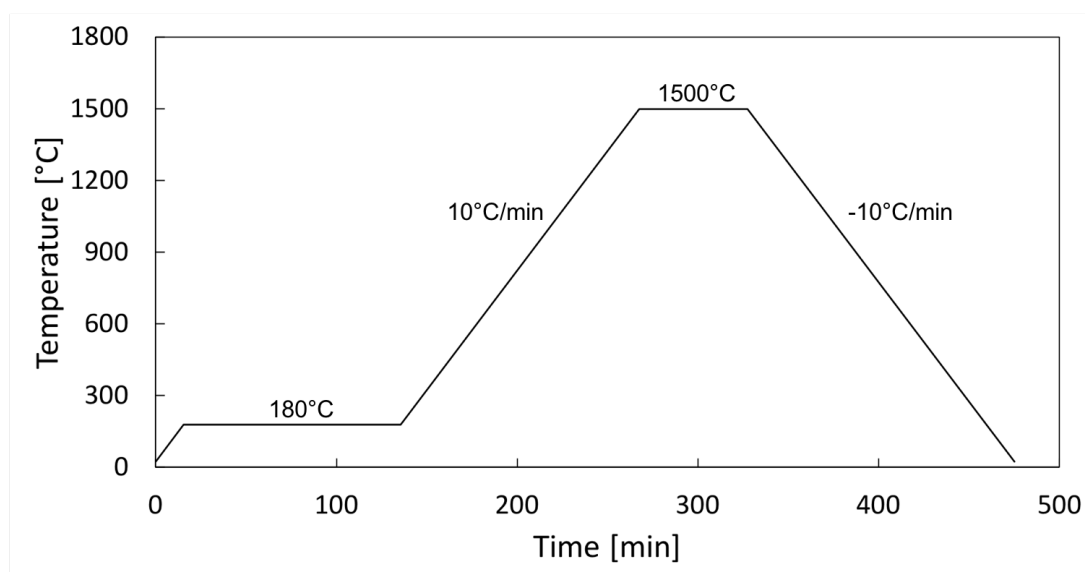
Figure 3.2.3: Graphic illustration of the temperature program used for TGA.

41

3.2.3   Raman spectroscopy

The raman spectra were acquired by a micro-Raman system connected to a microscope (Alpha 300 R, WITec, Germany). The system has a backscattering geometry with a spectral resolution of 1 cm^{-1} and an excitation wavelength of 532nm (frequency-doubled NdYag laser with a maximum power of 66 mW). Raman was used to characterize both sintered bodies and residual carbon after pyrolysis. The sintered bodies investigated were polished in order to get bulk properties. The residual carbon samples were just flattened between to glass plates before they were put under the microscope. 5 scans were done on each sample on different positions on the sample to get an average result that were more homogeneous that just running one scan. An objective of 50x magnification (numerical aperture of 0.75) was used when running the scans. The background was removed and the curve was smoothed for each scan before the average of the 5 scans were made. Then that average scan was used for further analysis. The analysis was done using the Fityk software [66]. The main goal of using Raman spectroscopy in this project was to look at the reactivity of different carbon sources. That was done by comparing the area underneath the D-peak and the G-peak. The Fityk sofware was used to deconvolute the peaks and get the area under the given peaks.

3.2.4   Spark plasma sintering

Spark Plasma Sintering (SPS) was the used sintering technique for this study. One of the greatest features of SPS is the internal and thus rapid heating. An explanation of the technique can be found in Section 2.3.2. The sintering was performed at a sintering unit called SPS 825 Dr. Sinter. The powder was placed in the middle of a symmetric graphite die with an inner diameter of 28 mm and a drilled hole at the centre of the lateral side. Graphite paper was used on the inside of the die as well as on the top and bottom before two punches were placed in each opening of the die. The purpose of the graphite paper was to avoid direct contact between the powder and the graphite die. The thickness of the graphite paper used was 0.25 mm after seeing negative effects on the sintering results using thinner paper [67]. Graphite wool, tied together with graphite thread, was put around the whole die for thermal insulation at high temperatures. For stability reasons, an initial pressure of 2MPa was applied on the punches with a uniaxial hydraulic press. Then the

die was placed between graphite disks inside the sintering chamber. The disks are there to regulate the height and it is of high importance that the die with the powder inside is placed symmetrical on the graphite disks to obtain a uniform pressure on the sample. Another layer of graphite wool was placed around the die and the graphite disks, another measure to increase insulation at elevated temperatures. An image of the sintering unit as well as the die and punches used can be seen in Figure 3.2.4. The hole in the graphite wool and in the die is there to enable temperature measurements by the pyrometer and correct alignment is required to obtain accurate temperature measurement. The pyrometer only starts measuring the temperature at 400 °C.


(a) SPS 825 Dr. Sinter


(b) Die and punches

Figure 3.2.4: The left picture shows the SPS unit used in this project and the picture to the right shows the graphite die and punches used.

Figure 3.2.5 shows a schematic of the sintering program, with temperature, time and pressure profiles, used for this project. Temperature only starts at 400°C because, as mentioned above, that is where the pyrometer starts its measurements. The sintering program is inspired by previous work on similar powders where an optimisation of the sintering program was done to maximize density and simultaneously minimize grain growth [67].
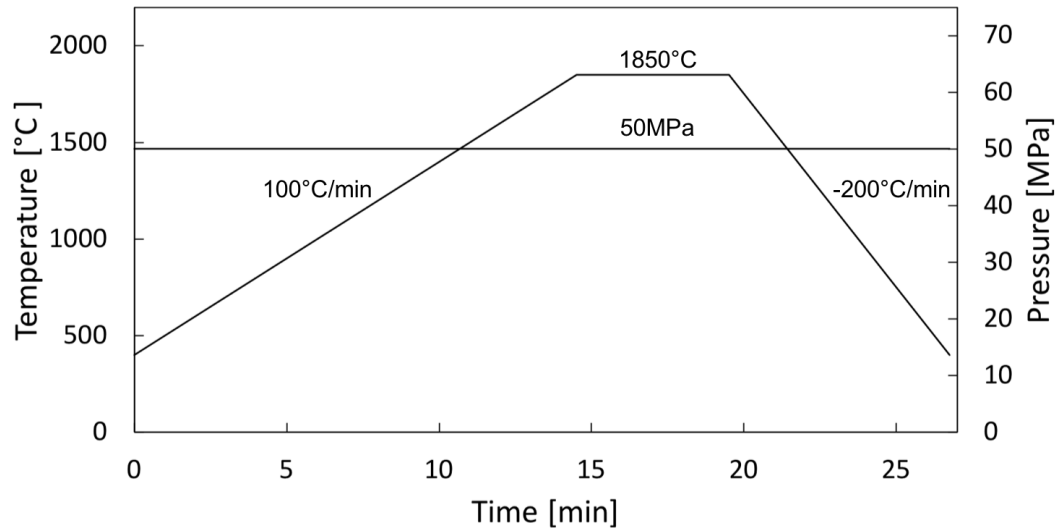
Figure 3.2.5: Time - temperature - pressure profile used for spark plasma sintering (SPS) of SiC - powders with different carbon sources. The purpose of this sintering program was to obtain a high density for all precursor powders.

A sintering temperature of 1850 °C with a holding time of 5 minutes together with an applied pressure of 50MPa throughout the whole sintering process are all strong drivers for dense sintering. With this program the goal was to get as high densities as possible to confirm if all the precursor powders were capable of obtaining high densities. This sintering program was applied on three samples of each precursor powder. One parallel was done with a reduced pressure, as can be seen in Figure 3.2.6. Here, the aim was to see if there was a difference in the precursors when one sintering driver was drastically reduced. The pressure was set to 3.3MPa, which corresponds to a load of 2kN when using a die with an inner diameter of 28mm. 3.3kN is the minimum pressure on the SPS instrument used. A lower pressure than that would not give sufficient contact between the graphite die and the electrodes where the pulsed current is sent through.
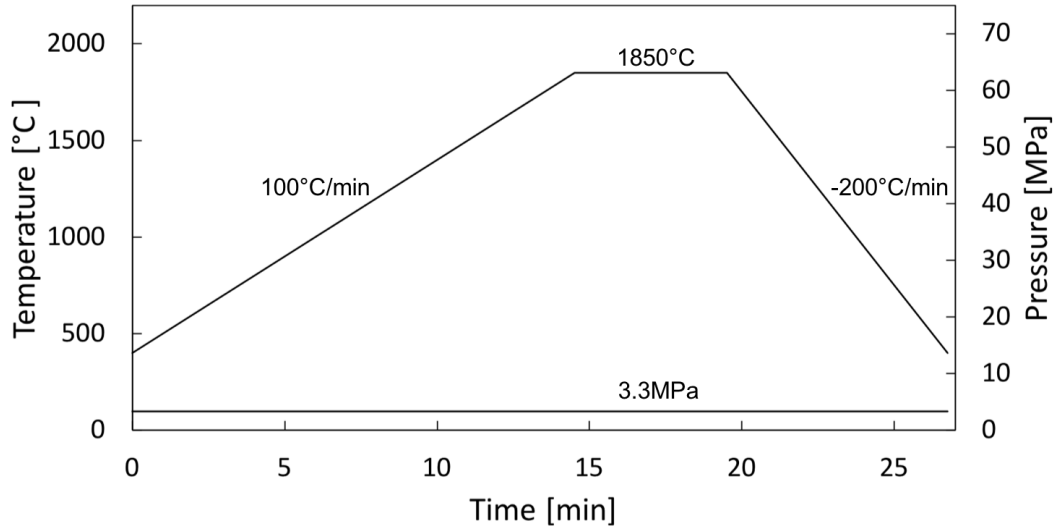
Figure 3.2.6: Time - temperature - pressure profile used for SPS of SiC - powders with different carbon sources. Here the pressure was reduces from 50MPa to 3.3MPa to investigate the effects that had on the different precursors.

The sintering program was made before sintering and was thus automatic during sintering. A great advantage of SPS, like discussed in Section 2.3.2, is that various sintering parameters can be observed and monitored during sintering. This was utilized to investigate what happens to the different carbon sources when reacting with silica on the surface of SiC particles at around 1500°C. Here, looking at changes in vacuum (i.e. how much gas is released) with regards to time was of interest. To get a more detailed view of what was happening during sintering, the heating rate was set to 100 °per minute for all the samples. The cooling rate was just set to 200 °per minute although there is only natural cooling happening and that takes significantly longer time that heating. The system was cooled down to around 300 °C before the sintered body was removed from the die using a uniaxial press.

3.2.5 Density measurements

Density, open porosity and closed porosity are all parameters that were found using Archimedes' principle. The bulk density is a direct result from the measurements whilst the relative density is based on the theoretical density of the precursor. Here, the theoretical density is assumed to be the density of silicon carbide, $3.21 g/cm^{-3}$. The approximation is that the additives are in such small amounts compared to silicon carbide

that it will not affect the overall density significantly. The equations used for calculations can be found in Appendix A. Isopropanol was used as immersion liquid for the density measurements. The weight of dry sample (m_1), immersed sample (m_2) and wet sample (m_3) were measured and used for calculations.

3.2.6 Surface polishing and etching

After sintering, the samples were micro blasted using walnut shells with a small grit size to remove the access graphite from the sintering process. When the surface was completely clean from graphite the samples, all in the shape of tablets, were placed in a mould, cast in epoxy resin and cured over night. The samples were then grinded and polished according to the polishing programme displayed in detail in Table 3.2.2. All the polishing steps were performed on Struers Tegrapol-31, an automatic polishing instrument. The first step in the programme were extended with an hour compared to the specialisation project by the same author [68], to ensure that the surface polished was in the bulk. The three first steps of the polishing programme were done on diamond disks with variable grit size using water as the lubricant. In between these steps, the samples and the samples holder were washed in distilled water. The three last steps were done using diamond suspensions with particle sizes of $9\mu m$, $3\mu m$ and $1\mu m$ respectively. In between these steps, the samples were put in an ultrasonic bath with ethanol to remove any remaining particles from the previous step. The sample holder was washed in distilled water between these steps as well.

Table 3.2.2: An overview of the different steps in the polishing routine used in this project. The sample holder speed was 150 rpm for every step and all the samples polished had a diameter of 28mm.

Step	Polishing disk	Lubricant	Time [min]	Force on single sample [N]	Disc rotation speed [rpm]
1	MD - Piano 80	Water	120	45	300
2	MD - Piano 220	Water	15	35	300
3	MD - Piano 1200	Water	15	20	300
4	MD - Allegro	DiaPro Allegro	15	15	150
5	MD - Dac	DiaPro Dac	10	10	150
6	MD - Nap	DiaPro Nap - B	5	10	150

After polishing, most of the epoxy was cut of using a Minitom, an automatic precision cut-off machine, to fit in the sample holders for XRD and SEM.

3.2.7 Scanning Electron Microscopy

Scanning electron microscope (SEM) was used to analyse the microstructure of the precursor powders and the sintered samples. Zeiss Supra FESEM 55 is the SEM unit used in this project. Different parameters was used for different purposes but mostly the acceleration voltage used was 5kV and the working distance was around 12.

3.2.8 Electron Backscatter Diffraction

Electron backscatter diffraction (EBSD) was used for characterisation of sintered samples. The samples were polished according to the polishing programme described in Section 3.2.6. Following the polishing was ion milling for an hour. A small section of the surface was bombarded with ions to clean the surface and improve the EBSD pattern. The online EBSD raw data collection was carried out on a Zeiss Supra FESEM 55 by using a NORDIF UF-420 EBSD acquisition detector. The NORDIF EBSD version 3 software was employed to acquire and stream the diffraction patterns directly offline. Calibration patterns were obtained and matched with silicon carbide 4H and 6H, which gave the highest match, namely confidence index. An EBSD pattern was obtained for magnifications of 200 and

400 for all three samples. A magnification of 400 gave a significantly higher confidence index than 200.

3.2.9 X-ray diffraction

X-ray diffraction was used to analyse phase composition. Pyrolysed carbon, precursor powders and sintered samples were scanned. D8 Advance DaVinci diffractometer operating with Bragg- Brentano geometry ($\Theta - 2\Theta$) was used to perform the scans. D8 Advance uses CuKα radiation (i.e. radiation with wavelength of 1.54 Å). The three precursor powders, the four various carbon sources and the sintered tablets, was analyzed together as the diffractometer has a multi-position sample holder. The pyrolysed carbon had to be placed on special sample holders where vacuum fat was used to keep the little carbon in place. The samples (carbon, precursor and sintered tablets) were scanned for 60 minutes with $2\theta = 10° - 80°$. Divergence slit of 0,2 mm was used for the scans.

Obtained patterns were later analyzed using the EVA software to identify the phase composition by comparison with patterns found in the International Centre for Diffraction Data (ICDD). Rietveld refinement was performed in TOPAS software [69] with the purpose of quantifying the amounts of compounds in the samples.

3.2.10 Fracture analysis

The fracture surface analysis was executed using the Zeiss Supra 55 PV field emission SEM, the same SEM instrument as used throughout the whole project. The samples, one from each precursor, were sintered using the program that gave the highest densities (i. e. using 50MPa as the sintering pressure). After sintering, the samples were simply broken into several pieces using a pointy chisel to provoke a natural fracture. One piece of each sample was then mounted on a SEM sample holder using a two sided tape. There was no need for coating due to silicon carbide having sufficient conducting properties. Settings on the SEM, like acceleration voltage, probe current and working distance, was chosen to obtain the sharpest images. However, these properties were similar in value to those explained for normal SEM analysis.

Chapter 4

Results

In the following chapter the results will be presented. They will come in order after experimental method used, but are sorted so that the methods used primarily on carbon sources are presented first, followed by results obtained on precursor powders and sintered bodies. It will be clearly stated whether pure carbon sources, precursor powders or sintered samples are the discussed item.

4.1 Carbon Sources

4.1.1 Thermogravimetric analysis (TGA)

All the carbon sources behaved as expected with regards to mass loss at increasing temperatures, as can be seen in Figure 4.1.1. Sucrose had the biggest mass loss out of the four investigated carbon sources, while carbon black had no mass loss. The resin used in this research project is originally in liquid form, but as a result from storing it in high temperature the water had evaporated before this experiment. That is worth mentioning as it will effect the result. Starch started off in liquid form, while sucrose and carbon black were both solid. Resin and starch have a very similar behavior apart from starch loosing more mass. Sucrose has a slow, but continuous mass drop until around 190 °C, where the mass decreases from 90 % to under 30 % in a short time interval. Resin and starch seem to be fairly stable during the dwelling time at 180 °C, before they also experience a rapid mass loss at around 190 °C, albeit less rapid than for

sucrose. All carbon sources became more or less stable with regards to mass at the end of the temperature program thus it can be said that all carbon sources (except carbon black) went through a pyrolysis and that the residues are pure carbon. No pyrolysis was expected for carbon black as that starts off as pure carbon. The slight drop in mass at the end might be caused by some oxygen in the system although great measure was taken to avoid that.
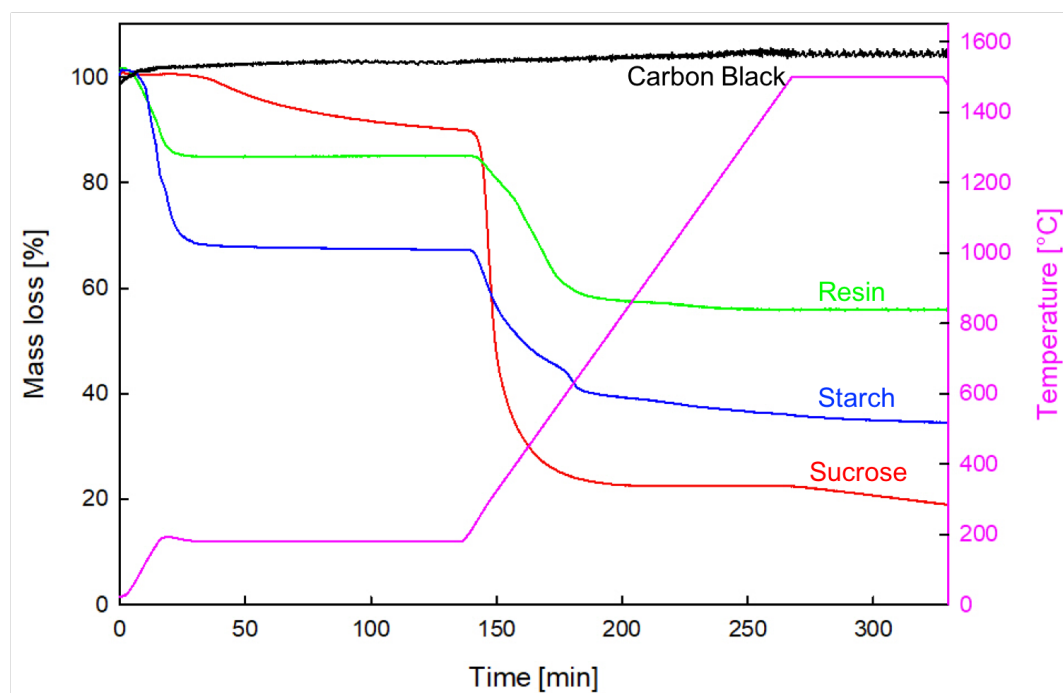
Figure 4.1.1: Results from the thermogravimetric analysis (TGA). Carbon black, resin, starch and sucrose are represented by the colours black, green, blue and red respectively. The magenta curve is the temperature program during the analysis. There were two holding times in the program; two hours at 180°C and one hour at 1500°C.

The exact mass loss is presented in Table 4.1.1. Here, it is clear that sucrose has the least carbon in it and resin has the most. This has, as mentioned before, been taken into account when producing the various powders so that by the time the reaction between silica and carbon starts, there are similar amounts of carbon present in the powder. This correlates well with the SPS curves presented below, where there is more gas evolution in the beginning of sintering with sucrose compared to resin, and that is due to less resin being added and less volatiles leaving resin in the first place.

Table 4.1.1: A tabulated overview of the residual carbon after pyrolysis at 1500 °C for an hour. It is assumed that everything left is pure carbon.

| Carbon source	Residual carbon [%]
Resin	56.4
Starch	34.7
Sucrose	19.1
Carbon Black	100

4.1.2 Raman Spectroscopy

An average of 5 spectra for each pyrolysed carbon sample is presented in Figure 4.1.2. The peaks occur at approximately the same shift for all carbon sources and the position is a match with the D peak and G peak in literature.
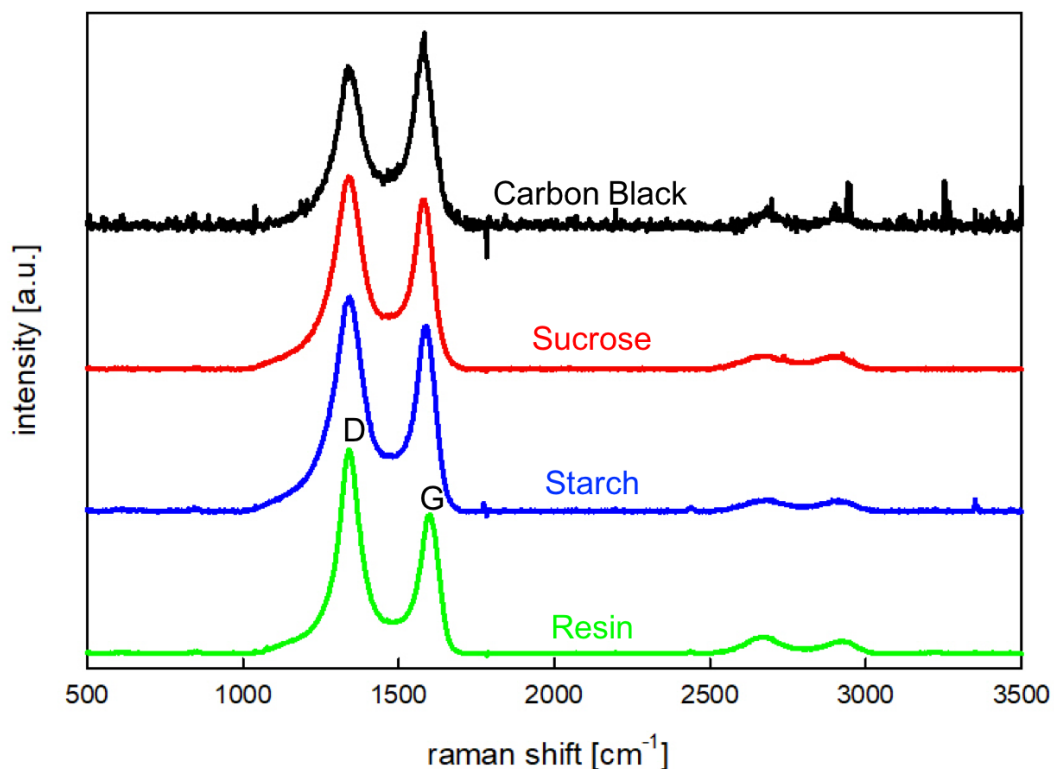
Figure 4.1.2: An average of 5 spectra for each pyrolysed carbon sample presented in a stacked plot. Carbon black experienced more noise due to having smaller particles. The D peak and G peak is clearly marked and is the same for all the samples.

For sintered bodies there are, as expected, observed peaks of higher intensities for silicon carbide. Figure 4.1.3 show the TO peak and the LO peak together with the above mentioned peaks. The TO peak stems from the transverse optical mode of silicon carbide and it occurs when the vibrational mode and the optical mode is perpendicular on each other. The LO peak is the longitudinal optical mode of silicon carbide. This peak occurs from the vibrational mode being parallel to the optical mode. As with the pure carbon sources, the positions of the peaks match well with values from literature.
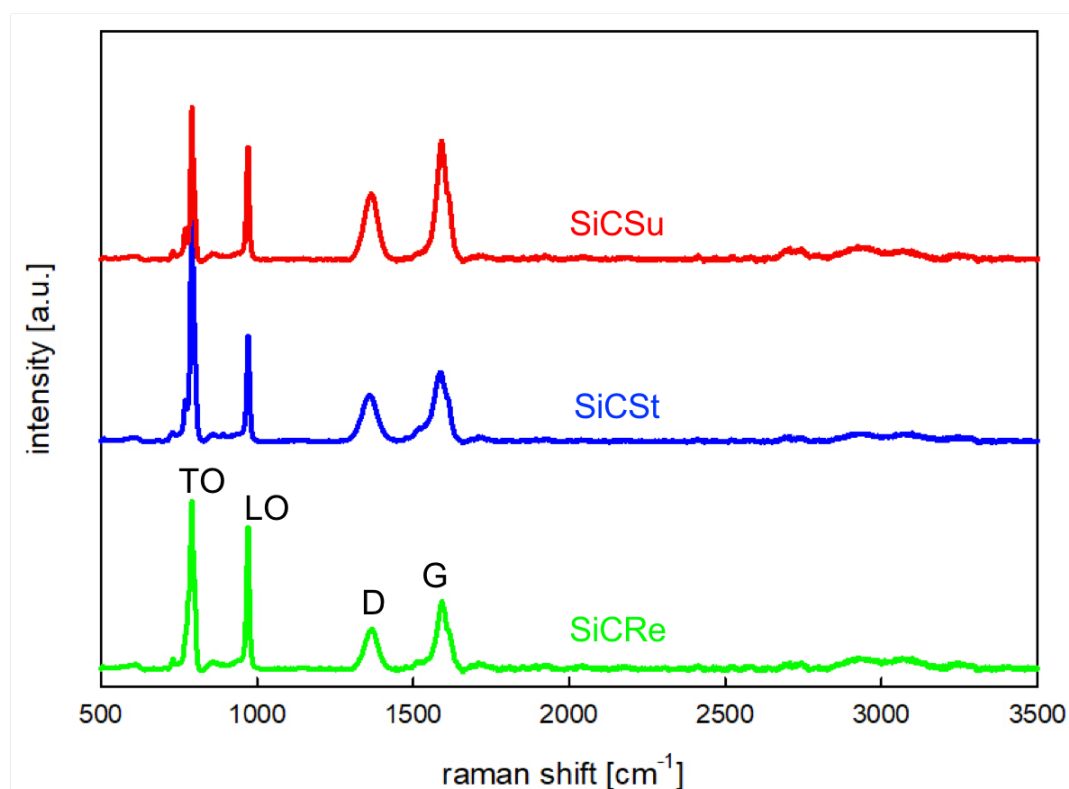
Figure 4.1.3: An average of 5 spectra for each sintered and polished sample presented in a stacked plot. All the samples have similar Raman spectra with the same characteristic peaks at the same positions. The most prominent and important peaks are marked clearly. D and G is the same as for the pure carbon sources. TO is the transverse optical mode of silicon carbide and LO is the longitudinal optical mode of silicon carbide.

A fitting of the carbon peaks, namely the D and G peak, was necessary in order to deconvolute the curves and find the ratio between the area under the curves. In this study the fitting was done according to the procedure developed by Brunetto et. al. although there are many different ways to go about this in literature. An illustration of

how the fitting was done can be found in Figure 4.1.4.
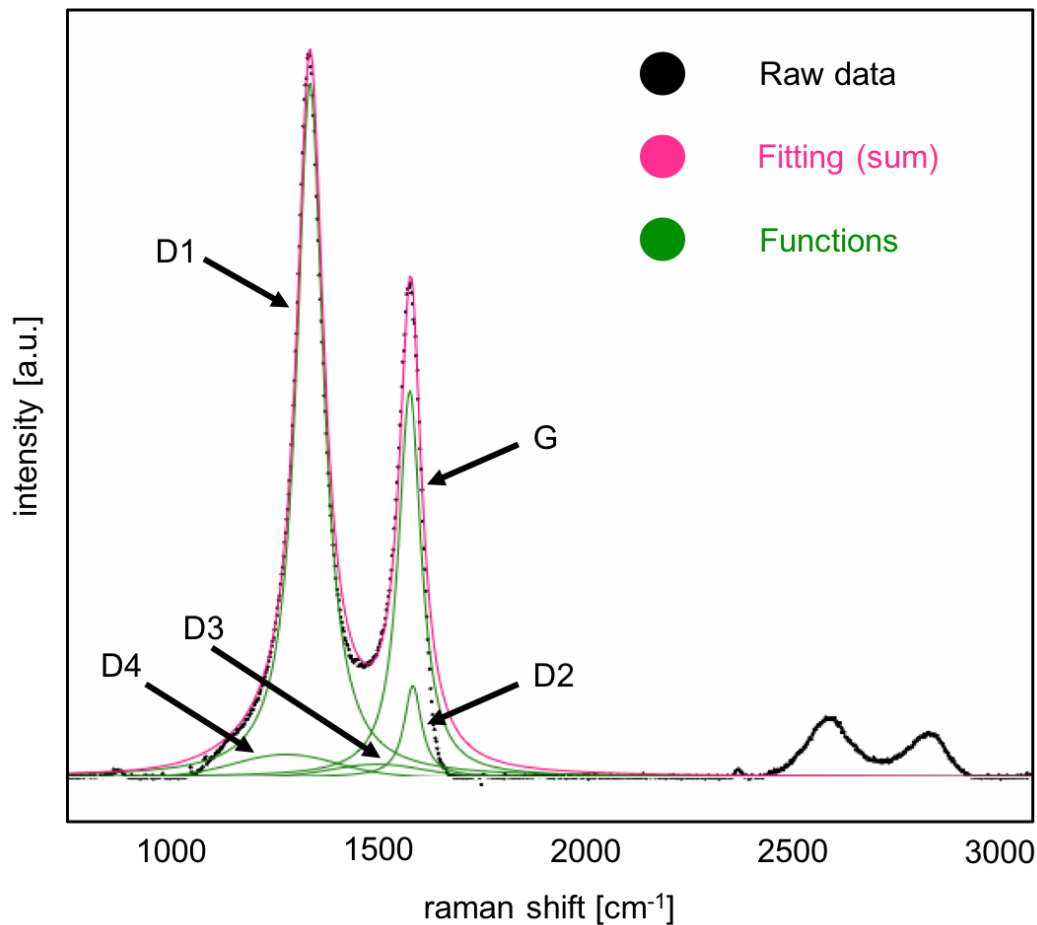
Figure 4.1.4: Illustration of the fitting done in Fityk software. The fitting is done following the procedure of Brunetto et. al. [40]. The black dotted line represents the raw data file, the pink line is the sum of all the functions used to get a fitting and the green curves are all the single functions. The three peaks marked G, D1 and D2 are fitted using Lorentzian curves whilst the peaks marked D3 and D4 are fitted with Gaussian curves. Here, the focus was to fit the carbon peaks, hence the 1000 - 2000 range in raman shift.

Following the fitting was calculating the ratio between the area underneath the D peak and the G peak. The result from doing so can be seen in Figure 4.1.5. The three main carbon sources investigated here, namely resin, starch and sucrose, all have a similar ratio between the area under the D peak and the G peak. This indicates that they all have a similar reactivity after pyrolysis. The biggest deviation in ratio is for carbon black, which is the only carbon source out of the four with more graphite-like carbon than diamond-like carbon, hence a ration below zero. For the sintered bodies, a lower ratio is

observed for all precursors, but the trend between them are still the same where starch has the most diamond-like structure.
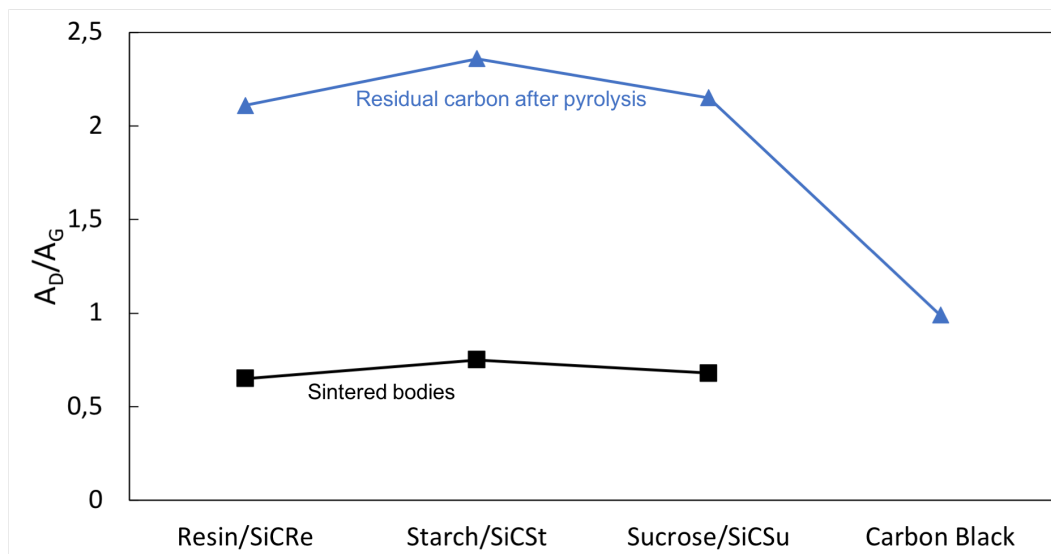
Figure 4.1.5: An overview of the ratio between the D peak and the G peak from Raman spectroscopy. The blue curve with triangles represent the residual carbon after pyrolysis (after TGA) and the black curve with squares represent sintered samples that were polished beforehand to ensure bulk properties.

More details about the features of pure carbon sources and sintered bodies found from raman spectroscopy, can be seen in Appendix B.

4.2 Precursor powders and sintered samples

4.2.1 Spark Plasma Sintering

Spark plasma sintering (SPS) was the only sintering technique used in this study. The sintering program was made with the aim to get the highest possible densities. With SPS, vacuum, temperature, pressure and compression can be monitored closely. Figure 4.2.1 show an example of the information obtained from the sintering, here SiCRe. The same plots for SiCSt and SiCSu, as well as plots for all precursors using a lower sintering pressure, can be found in Appendix B.

In Figure 4.2.1 the magenta curve represent the vacuum in the sintering chamber during sintering. The green curve is the sintering, or compression curve. Due to the setup of

the system, compression is here an increase in the curve. For example after around 14 minutes carbon starts to react with silica on the surface of the SiC particles (as can be seen by the CO gas peak), and then an immediate sintering starts. The red curve is the temperature, and the heating rate is here, as for all the sintering, $100°Cmin^{-1}$.
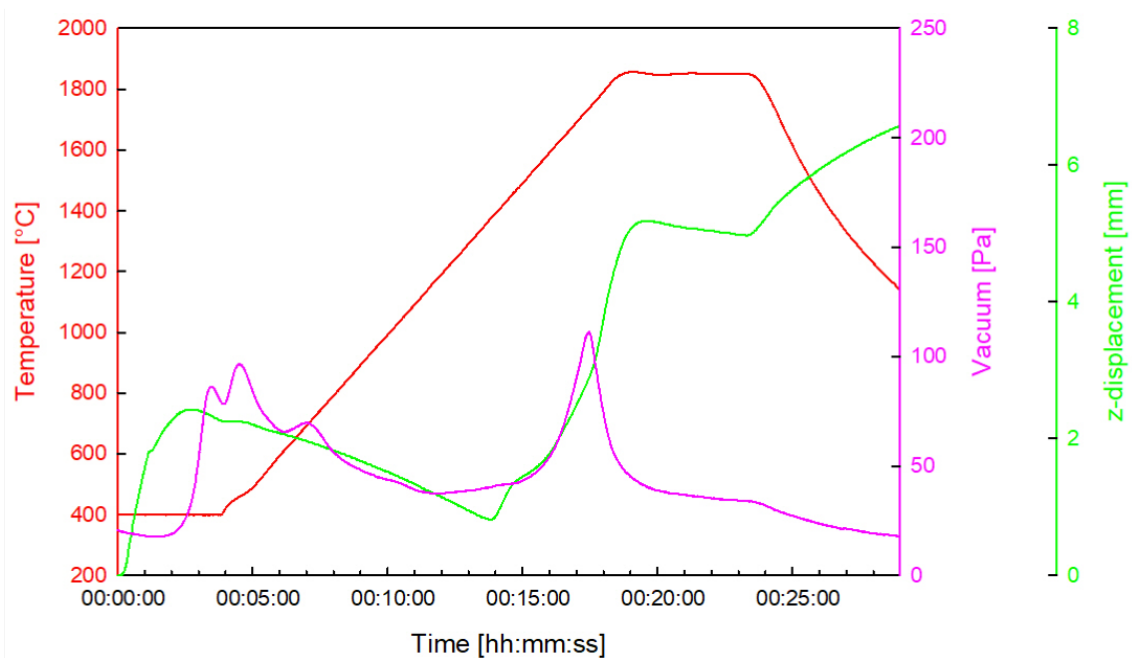

Figure 4.2.1: An overview of the sintering of SiCRe. The curve in magenta is the vacuum in the sintering chamber, the green curve is the sintering curve (or compression) and an increase here is compression. The red curve is the temperature profile.

At the beginning there are some gas evolution, as can be seen from the vacuum curve. This is mostly volatiles from the carbon source, as is also observed during TGA. What is really of interest on the vacuum curve, however, is the peak caused by CO gas being produced as a result from the reaction between carbon and silica. Figure 4.2.2 show a comparison of the CO gas evolution occurring around 1500 °C for samples sintered with a sintering pressure of 50MPa. When using a sintering pressure of 3.3MPa, the vacuum curve looked slightly different, as can be seen in Figure 4.2.3. In both figures, SiCRe, SiCSt and SiCSu is represented by the respective colours; green, blue and red. When using a high sintering pressure the vacuum curves look similar for all precursor powders. With a lower sintering pressure, however, there are more variations and resin looks like the most reactive carbon source. For higher sintering pressures the difference is insignificant.
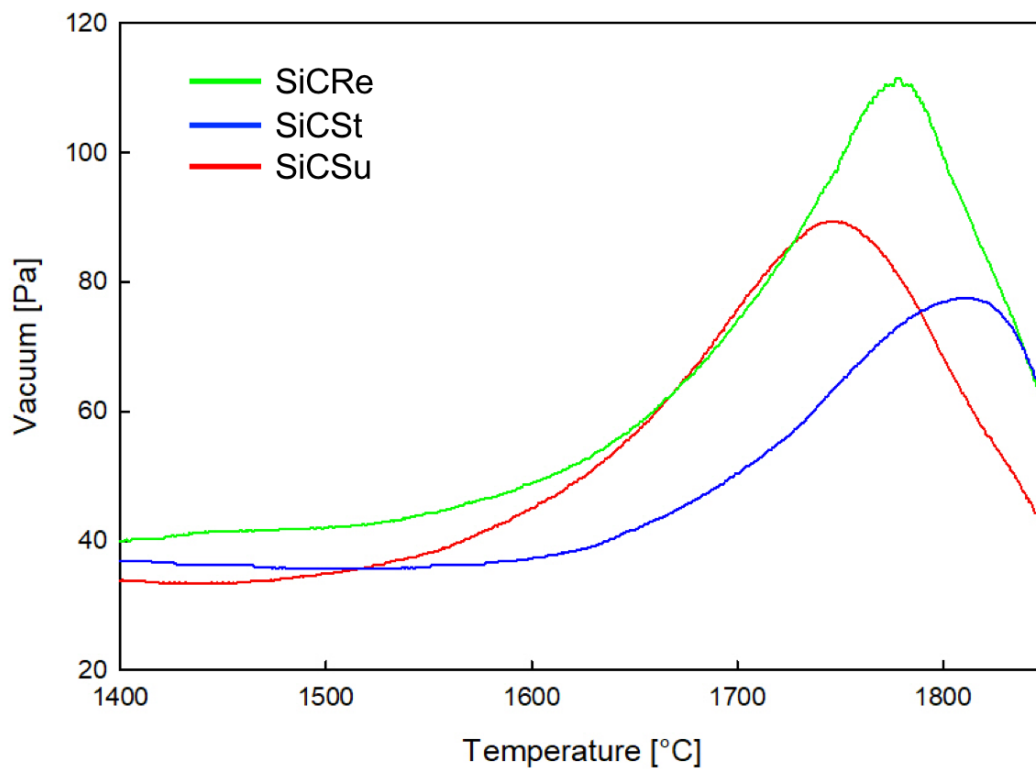
Figure 4.2.2: Comparison of the vacuum curve during sintering with a sintering pressure of 50MPa. This peak arises from the evolution of CO gas from the reaction between carbon and silica.
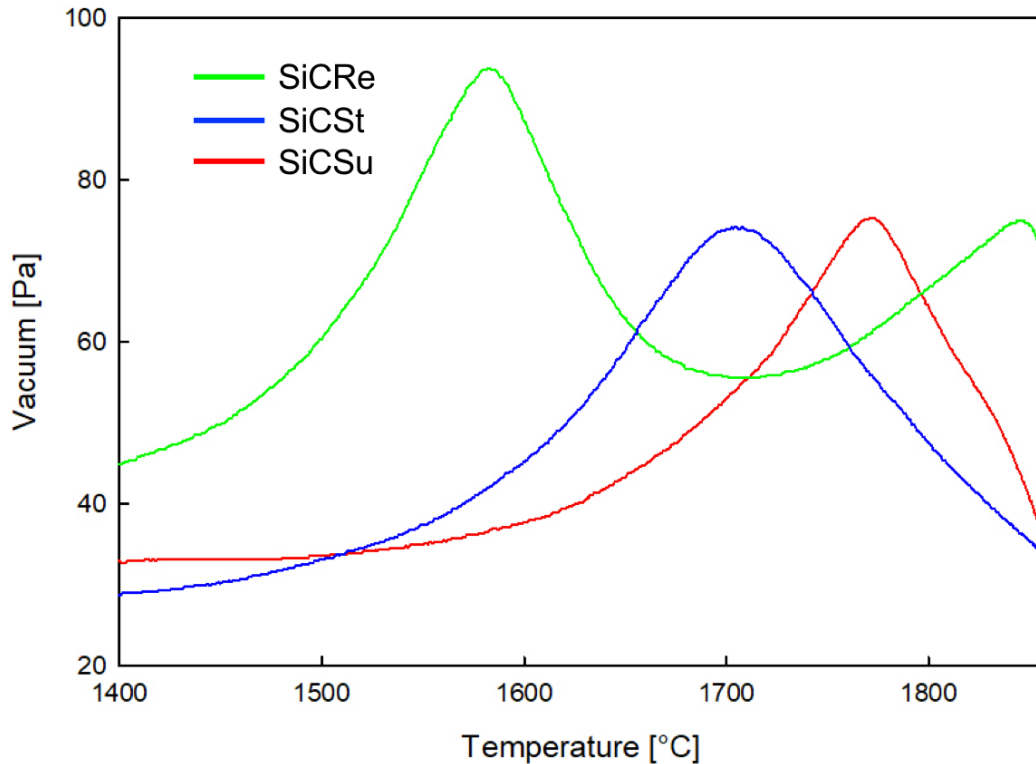
Figure 4.2.3: Comparison of the vacuum curve during sintering with a sintering pressure of 3.3MPa. This peak arises from the evolution of CO gas from the reaction between carbon and silica.

The densification started right after the silica was removed from the surface of the particles, as seen in Figure 4.2.1. The densification curve for all the precursor powders are compared in Figure 4.2.4, where densification equals a decrease in the sintering curve. The displacement cannot be compared directly as that is influenced by the amount of powder in the die, but when sintering starts and how fast it happens is comparable. The sintering look similar for all precursors with densification starting after around 14 minutes which corresponds to around 1400°C. It is clear that removal of silica on the surface of the SiC particles is necessary in order to start sintering. The expansion in the beginning and and at the end is due to the nature of the graphite die. SiCSt has a less steep sintering curve (densification curve) than the other two precursors without that affecting the density. As presented in the following section, the density is fairly similar for all the samples confirming the similar sintering curves.
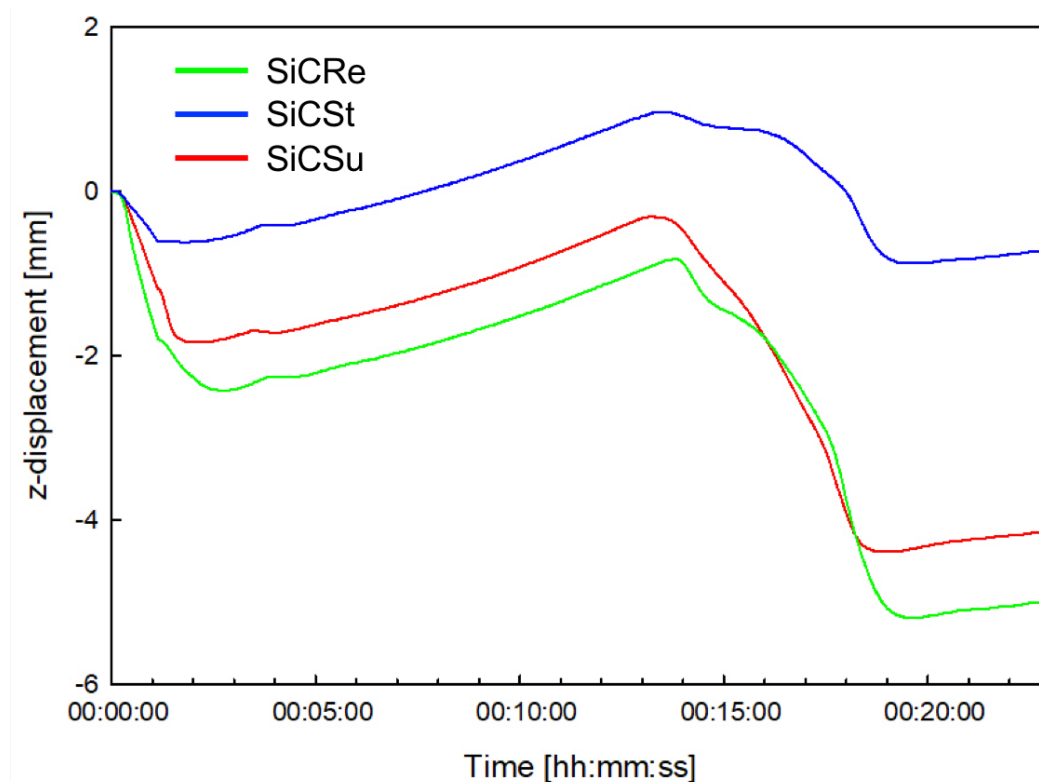
Figure 4.2.4: Comparison of the densification curve for the three different precursors. Sintering pressure here was 50MPa.

4.2.2 Density measurements

The three samples with the low sintering pressure was used, together with a random series of the samples sintered at 50MPa, just to illustrate the difference, found in Figure 4.2.5. All parallels using a sintering pressure of 50MPa had a fairly similar density, as can be seen in Appendix B.

Density measurements, using Archimedes' principle, show that there is not a big difference in density with different carbon sources as sintering additive. Figure 4.2.5 show high densities for all samples where a high pressure (here 50MPa) has been used during sintering. A density above 98% of theoretical density was obtained for all precursor powders. The highest density was observed for SiCRe with an average of 3.18 gcm^{-3} followed by SiCSt and SiCSu with 3.16 gcm^{-3} and 3.15 gcm^{-3} as an average, respectively. When lowering the sintering pressure (i.e. lowering one strong driver for sintering) a larger deviation was observed, also illustrated in Figure 4.2.5. All the precursors had a lower density resulting from a lower sintering pressure, but SiCSu indicates the need for strong

sintering drivers more than the other to precursors.
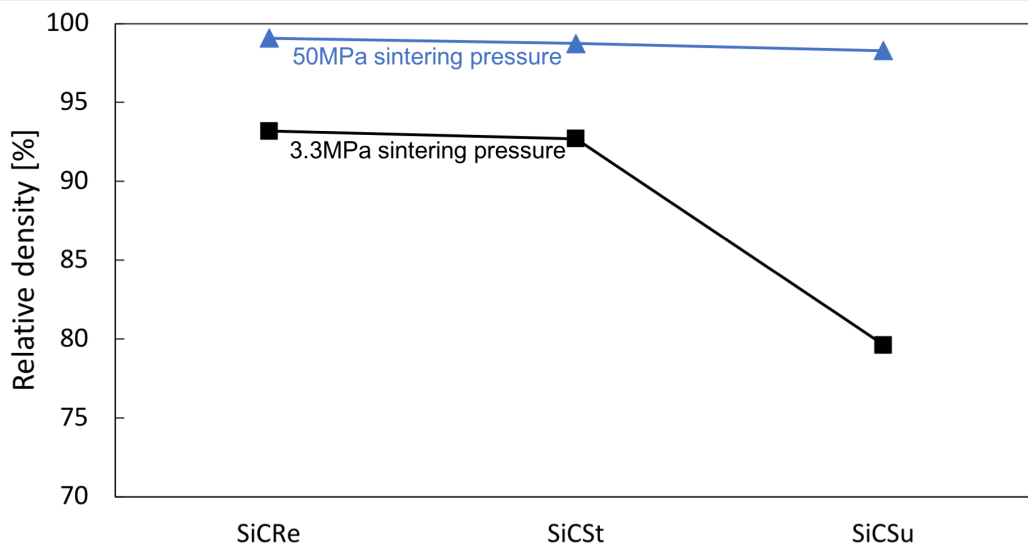
Figure 4.2.5: An illustration of the difference in relative density between using a sintering pressure of 50MPa and 3.3MPa. 50MPa is marked with a blue line whilst 3.3MPa is black.

As seen in Figure 4.2.6, the total porosity was lowest for the sintered body with resin as the carbon source. That was also the only sample with higher open porosity than closed porosity.
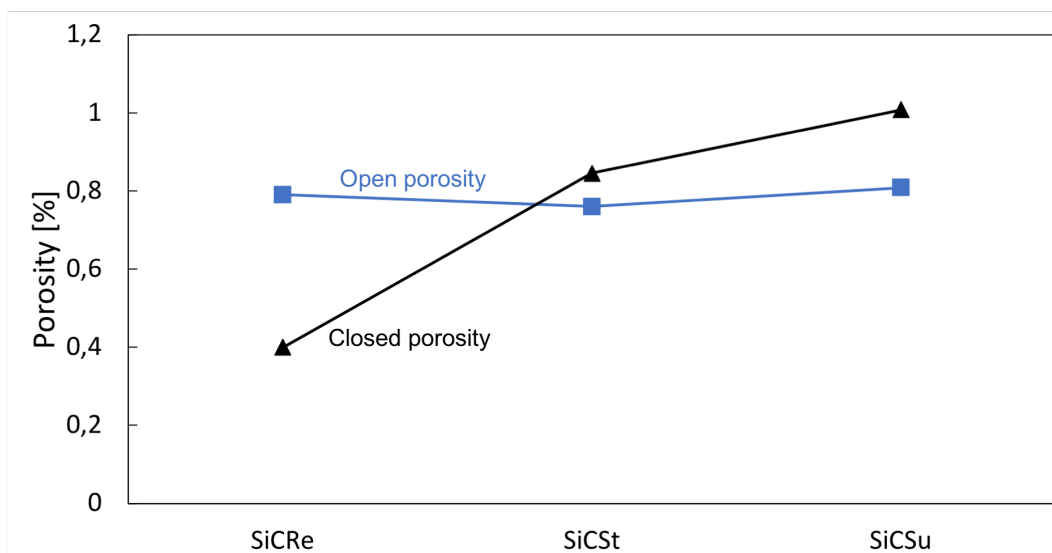
Figure 4.2.6: An illustration of the difference between open (blue line) and closed (black line) porosity for the various samples.

4.2.3   Microstructure

The microstructure of the sintered samples were investigated in SEM, using secondary electron mode, and the images are presented in Figure 4.2.7 with two magnifications (400x and 6000x) for each sample. The first obvious observation here is that the amount of black spots increase from using resin as a carbon source, to starch and then sucrose. It is hard to say if the black spots are pores or carbon, but they are assumed to be pores as they increase in amount with a decrease in density. There are also some black spots that have a different shape, looking thin and curved. This feature become more prominent at the higher magnification. The limps on the surface in the light grey colour are assumed to be result of the ion milling as the bombardment of ions can be a rough treatment. A slight outline of the grain boundaries can be seen at the higher magnification, but they are more clear after etching, as can be seen below.

(a) SiCRe, 400x

(b) SiCRe, 6000x

(c) SiCSt, 400x

(d) SiCSt, 6000x

(e) SiCSu, 400x
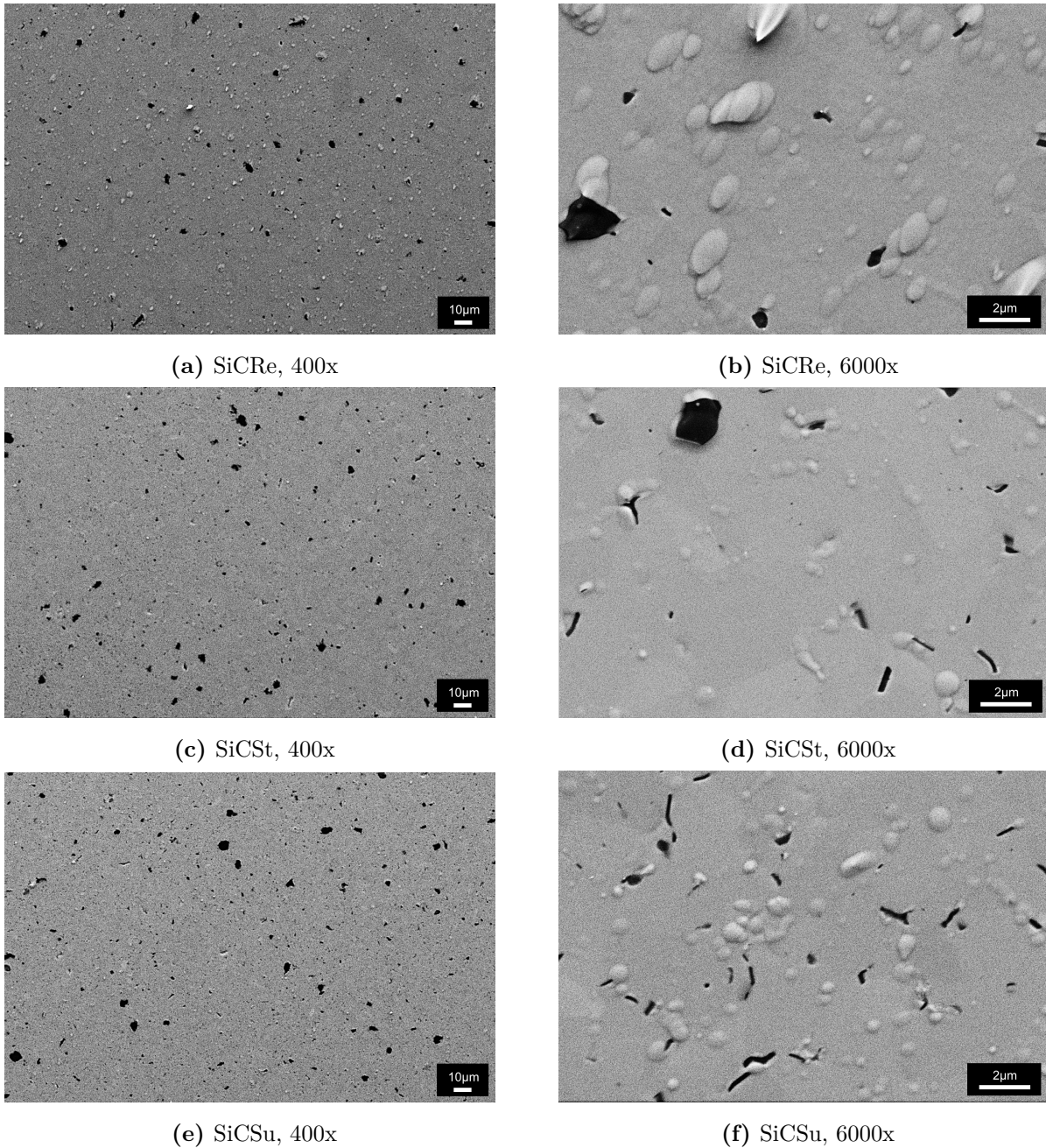
(f) SiCSu, 6000x

Figure 4.2.7: SEM images of sintered, polished and ion milled samples. The top two pictures are of SiCRe, the middle two are SiCSt and the bottom two are SiCSu, all represented with two different magnifications; 400x and 6000x. All pictures are taken in SE mode.

Sintered and polished sampled were etched by Fiven Norge AS. The etched sampeld were then investigated in SEM and the result is found in Figure 4.2.8. Each sample is represented with two different magnifications; 400x and 2000x. Looking at the overview at the lowest magnification, the increase in pores from using resin as the carbon source

to using sucrose, is evident. At the higher magnification, the grain boundaries are clear and the grain size is variable. For SiCRe the grain size is in a range of 2-10μm, while for SiCSt the grains look slightly smaller, in the range of 1-5μm. SiCSu has grains in the same size range as SiCRe. There is however a difference in the shape of the grains. SiCSu have large elongated grains, while SiCRe and SiCSt are more similar with far less anisotropic grain growth.

(a) SiCRe etched, 400x

(b) SiCRe etched, 2000x

(c) SiCSt etched, 400x

(d) SiCSt etched, 2000x

(e) SiCSu etched, 400x

(f) SiCSu etched, 2000x
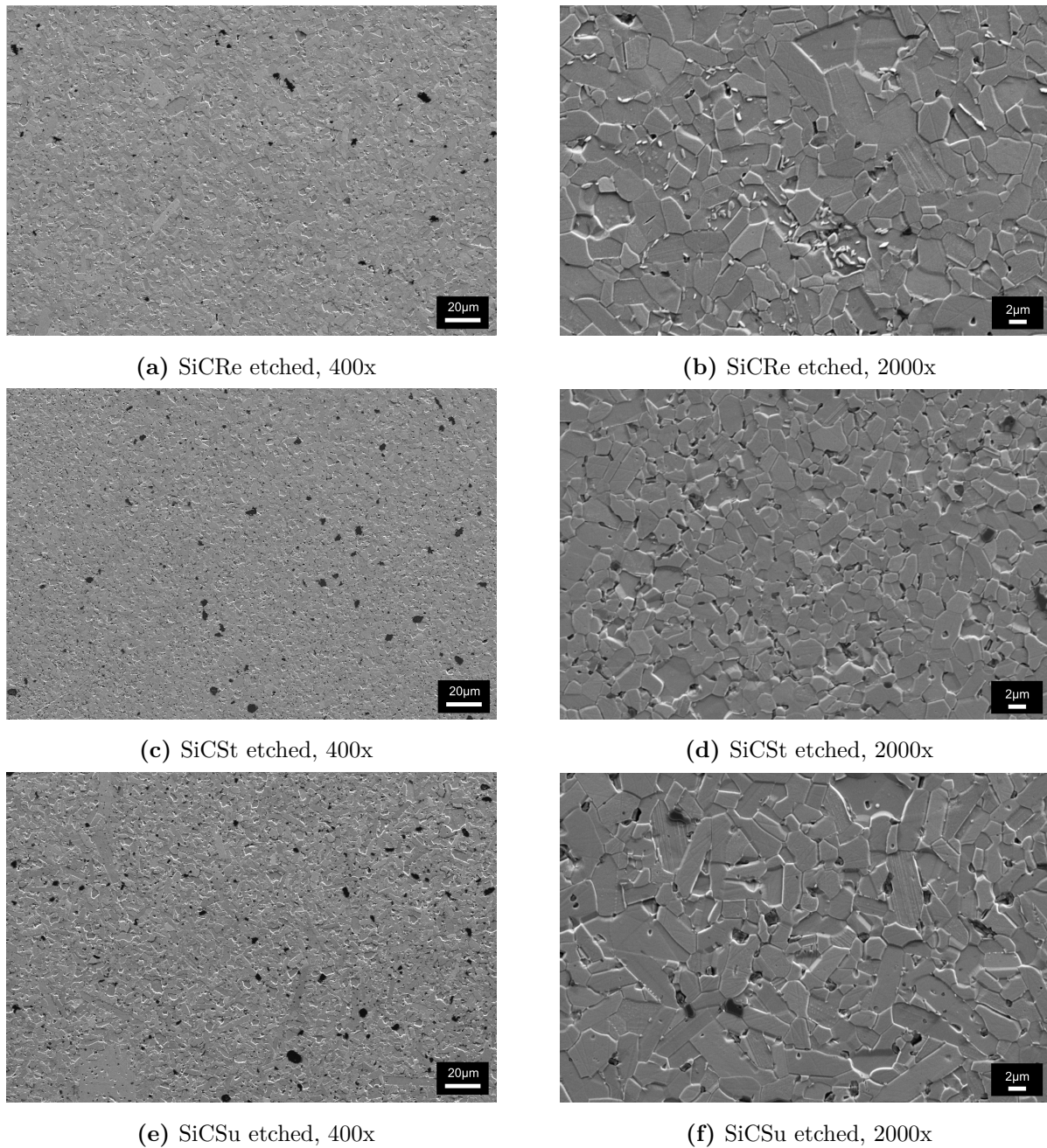
Figure 4.2.8: SEM images of sintered, polished and etched tablets. The etching was done by Fiven Norge AS. The images to the left, a), c) and e) are taken at a lower magnification than the ones to the right, b), d) and f). The magnifications used are 400x and 2000x, respectively. All images are taken using SE mode.

4.2.4 Fracture Analysis

SEM images of the fracture surfaces can be found in Figure 4.2.9. To the blunt eye, all the fracture surfaces showed evidence of a brittle fracture. There is no sign of any neck

forming. Figure 4.2.9a show the fracture surface of SiCRe which have some segments of smooth surface, but mostly looks rough. It is challenging to identify the grains which indicates transgranular fractures. The second image, Figure 4.2.9b, is the least smooth surface and it is even harder to distinguish between different grains here. Out of the three samples, SiCSt seem to have the highest degree of transgranular fractures. The bottom left image, Figure 4.2.9c, looks like something in between the other two samples in terms of fracture modes with a strong topography. The fracture mode is strongly dependent on the grain sizes and strain stresses. Smaller grains promote transgranular fractures, while larger grains promote intergranular fractures. Another factor that influence the fracture mode is homogenisation of the strain, which again correlates with grain size. The trend observed here is that SiCSt has the highest degree of transgranular fractures followed by SiCSu and SiCRe, although the difference is small. There is also some black spots observed on the fracture surfaces of all samples, which are most likely pores, but could possible also be carbon. SiCSu is the sample with the most black areas, and SiCRe is the one with the least, which strongly indicates that the black areas are indeed pores (the trend correlates well with the density trend).

The bottom right picture, Figure 4.2.9d, is taken at a very low magnification to get an idea of how the fractures look and to confirm that the fracture is very brittle.

(a) SiCRe fracture surface, 2k

(b) SiCSt fracture surface, 2k

(c) SiCSu fracture surface, 2k


(d) SiCSt fracture surface, low magnification
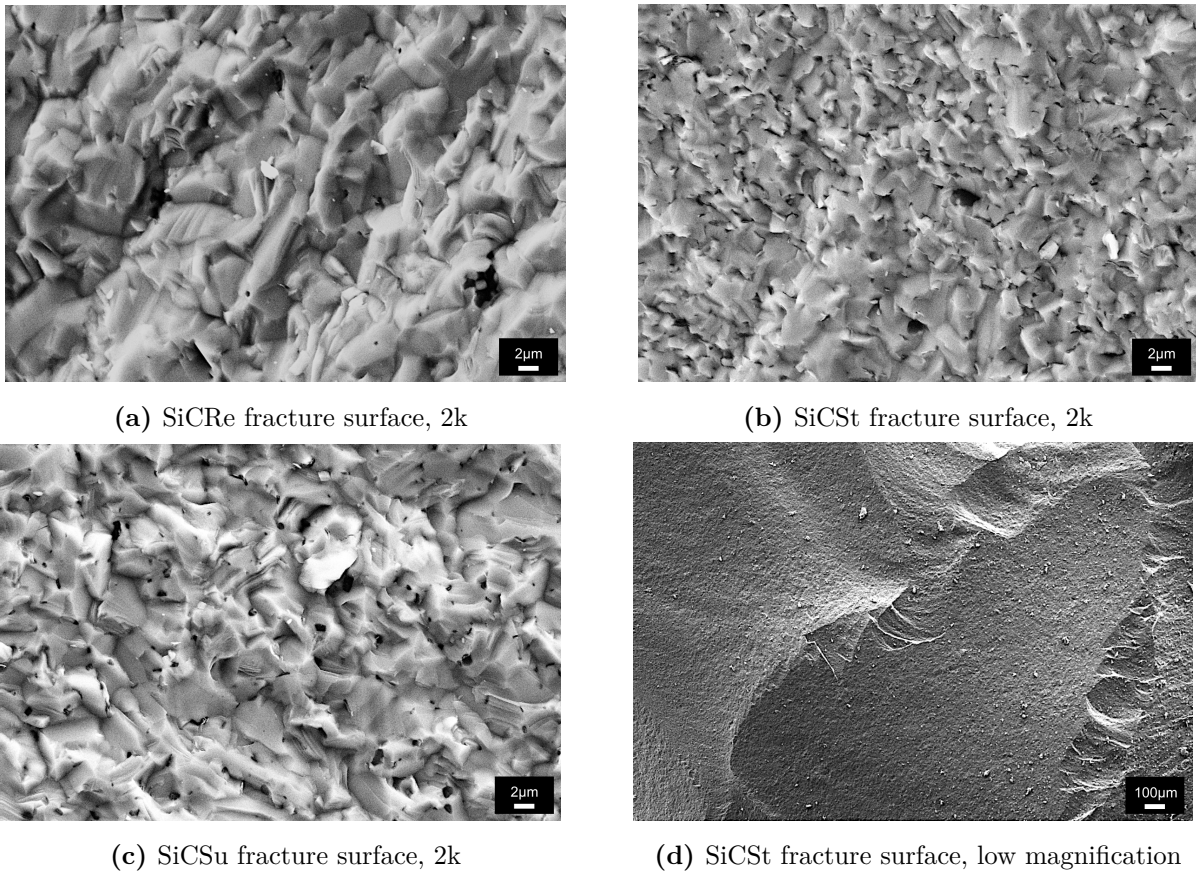
Figure 4.2.9: SEM images of fracture surfaces of sintered bodies using the three different precursors. The first three pictures show the fracture surface of SiCRe, SiCSt and SiCSu at a magnification of 2000x, and the last picture, d), is there to illustrate how a typical fracture surface looked at a low magnification, here using SiCSt as an example. All images are taken using SE mode.

4.2.5   Phase composition (XRD)

X-ray diffraction (XRD) diagram for precursor powders can be found in Figure 4.2.10. Figure 4.2.11 show the diffractograms of sintered samples using 50MPa as sintering pressure, hence the samples with the highest densities. When a lower sintering pressure was used, here 3.3MPa, a decrease in density was observed. The diffractograms for these samples are found in Figure 4.2.12. For all diffractograms, the circular symbol represents the 6H polytype of silicon carbide, the star symbol represent the 4H polytype and the 3C silicon carbide polytype and graphite is represented by a square and a triangle symbol respectively. Looking at the precursors there are no observation of graphite, as is confirmed by the numerical values tabulated in Table 4.2.1 that are calculated by

performing a Rietveld refinement in the TOPAS software [69]. All the precursors look similar in terms of position of the diffraction peaks. Fot he precursor powders, the composition is fairly similar apart from SiCRe having significantly more 4H polytype than the other two. It is difficult to distinguish between the different polytypes as they often have overlapping peaks.
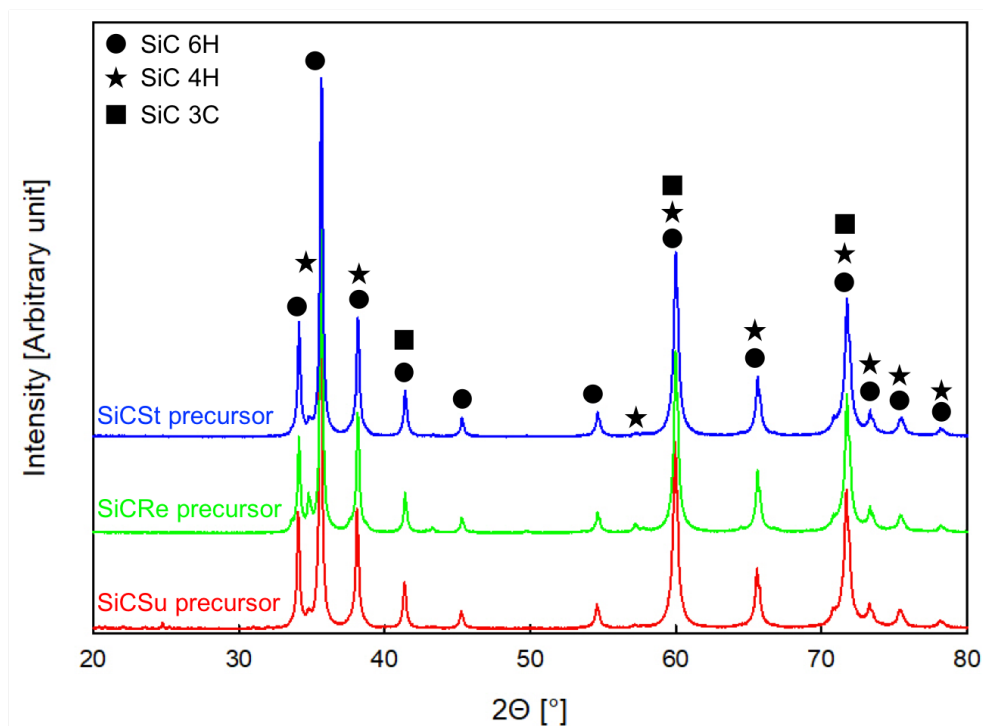
Figure 4.2.10: X-ray diffractogram for the three precursor powders. No graphite was observed here.
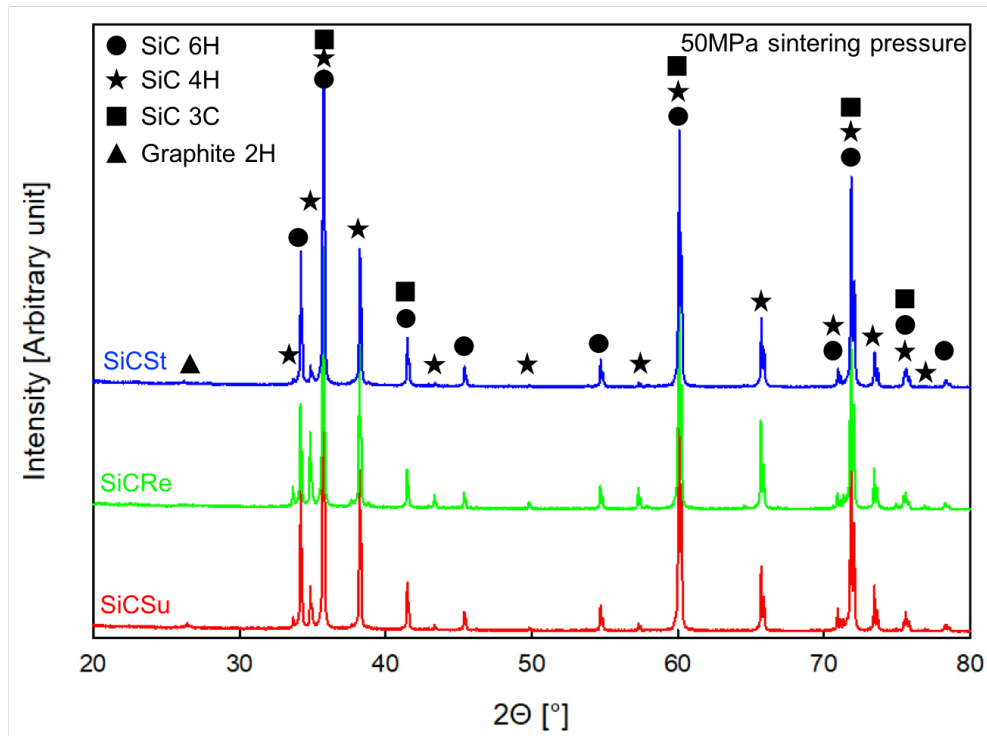
Figure 4.2.11: X-ray diffractogram for sintered samples using a sintering pressure of 50MPa (i.e. the samples with the highest densities).
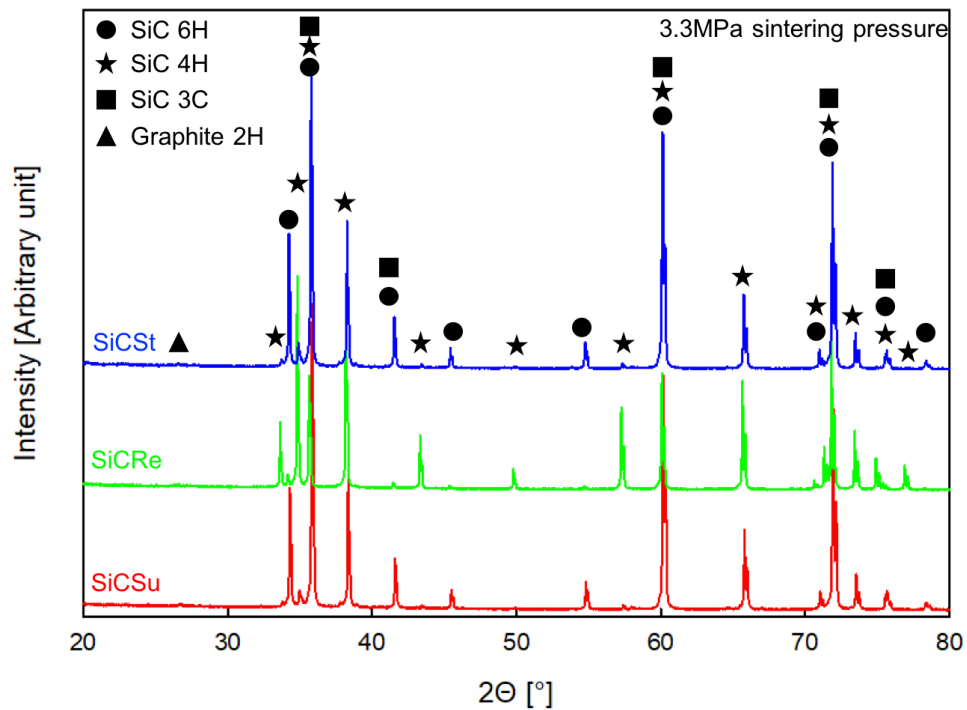
Figure 4.2.12: X-ray diffractogram for sintered samples using a sintering pressure of 3.3MPa (i.e. the samples with the lowest densities).

All the exact values for compositions found from the Rietvelt refinement are tabulated in Table 4.2.1. All the refinements had a rwp value around 20, which indicates a reasonable, but far from perfect fit. As mentioned, no graphite was found in the precursor powders. The precursor with starch and sucrose as the carbon source had very similar compositions where variations are within the margin of error. For the precursor with resin as the carbon source there is observed a significantly larger amount of 4H prior to sintering and a slightly larger amount of the 3C polytype than the other two precursors. The same trend is evident in the sintered samples where SiCRe has by far the most 4H when both using 3.3MPa and 50MPa as sintering pressure. Especially for the samples sintered with the lowest sintering pressure there is an enormous difference in the phase composition with SiCRe having over 91 % 4H while SiCSt and SiCSu only have around 11 %. For the samples sintered with 3.3MPa SiCSt and SiCSu have very similar compositions. The difference is bigger when the sintering pressure is higher. For a sintering pressure of 50MPa, SiCRe still has by far the most 4H present, but the amount is drastically reduced from that of 3.3MPa sintering pressure. There is also a bigger difference between SiCSt and SiCSu when the sintering pressure is higher. Then, SiCSt had more 6H, but SiCSu had more 4H, 3C and graphite. The amount of graphite varies with sintering pressure, except for SiCSt where the amount of graphite is fairly similar regardless of the pressure applied during sintering.

Table 4.2.1: Tabulated values from the Rietveld refinement done in TOPAS [69]. Rwp value was around 20 for all refinements.

Sample	SiC 6H [wt%]	SiC 4H [wt%]	SiC 3C [wt%]	Graphite 2H [wt%]
Precursor SiCRe	79.95	17.97	2.05	0.04
Precursor SiCSt	90.71	7.52	1.74	0.03
Precursor SiCSu	90.21	8.20	1.55	0.05
SiCRe 3MPa	5.52	91.05	0.68	2.75
SiCSt 3MPa	82.18	11.73	4.66	1.43
SiCSu 3MPa	82.39	11.21	4.21	2.18
SiCRe 50MPa	69.43	27.91	1.91	0.75
SiCSt 50MPa	82.46	11.51	4.09	1.93
SiCSu 50MPa	75.53	13.05	9.12	2.30

The X-ray diffractogram of pyrolysed carbon can be found in Figure 4.2.13. The peaks here are graphite, so this confirms the graphitisation of the carbon sources after being subjected to elevated temperatures.
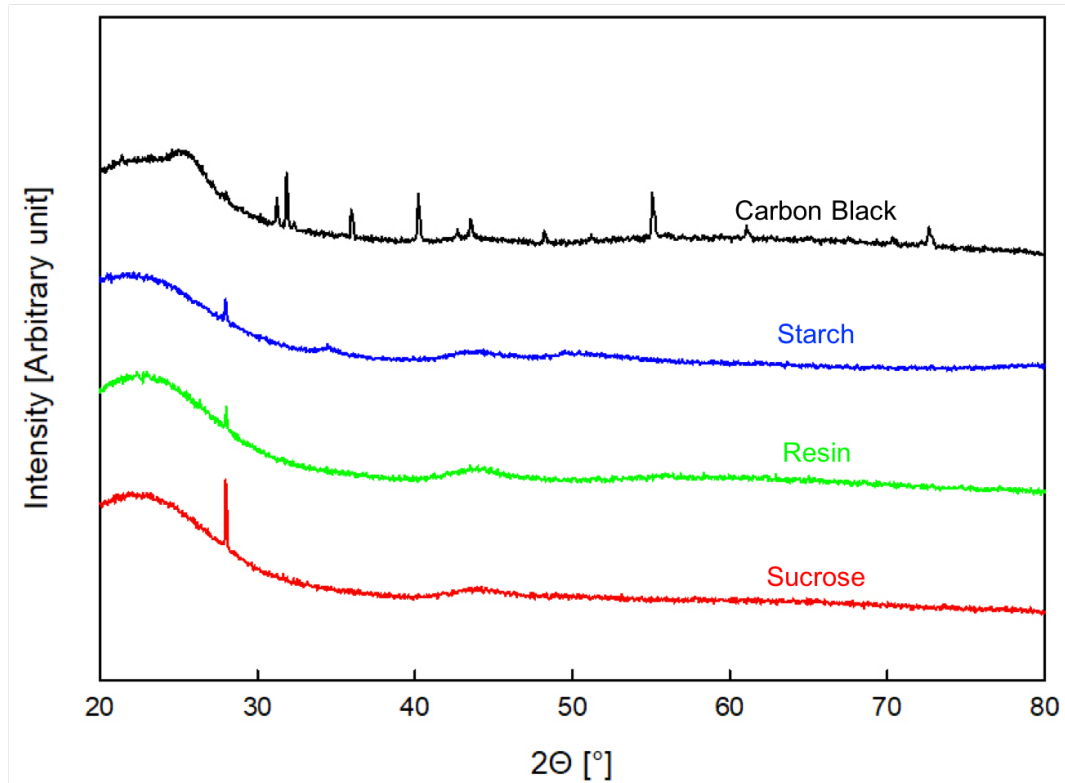

Figure 4.2.13: X-ray diffractogram of carbon sources after pyrolysis at 1500 °C for an hour. It is here assumed that the samples contain only carbon and that the peaks showing on the diffractogram stems from graphite due to its crystalinity.

4.2.6   EBSD

Figure 4.2.14 show the inverse pole figures of SiCRe, SiCSt and SiCSu, respectively. For the offline analysis, a confidence index is given to indicate the performance of the fit. For silicon carbide it was hard to find a good fit and a lower confidence index then what is normally required (when working with for example metals) was tolerated. However, the same analysis has been done for all samples so for comparability, this study is valid. SiCRe have the most abnormal growth here with some elongated grains in the size of around 40 μm. The areas scanned here are small and can not be considered a true picture of the whole sample so SiCSt and SiCSu might have abnormal grain growth elsewhere on the sample. SiCSt have small grains in the whole area scanned with no particular anisotropic

growth observed. All the grains are in the size region of 1 μm to 5 μm. For SiCSu there are more observed anisotropic grain growth with some grains in the size of up to 10 μm, but the quality of the pattern is also the worst for this sample. No preferred orientation is seen for any of the samples.
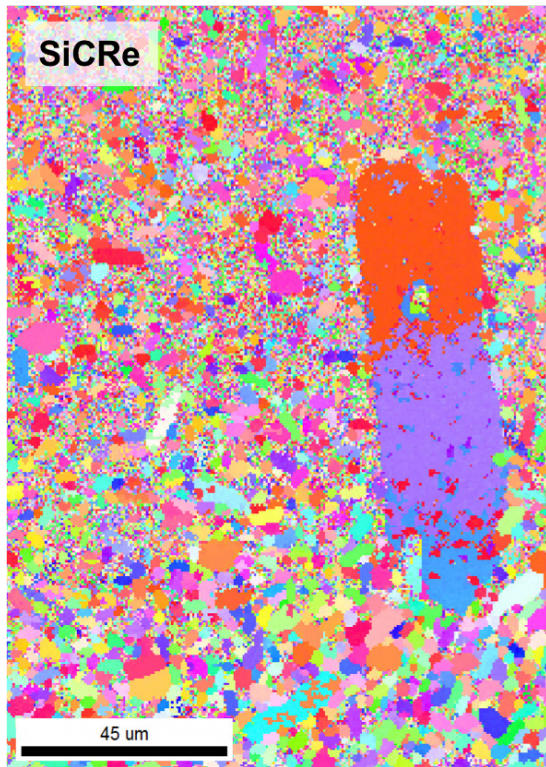
(a) SiCRe, inverse pole figure (IPF)
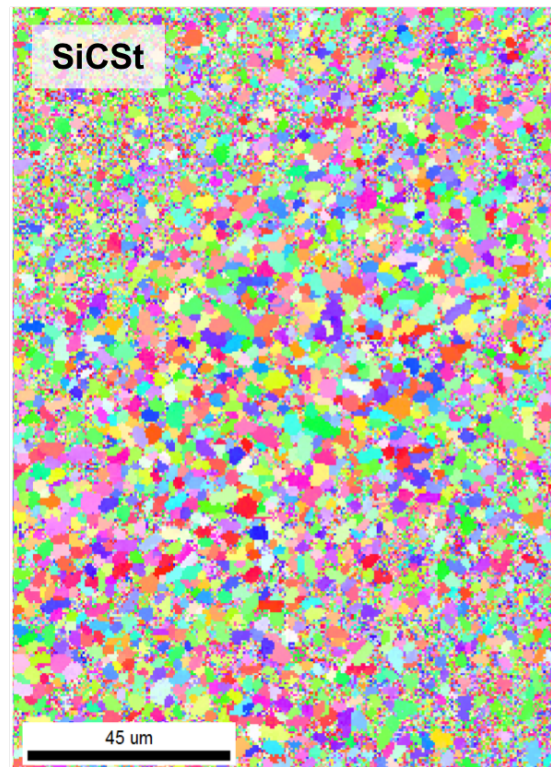
(b) SiCSt, inverse pole figure (IPF)
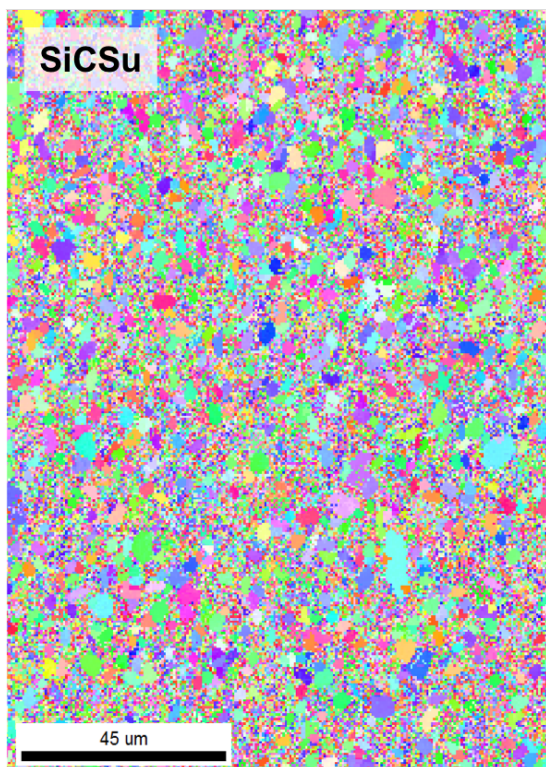
(c) SiCSu, inverse pole figure (IPF)
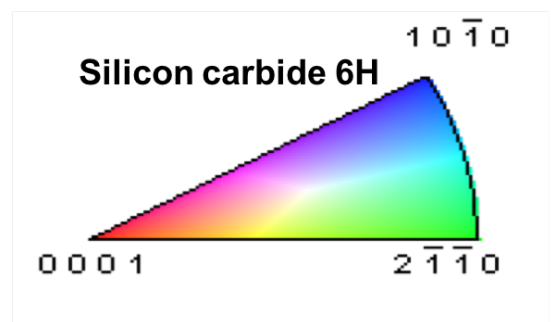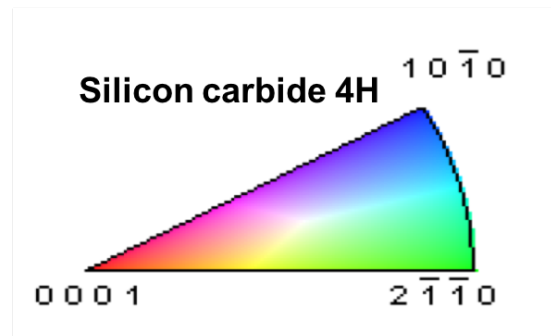
(d) Colour representation of grain direction.

Figure 4.2.14: Inverse pole figure (IPF) for three variable sintered samples. The colours change with direction of the grain; red is the [0001] direction out of the plane, while blue is [10$\bar{1}$0] and green [2$\bar{1}\bar{1}$0], the latter two directions being in-plane.

71

The average grain size for the EDSB maps was calculated by the software and is presented in Table 4.2.2. From this, SiCSu has the largest grain size and SiCRe and SiCSt are almost identical.

Table 4.2.2: Average grain size calculated by the EBSD software. The calculation is done by using the patterns from Figure 4.2.14.

Sample	Average grain size [μm]
SiCRe	2.79
SiCSt	2.75
SiCSu	3.77

The distribution of phases can be found in Figure 4.2.15. An assumption was made that there is only two phases present, namely 4H and 6H. Here, 4H is represented by the colour green and 6H is represented by the colour red. These phase maps are generated fro the exact same area as the inverse pole figures in Figure 4.2.14. The largest grains in the SiCRe sample are 6H whilst for the rest of the sample the largest grains seem to be the 4H polytype. SiCSt have a prominent amount of 4H structure and SiCSu have an even distribution for the blunt eye.

(a) SiCRe

(b) SiCSt

(c) SiCSu
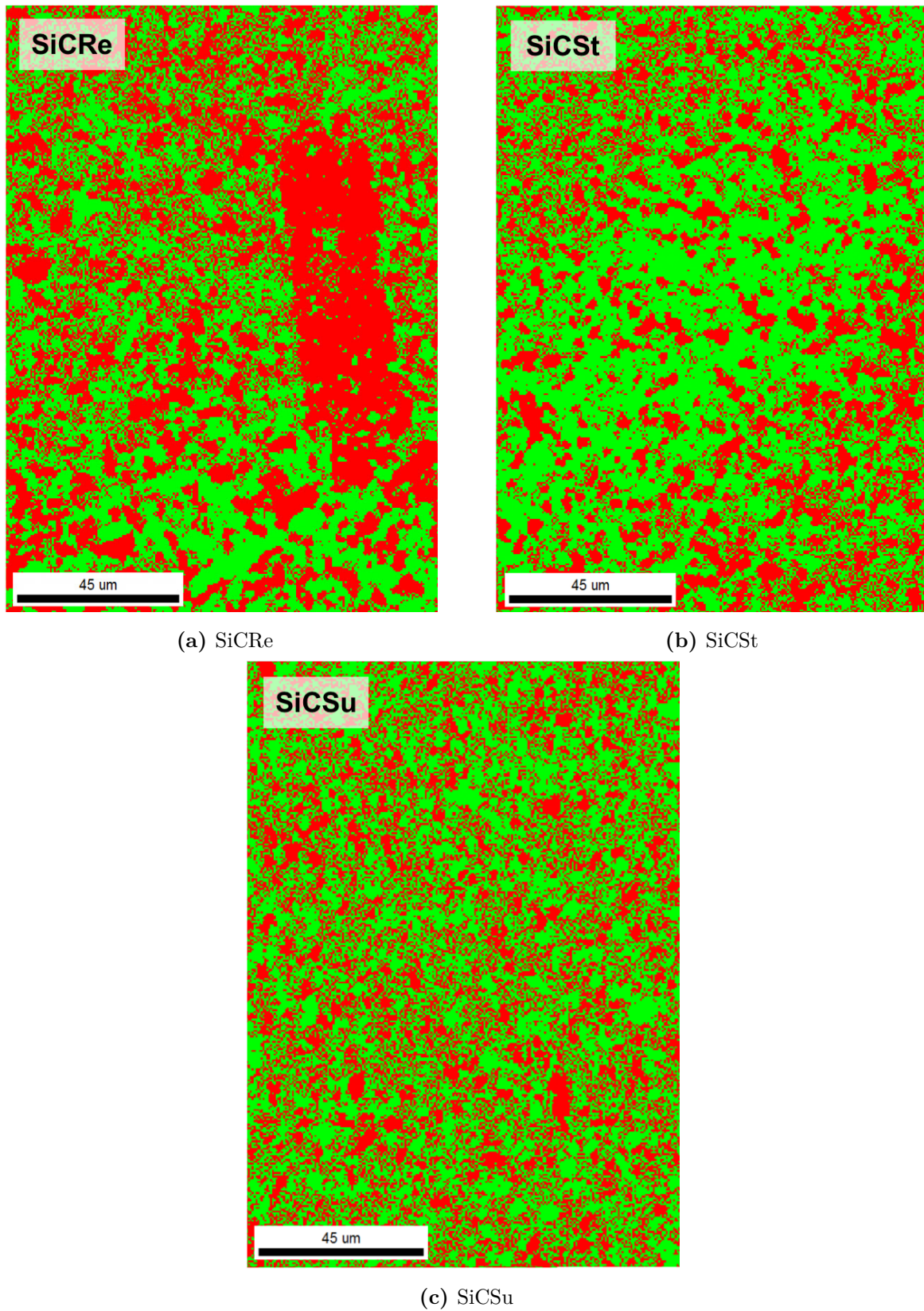
Figure 4.2.15: Phase maps for the three different sintered samples generated from the same area as the IPF.

Table 4.2.3 shows the amounts of the two SiC polytypes, 6H and 4H, calculated by the EBSD software. The calculated area is the same as the areas used for the IPF and phase maps seen in Figure 4.2.14 and 4.2.15.

Table 4.2.3: Numerical values for the phase composition calculated using the EBSD software. The area used for calculations is the same as for the inverse pole figures and the phase maps found using EBSD.

Sample	SiC 6H [%]	SiC 4H [%]
SiCRe	0.491	0.509
SiCSt	0.618	0.382
SiCSu	0.585	0.415

Compared to the values found for phase composition using XRD, the same trend can be seen. From XRD the sintered samples with resin had the most 4H polytype present. From EBSD, the same trend is present although with less difference and with different numerical values. The samples containing starch and sucrose have the most 6H and vise versa for the sample with resin.

Chapter 5

Discussion

In this chapter, the results presented in the previous chapter are discussed. The discussion will come in a slightly different order than the results were presented. Here, the carbon sources and their properties will be discussed first. Secondly, densification will be discussed before characterisation comes lastly.

5.1 Carbon Sources

The results obtained from the thermogravimetric analysis (TGA) was as expected. Sucrose had the least residual carbon after a 60 minute dwelling time at 1500°C in argon atmosphere. Sucrose lose mass early in the heating process which is probably due to evaporation of water mostly, and other volatiles that have not been identified. For the other carbon sources, except carbon black, the same is observed although they lose more mass in the beginning and less when sucrose has its significant drop in mass around 190 °C. For resin and starch, which behave fairly similar during the heating, there is no mass loss during the first dwelling time at 180 °C. This indicates that the volatiles do not need time to leave the system, but rather a certain temperature. For sucrose there is a slight decrease in mass during the dwelling time but the largest drop in mass occurs just after increasing the temperature again indicating that there are some components in sucrose as well that need a higher temperature to decompose. The release of volatiles at relatively low temperatures are also seen when looking at the variation in vacuum during sintering, as will be discussed shortly below. The results found here is a good match with results

from literature. Venugopal et. al. showed a similar trend for sucrose and resin where resin started losing mass at a lower temperature than sucrose, but sucrose had the largest drop around 200 °C, which is similar to the trend here [35]. After around 800 °C, all the carbon sources (except carbon black) seem to stabilize. The trend is similar in literature and the slight loss of mass after 800 °C could come from some oxygen in the system although great measures was taken to avoid that. The residual carbon after pyrolysis for an hour at 1500 °C was 56.4, 34.7, 19.1 and 100% for resin, starch, sucrose and carbon black respectively. Here, it is assumed that carbon is the only component left after pyrolysis, which is a valid assumtion according to literature. From the results found by Venugopal et. al. the trend is similar. Sucrose is the carbon source with the least amount of carbon left after pyrolysis, starch is second and resin has the most carbon left. Carbon black is not comparable here as it does not undergo pyrolysis. Carbon black start off with pure carbon and is not expected to have any mass loss even at elevated temperatures. It is worth mentioning that the resin used for this experiment had lost some water by being stored for a long time, hence is a higher residual carbon yield expected. The difference in carbon yield was taken into account when making the precursor powders. The carbon source was added so that there would be 1wt% pure carbon present in the precursor during sintering. For this reason, the amount of carbon present in the precursor will not be discussed or considered as a variable.

After TGA (or pyrolysis) the residual carbon was analysed using Raman spectroscopy. The main aim of performing Raman spectroscopy was to look at the degree of graphitisation that had occurred during pyrolysis, and that would thus occur during sintering at the same temperatures. From literature, pure diamond will have one single Raman peak at around 1360 cm^{-1}, namely the D peak, while pure graphite will have one Raman peak at around 1560 cm^{-1}, the G peak. Most carbon materials have a mix of the two features as seen in Figure 2.2.2, and by comparing the area under the two peaks (A_D/A_G for the carbon materials investigated here, an indication of the degree of graphitisation was found, and hence a degree of reactivity. The ratio between the two peaks was similar for all carbon materials except carbon black. Carbon black was the only material with more graphite like structure and thus a ratio below zero. For resin, starch and sucrose the ratio was fairly similar and within the margin of error. In order to find these ratios the Raman spectra had to be deconvoluted using a computer software. The fitting is

just an approximation and small adjustments can change the result. Therefore, the ratios found here are considered to be similar. Figure 4.1.5 show the area ratio for pure carbon sources together with the ratio between the same peaks but found when looking at sintered samples. The trend is the same with starch and SiCSt having the highest ratio, although the variations are to small to draw any conclusions as to what carbon source is the most reactive. However, this result indicated that what the pure carbon sources went through in TGA, can be compared to what happens during sintering. The ratio being significantly lower for all sintered bodies than for pure carbon sources can be caused the higher temperature during sintering (1850°C when sintering, 1500°C when performing TGA).

It is hard to come to a single conclusion on what carbon source has the best potential to sinter silicon carbide close to theoretical density. However, as discussed in Chapter 2, there are some theories that the particle size of the carbon used as a sintering additive will indeed strongly influence the microstructure of the final product, illustrated in Figure 2.4.2. With a larger specific surface area there are more carbon particles to react with silica on the surface of the SiC and thus start the sintering. When looking at the removal of silica on the vacuum curve from sintering, reactivity of the carbon source is one aspect, while another is the particle size of the carbon. Microstructure of sintered bodies will be discussed further down, but the particle size of the carbon sources used was beyond the scope of this study. What can be said about the carbon sources investigated here is that they behave similarly when looking at them with Raman spectroscopy. The fact that they have very different carbon yield after pyrolysis can easily be adjusted for by increasing the amount added to the silicon carbide slurry before mixing and spray drying.

5.2 Densification

The densification method used here was spark plasma sintering. All the precursor powders were sintered according to the same sintering program (only varying the sintering pressure), a program that was made to ensure dense samples was obtained. When the sintering pressure was lowered, that was to see if all the precursor powders handled less sintering drivers as well. When looking at the sintering parameters for the various precursors there are not many differences to point out. With regards to the gas evolution

during sintering, it is clear that sucrose realise the most volatiles in the beginning of the sintering program. This makes perfect sense when looking at the TGA results for the pure carbon sources. Sucrose had the largest mass loss out of all the carbon sources investigated, and because of the low carbon yield, more sucrose was added to the precursor to compensate. These two factors are the explanation for the gas evolution happening with SiCSu (and somewhat also SiCSt). Compared to the precursor powders used for the specialisation project [68], far less gas evolution is observed for all samples. The reason for this is that all the precursors for this study were made for hot pressing, i. e they were made with less additives because more sintering drivers would be applied. For the specialisation project, powders made for pressure-less sintering was used, hence the need for more additives. The second peak on the vacuum curve is CO gas from the reaction between silica and carbon at around 1500°C. The CO peak was compared in Figure 4.2.2 and 4.2.3 for 50MPa and 3.3MPa sintering pressure respectively. When looking at the gas behaviour at the highest sintering pressure there is no significant differences, although in SiCRe the reaction seem to start slightly earlier than for the other two. However, the difference is bigger when looking at a lowering sintering pressure. Here, it is clear that resin is able to remove the silica layer faster than the other two carbon sources. The reason the difference is more significant at a lower sintering pressure is unknown. A likely theory is that at a high pressure, the gas struggles more to leave the system, leaving the curves looking similar, compared to when a low pressure is used and the gas is able to release whenever it wants to. This reasoning indicates that at a lower sintering pressure a more accurate picture of the situation is made and resin looks like the most reactive carbon source. On the counter side it looks like all the carbon sources do their job and remove the silica. The holding time at 1850°C was 5 minutes for all samples and using a shorter holding time might make the reactivity a more important factor.

As far as the densification curves go, found in Figure 4.2.4, they look similar for all precursors, which is later confirmed when measuring density. Density was measured for all sintered samples and the complete data set can be found in Appendix B. An overview of both density and porosity was presented in Section 4. Generally, a higher density was found for samples sintered with the highest pressure. SiCRe had the highest average bulk density of 3.18 gcm^{-3} which. is considered to be really high, but not unusual for precursors with resin as sintering additive. SiCSt followed up with an average of 3.16

gcm^{-3} and SiCSu had the lowest density with 3.15 gcm^{-3} in average. The trend is clear; resin gives the highest densities, followed by starch and sucrose. However, the densities obtained with starch, and especially sucrose, in this study is high and confirms that there are alternatives to resin. When the sintering pressure was lowered, the picture was different. Like mentioned, all densities were significantly lower with not even SiCRe reaching a value above 3.00 gcm^{-3}. However, the samples with resin and starch decreased their density from over 98% of theoretical density to around 93%, but SiCSu when from over 98% to just below 80%. This is a strong indication that sucrose as a carbon source is more prone to environment changes, and that resin and starch handle that better. It is worth mentioning here that all precursor powders were made for hot pressing, and using 3.3MPa as the sintering pressure hardly fall under the category of hot pressing, but it was done as an experiment to see how the different precursors reacted.

The porosity was presented in Figure 4.2.6. With densities higher than 98%, there should be very little open porosity left in the samples, if any. The open porosity was, however, higher than expected for all samples, but especially for SiCRe having more open than closed porosity. This could be due to inaccuracy using Archimedes' method, for example when moving the sample from the immersed liquid to measure the wet weight.

In general, when using enough sintering drivers, i.e. high temperature, high pressure and a long holding time, all the precursors obtain high densities.

5.3 Characterisation

5.3.1 Microstructure

Several characterisation methods were performed on the sintered samples. By looking at the samples in SEM some black spots were discovered, increasing in occurrence from SiCRe to SiCSu. This is assumed to be pores in the material, although a counter theory is that it might be carbon. Another discovery from the SEM images was that some of the black spots look different than the others, having a very different shape being thin and curved. Something similar was discovered by Celik et. al. [64], although at a significantly larger size. The curve shaped black spots found by Celik et. al. was in the size range of 10 - 50μm compared to similar finding here in the size of a couple microns.

As mentioned in the literature review, the curved black spots were concluded to be carbon accumulations (from using carbon black as a sintering additive), as seen in Figure 2.4.3. The theory was that the curve shape was a result from the carbon segregation during the spray-drying of the agglomerates, which is the same powder preparation method used in this study. By looking at Figure 2.4.2, also by Celik et. al., it is clear that carbon segregation is a problem during spray-drying although it might vary for different carbon sources depending on its solubility in water. All the three precursors used in this study have been spray-dried, SiCRe on a commercial scale and SiCSt and SiCSu on a pilot scale. It can not be confirmed that the curve shaped black spots are segregated carbon resulting from the spray-drying, it is just one hypothesis that should be looked more into. From literature, there is limited research found on the specific topic.

A series of the polished samples were etched by Fiven Norge AS and the results were presented in Figure 4.2.8. Here, the grain boundaries are seen clearly and the anisotropic grain growth in inevitable. The large and elongated grains are most prominent for SiCSu although it is seen for the other two samples as well. Densifying using SPS will affect the microstructure, although how and if it is for the better or worse is widely debated in literature. On the one side SPS is thought to inhibit the grain growth compared to hot pressing. Tamari et. al. [54] compared SPS and hot press and found that using SPS as the sintering method not only increased the density but also the bending strength. Hayun et. al. [53] also concluded that SPS is highly competitive with hot press. The opposing theory, presented by Zhou et. al. [55], is that the fast heating rate provided by SPS actually promotes anisotropic grain growth as well as the polytype transformation from cubic structure to hexagonal structure ($\beta \rightarrow \alpha$), which in turn is also a strong driver for anisotropic grain growth. From the SEM images of the etched surfaces it looks like all samples are prone to some anisotropic grain growth, possibly from the fast heating rate (heating rate used for all samples here were 100°C per minute which is considerably low for SPS that can have heating rates in the values of 400°C per minute). The polytype transition will be further discussed below.

EBSD was also used to understand the microstructure of the various sintered samples. Figure 4.2.14 show the EBDS patterns obtained for all samples. The confidence index (CI) for these patterns were not as high as wanted, but it was approximately the same

for all samples (0.4) and it is therefore considered valuable for comparable reasons. The reason for the low CI is most likely poor surface treatment, and even though the surface was carefully polished and ion milled, silicon carbide is a challenging material to work with due to high hardness. There are some anisotropic grain growth observed here as well, and a variable grain size, like what was seen in the SEM images. In the pattern for SiCRe there is one large grain, but the area scanned here is small and there might be similar grains on the other samples. The grains are small for all samples, but compared to the EBSD pattern from Mogstad [25], at a higher magnification, the size range is similar. At the magnification used here, the grain size is most likely smaller than the resolution limit, making it difficult to distinguish between some of the grains. The EBSD software calculated the average grain size from the patterns and found that SiCSu had the largest grain size followed by SiCRe and SiCSt, which had close to identical average grain size. Again, this is just based on a small area on the surface of the sample. The trend is however similar to that of the SEM images, increasing the credibility of the EBSD patterns. There is no preferred orientation observed for any of the samples, nor is the abnormal grain growth directionally controlled.

5.3.2 Phase composition

The phase composition was investigated by XRD and EBSD. From XRD the precursor powders have similar diffractograms with no graphite observed, as expected. In the precursors there should not be any graphite as the carbon has not been exposed to elevated temperatures. The Rietveld refinement give quantitative information about the polytypes present, and the findings are presented in Table 4.2.1. The Rietveld analysis also confirms that there is no graphite present in the precursor powders. The precursor with resin has by far the largest amount of the 4H polytype before sintering. When looking at the sintered samples, both for 3.3 and 50MPa sintering pressure, the trend is the same with SiCRe having the most 4H. The same trend is seen from the research done by Skarpeid [50]. It is reasonable that when the precursor has more 4H prior to sintering, the sintered samples from the same precursor also has more 4H than the other samples. Even though the precursors were made as similar as possible, the one with resin was made in a commercial scale on a big spray-dryer, while both the powder with starch and sucrose was made on a small pilot scale spray-dryer. It is likely that the processing of the

precursors would have a affected the polytype distribution, that would in turn influence the sintered bodies. The 3C polytype is expected to be almost negligible after sintering at 1850°C due to only showing high stability at lower temperatures. There is however some 3C observed in all samples, the highest content for SiCSt and SiCSu. According to theory, both 4H and 6H can be stable at the sintering temperature used here , but it is challenging to distinguish between the various polytypes as many have overlapping peaks.

The fact that samples with resin have the highest content of 4H can be caused by less grain growth occurring in those samples, as was seen when looking at the microstructure. All these samples have been subjected to the same heating rate, which can have a massive impact on the polytype transition (especially from cubic to hexagonal structure) [55]. For all the sintered samples, graphite is easily detected which confirms the graphite seen in the pyrolysed carbon samples, in Figure 4.2.13.

The EBSD results on phase distribution show a similar trend where the sample with resin has the most 4H. It looks like the most abnormal grin growth is 6H. EBSD analysis was performed with only two polytypes, namely 4H and 6H. Based on the calculated fraction of the two in all samples, seen in Table 4.2.3, there are more or less equal amounts of 4H and 6H present. From the EBSD results there are more 4H in all samples than when comparing with the XRD results.

5.3.3 Fracture analysis

Looking at the fracture surfaces with the blunt eye the fracture all look brittle and no neck formation is seen. Studying the surfaces in SEM give a more detailed view. All the fractures look like a mix of transgranular and intergranular fracture modes. It is hard to distinguish between the different grains for all samples, indicating trnasgranular fractures. Smaller grains promote transgranular fracture and larger grains intergranular fractures. According to this, SiCRe and SiCSt should have the most prominiant transgranular fracture mode, although it is challenging to say from the SEM images taken. The black spots seen on the fracture surface could be either pores or accumulated carbon. Some of the black spots have to be pores as there are some pores in the material. There could be some carbon as well based on what was discussed on microstructure.

Chapter 6

Conclusion

The three different silicon carbide powders given by Fiven Norge AS, contained various carbon sources, namely resin, starch and sucrose. The precursor with resin as the carbon source was the only commercial powder of the three, the other two being made solely for this study. The three carbon sources (and carbon black for comparability reasons), in pure form, were investigated using TGA and Raman spectroscopy to analyse pyrolysis properties and reactivity. The precursor powders were sintered using the spark plasma sintering method and then characterised with numerous methods like SEM, EBSD and XRD. Following conclusion were made:

- The carbon sources used in this study behave differently when subjected to heat, where sucrose had the least carbon yield after pyrolysis for an hour at 1500°C, followed by starch and resin. Carbon black had, like expected, no mass loss at elevated temperatures.

- Raman spectroscopy showed little difference between the carbon sources. In terms of reactivity they are considered to be almost similar, with resin slightly more reactive than the others (based on the gas evolution during sintering).

- All precursors obtained high densities with an average bulk density of 3.18, 3.16 and 3.15 gcm^{-3} for SiCRe, SiCSt and SiCSu respectively. When lowering the sintering pressure, the sample with sucrose as the carbon source got a significantly lower density than the other two.

- The sintered samples with sucrose has the largest grain size and also the most

prominent anisotropic grain growth.

- Both the precursor with resin and the resulting sintered samples with resin have the highest amount of 4H polytype.

- All fracture surfaces looks brittle with a combination of intergranular and transgranular fractures.

The carbon sources investigated have the potential to substitute phenolic resin and be a more environmentally friendly sintering aid. High densities were obtained with all carbon sources, albeit with SPS as the sintering method. More research need to be executed on the topic to understand better what makes a good carbon for sintering silicon carbide.

Chapter 7

Further work

For future work on the topic it is important to look at different carbon sources (both the ones used here and other alternatives) and use other densification techniques. SPS is not yet commonly used in industry, and based on literature, there are many advantages of using SPS versus for example hot press. There are even examples of reaching densities close to theoretical without sintering additives using SPS, so the need to investigate alternative carbon sources using methods that are actually in use in industry, is of high importance. Another interesting aspect of the sintering is to see if a decrease in holding time would require a carbon source of higher reactivity. It is clear from the results here, that sucrose needed more sintering drivers to obtain high densities than the other two carbon sources so maybe the differences are just small in this study due to the use of SPS with high temperature and high pressure.

The reactivity of the carbon sources have been investigated here, but the correlation between particle size of the carbon and densification properties is yet to be investigated.

As discussed in the previous chapter, some curve shaped black spots were discovered in the microstructure of the sintered samples, looking similar to what was found in literature, although smaller. Thus it would be interesting to look more into the segregation of carbon during spray-drying and investigate if what happens during the production of the agglomerates actually impact the densification properties, or even more so, the mechanical properties.

Bibliography

[1] David W Richerson. *Modern Ceramic Engineering: Properties, Processing, and Use in Design.* CRC Press, 2005.

[2] Koichi Yamada and Masahide Mohri. Properties and applications of silicon carbide ceramics. In *Silicon carbide ceramics—1*, pages 13–44. Springer, 1991.

[3] Svante Prochazka and Ronald M Scanlan. Effect of boron and carbon on sintering of sic. *Journal of the American Ceramic Society*, 58(1-2):72–72, 1975.

[4] Ludoslaw Stobierski and Agnieszka Gubernat. Sintering of silicon carbide ii. effect of boron. *Ceramics international*, 29(4):355–361, 2003.

[5] Ludoslaw Stobierski and Agnieszka Gubernat. Sintering of silicon carbidei. effect of carbon. *Ceramics international*, 29(3):287–292, 2003.

[6] Werner Benker. Process for producing ceramic components of silicon carbide, April 8 1997. US Patent 5,618,767.

[7] Giuseppe Magnani, Giuliano Sico, Alida Brentari, and Paride Fabbri. Solid-state pressureless sintering of silicon carbide below 2000° c. *Journal of the European Ceramic Society*, 34(15):4095–4098, 2014.

[8] Koushik Biswas. Solid state sintering of sic-ceramics. In *Materials Science Forum*, volume 624, pages 71–89. Trans Tech Publ, 2009.

[9] M Petrus, J Wozniak, A Jastrzebska, M Kostecki, T Cygan, and A Olszyna. The effect of the morphology of carbon used as a sintering aid on the sinterability of silicon carbide. *Ceramics International*, 44(6):7020–7025, 2018.

[10] Alfian Noviyanto, Bong-Ki Min, Hyun-Woo Yu, and Dang-Hyok Yoon. Highly dense and fine-grained sic with a sc-nitrate sintering additive. *Journal of the European Ceramic Society*, 34(3):825–830, 2014.

[11] A Qteish, Volker Heine, and RJ Needs. Structural and electronic properties of sic polytypes. *Physica B: Condensed Matter*, 185(1-4):366–378, 1993.

[12] PTB Shaffer. A review of the structure of silicon carbide. *Acta Crystallographica Section B: Structural Crystallography and Crystal Chemistry*, 25(3):477–488, 1969.

[13] NW Jepps and TF Page. Polytypic transformations in silicon carbide. *Progress in crystal growth and characterization*, 7(1-4):259–307, 1983.

[14] Ajit Ram Verma and Padmanabhan Krishna. Polymorphism and polytypism in crystals. *1966, 341 P. JOHN WILEY AND SONS, INC., 605 THIRD AVENUE, NEW YORK, N. Y. 10016*, 1965.

[15] JB Casady and R Wayne Johnson. Status of silicon carbide (sic) as a wide-bandgap semiconductor for high-temperature applications: A review. *Solid-State Electronics*, 39(10):1409–1422, 1996.

[16] D Pandey and P Krishna. The origin of polytype structures. *Progress in Crystal growth and Characterization*, 7(1-4):213–258, 1983.

[17] Yoshizo Inomata, Zenzaburo Inoue, Mamoru Mitomo, and Hiroshige Suzuki. Relation between growth temperature and the structure of sic crystals grown by the sublimation method. Technical report, EMMANUEL COLL BOSTON MASS ORIENTAL SCIENCE RESEARCH LIBRARY, 1969.

[18] A Taylor and RM Jones. The crystal structure and the thermal expansion of cubic and hexagonal silicon carbide, silicon carbide-a high temperature semiconductor, edited by jro connor, j. smiltens. Oxford, Symposium Publications Division, Pergamon Press, 1960.

[19] Gary Lynn Harris. *Properties of silicon carbide.* Number 13. Iet, 1995.

[20] Misasa Okayama, "VESTA crystallographic data". `http://www.misasa.okayama-u.ac.jp/~masami/pukiwiki/index.php?Vesta_data`. Accessed: 08.05.2019.

[21] Tim Maitland and Scott Sitzman. Backscattering detector and ebsd in nanomaterials characterization. In *Scanning Microscopy for Nanotechnology*, pages 41–75. Springer, 2006.

[22] Matt M Nowell and Stuart I Wright. Phase differentiation via combined ebsd and xeds. *Journal of Microscopy*, 213(3):296–305, 2004.

[23] Stuart I Wright. Fundamentals of automated ebsd. In *Electron backscatter diffraction in materials science*, pages 51–64. Springer, 2000.

[24] Yoshiki Mikami, Kazuo Oda, Masayuki Kamaya, and Masahito Mochizuki. Effect of reference point selection on microscopic stress measurement using ebsd. *Materials Science and Engineering: A*, 647:256–264, 2015.

[25] Kent Mogstad. A study on commercial sic-powders sintered by hot pressing. Master's thesis, NTNU, 2016.

[26] Florimond Delobel, Sébastien Lemonnier, and Julien Cambedouzou. Effects of density on the mechanical properties of spark plasma sintered β-sic. *Ceramics International*, 2020.

[27] Lionel Vargas-Gonzalez, Robert F Speyer, and James Campbell. Flexural strength, fracture toughness, and hardness of silicon carbide and boron carbide armor ceramics. *International Journal of Applied Ceramic Technology*, 7(5):643–651, 2010.

[28] Philip J Guichelaar. Acheson process. In *Carbide, Nitride and Boride Materials Synthesis and Processing*, pages 115–129. Springer, 1997.

[29] GS Gupta, P Vasanth Kumar, VR Rudolph, and M Gupta. Heat-transfer model for the acheson process. *Metallurgical and Materials Transactions A*, 32(6):1301–1308, 2001.

[30] Mohammed Mathlouthi and Philippe Reiser. *Sucrose: properties and applications*. Springer Science & Business Media, 2012.

[31] Arno Gardziella, Louis A Pilato, and Andre Knop. *Phenolic resins: chemistry, applications, standardization, safety and ecology*. Springer Science & Business Media, 2013.

[32] David R Lide. *CRC handbook of chemistry and physics*, volume 85. CRC press, 2004.

[33] George Ting-Kuo Fey and Yun-Chien Kao. Synthesis and characterization of pyrolyzed sugar carbons under nitrogen or argon atmospheres as anode materials for lithium-ion batteries. *Materials chemistry and physics*, 73(1):37–46, 2002.

[34] Roy L Whistler, James N BeMiller, and Eugene F Paschall. *Starch: chemistry and technology*. Academic Press, 2012.

[35] S Venugopal, A Paul, B Vaidhyanathan, JGP Binner, A Heaton, and PM Brown. Synthesis and spark plasma sintering of sub-micron hfb2: Effect of various carbon sources. *Journal of the European Ceramic Society*, 34(6):1471–1479, 2014.

[36] A Oberlin. Carbonization and graphitization. *Carbon*, 22(6):521–541, 1984.

[37] Andrea C Ferrari and John Robertson. Interpretation of raman spectra of disordered and amorphous carbon. *Physical review B*, 61(20):14095, 2000.

[38] S Piscanec, Francesco Mauri, AC Ferrari, M Lazzeri, and J Robertson. Ab initio resonant raman spectra of diamond-like carbons. *Diamond and related materials*, 14(3-7):1078–1083, 2005.

[39] John Robertson. Diamond-like amorphous carbon. *Materials science and engineering: R: Reports*, 37(4-6):129–281, 2002.

[40] R Brunetto, T Pino, E Dartois, A-T Cao, L d'Hendecourt, G Strazzulla, and Ph Bréchignac. Comparison of the raman spectra of ion irradiated soot and collected extraterrestrial carbon. *Icarus*, 200(1):323–337, 2009.

[41] Sigita Urbonaite, Lars Hälldahl, and Gunnar Svensson. Raman spectroscopy studies of carbide derived carbons. *Carbon*, 46(14):1942–1947, 2008.

[42] Gen Katagiri, Hideyuki Ishida, and Akira Ishitani. Raman spectra of graphite edge planes. *Carbon*, 26(4):565–571, 1988.

[43] Zhichao Chen, Ghatu Subhash, and James S Tulenko. Raman spectroscopic investigation of graphitization of diamond during spark plasma sintering of uo2-diamond composite nuclear fuel. *Journal of Nuclear Materials*, 475:1–5, 2016.

[44] Michio Inagaki, Naoto Ohta, and Yoshihiro Hishiyama. Aromatic polyimides as carbon precursors. *Carbon*, 61:1–21, 2013.

[45] Stylianos D Stefanidis, Konstantinos G Kalogiannis, Eleni F Iliopoulou, Chrysoula M Michailof, Petros A Pilavachi, and Angelos A Lappas. A study of lignocellulosic biomass pyrolysis via the pyrolysis of cellulose, hemicellulose and lignin. *Journal of analytical and applied pyrolysis*, 105:143–150, 2014.

[46] Jun Yi Yeo, Bridgid Lai Fui Chin, Jun Kit Tan, and Ying Sheng Loh. Comparative studies on the pyrolysis of cellulose, hemicellulose, and lignin based on combined kinetics. *Journal of the Energy Institute*, 92(1):27–37, 2019.

[47] I-Wei Chen and X-H Wang. Sintering dense nanocrystalline ceramics without final-stage grain growth. *Nature*, 404(6774):168–171, 2000.

[48] Zuhair A Munir, Dat V Quach, and Manshi Ohyanagi. Electric current activation of sintering: a review of the pulsed electric current sintering process. *Journal of the American Ceramic Society*, 94(1):1–19, 2011.

[49] Mohamed N Rahaman. *Ceramic processing and sintering*. CRC press, 2003.

[50] Henriette Skarpeid. The effect of carbon and boron carbide additions in pressure assisted sintered silicon carbide. Master's thesis, NTNU, 2017.

[51] W Beere. The second stage sintering kinetics of powder compacts. *Acta Metallurgica*, 23(1):139–145, 1975.

[52] V Mamedov. Spark plasma sintering as advanced pm sintering method. *Powder Metallurgy*, 45(4):322–328, 2002.

[53] S Hayun, V Paris, R Mitrani, S Kalabukhov, MP Dariel, E Zaretsky, and N Frage. Microstructure and mechanical properties of silicon carbide processed by spark plasma sintering (sps). *Ceramics International*, 38(8):6335–6340, 2012.

[54] Nobuyuki Tamari, Takahiro Tanaka, Koji Tanaka, Isao Kondoh, Masakazu Kawahara, and Masao Tokita. Effect of spark plasma sintering on densification and mechanical properties of silicon carbide. *Journal of the ceramic society of Japan*, 103(1199):740–742, 1995.

[55] You Zhou, Kiyoshi Hirao, Motohiro Toriyama, and Hidehiko Tanaka. Very rapid densification of nanometer silicon carbide powder by pulse electric current sintering. *Journal of the American Ceramic Society*, 83(3):654–656, 2000.

[56] Alexandre Maître, A Vande Put, Jean-Paul Laval, Stéphane Valette, and Gilles Trolliard. Role of boron on the spark plasma sintering of an α-sic powder. *Journal of the European Ceramic Society*, 28(9):1881–1890, 2008.

[57] Hidehiko Tanaka, Naoto Hirosaki, Toshiyuki Nishimura, Dong-Woo Shin, and Sam-Shik Park. Nonequiaxial grain growth and polytype transformation of sintered α-silicon carbide and β-silicon carbide. *Journal of the American Ceramic Society*, 86(12):2222–2224, 2003.

[58] W Van Rijswijk and Daniel J Shanefield. Effects of carbon as a sintering aid in silicon carbide. *Journal of the American Ceramic Society*, 73(1):148–149, 1990.

[59] John S Nadeau and NADEAU JS. Very high pressure hot pressing of silicon carbide. 1973.

[60] P Šajgalík, J Sedláček, Z Lenčéš, J Dusza, and H-T Lin. Additive-free hot-pressed silicon carbide ceramics—a material with exceptional mechanical properties. *Journal of the European Ceramic Society*, 36(6):1333–1341, 2016.

[61] Linus UJT Ogbuji. Oxidation of polycrystalline silicon carbide. *Ceramics international*, 12(3):173–178, 1986.

[62] You Zhou, Hidehiko Tanaka, Shigeki Otani, and Yoshio Bando. Low-temperature pressureless sintering of alpha-sic with al4c3-b4c-c additions. *Journal of the American Ceramic Society*, 82(8):1959–1964, 1999.

[63] S Contarini, SP Howlett, C Rizzo, and BA De Angelis. Xps study on the dispersion of carbon additives in silicon carbide powders. *Applied surface science*, 51(3-4):177–183, 1991.

[64] Ali Çelik, Alpagut Kara, Servet Turan, and Ferhat Kara. Processing of solid state sintered α-sic ceramics with carbon-black addition. *Materials Research Express*, 6(10):105606, 2019.

[65] Stephen Rugholm. *Private communication.* Fiven Norge AS, 2020.

[66] Marcin Wojdyr. Fityk: a general-purpose peak fitting program. *Journal of Applied Crystallography*, 43(5-1):1126–1128, 2010.

[67] Martin Madsen. Ceramic matrix composites based on silicon carbide and carbon fibers. Master's thesis, NTNU, 2019.

[68] S. Skjelstad. Effect of the carbon source on sintering properties of sic. 2019.

[69] J. Perl, J. Shin, J. Schumann, B. Faddegon, and H. Paganetti. TOPAS: An innovative proton Monte Carlo platform for research and clinical applications. *Medical Physics*, 39:6818, 2012.

Appendix A

Equations

The density of isopropanol is dependent on the temperature according to Equation (A.1).

$$\rho_{liq} = -0.0009T + 0.8018 \tag{A.1}$$

The bulk density is calculated from Equation (A.2).

$$\rho_b = \frac{m_1}{m_3 - m_2} \cdot \rho_{liq} \tag{A.2}$$

Equation (A.3) is used to calculate apparent porosity.

$$\pi_a = \frac{m_3 - m_1}{m_3 - m_2} \cdot 100 \tag{A.3}$$

And finally, the total porosity is calculated from Equation (A.4).

$$\pi_t = \frac{\rho_t - \rho_b}{\rho_t} \cdot 100 \tag{A.4}$$

# Appendix B

Raw data

Spark plasma sintering

A selection on sintering curves are presented below. In Figure B.0.1 and B.0.2 are the two other precursors, SiCSt and SiCSu, sintered with the highest sintering pressure. SiCRe is presented in Section 4. In the following three images, Figure B.0.3, B.0.4 and B.0.5, all three precursors are presented, but here a sintering pressure of 3.3MPa was used.
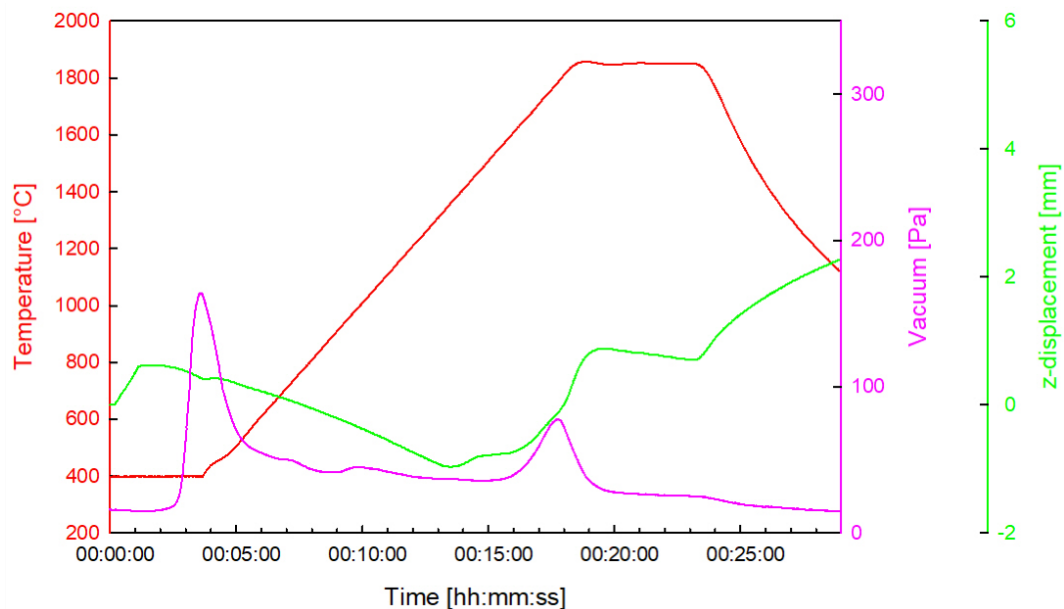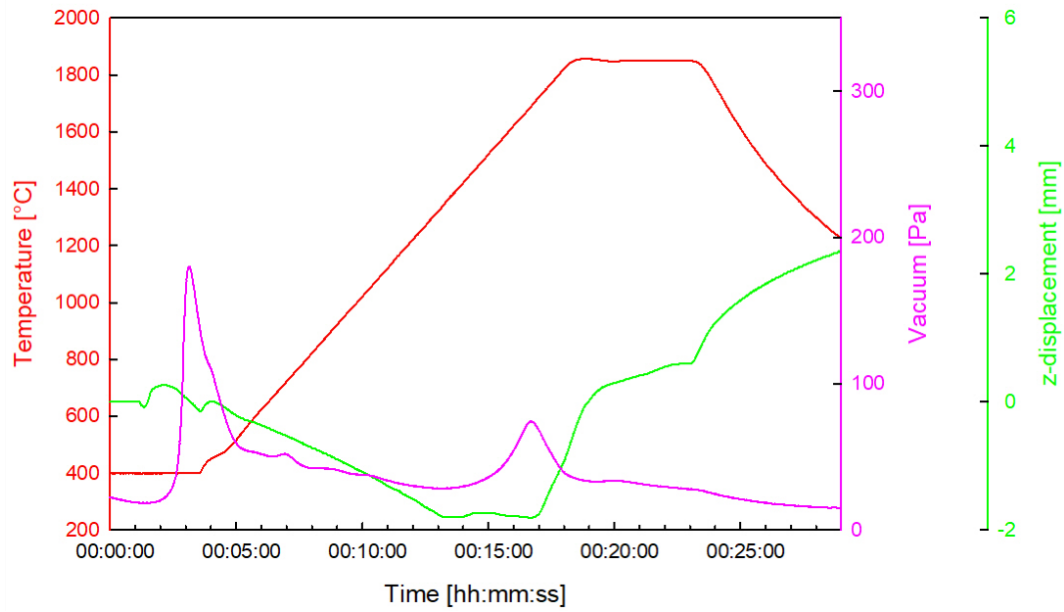

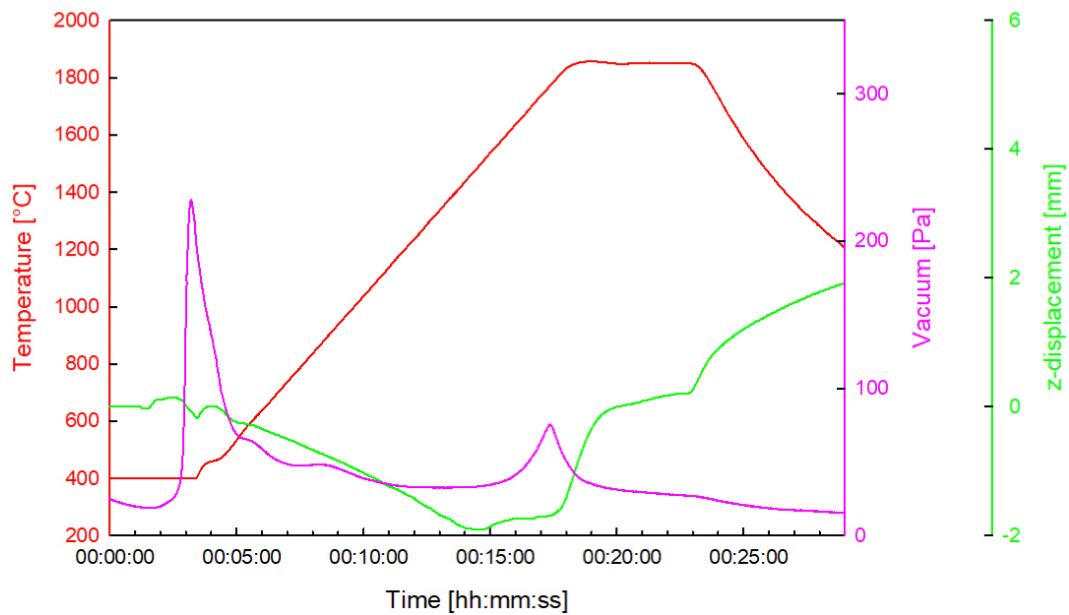**Figure B.0.1:** Sintering curves for SiCSt using 50MPa. Heating rate was 100 °C.
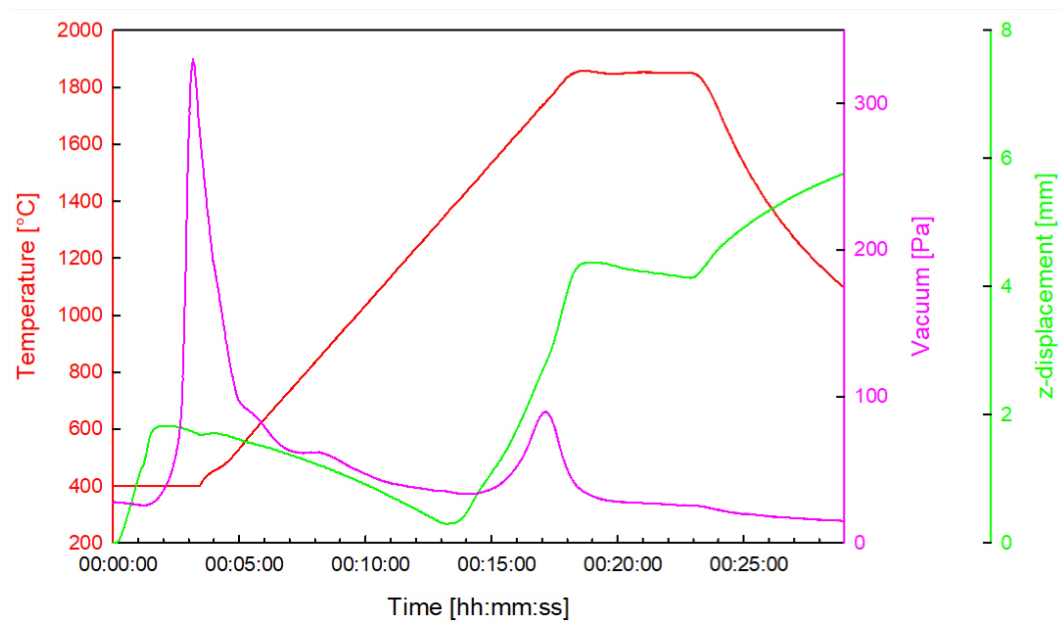
Figure B.0.2: Sintering curves for SiCSu using 50MPa. Heating rate was 100 °C.
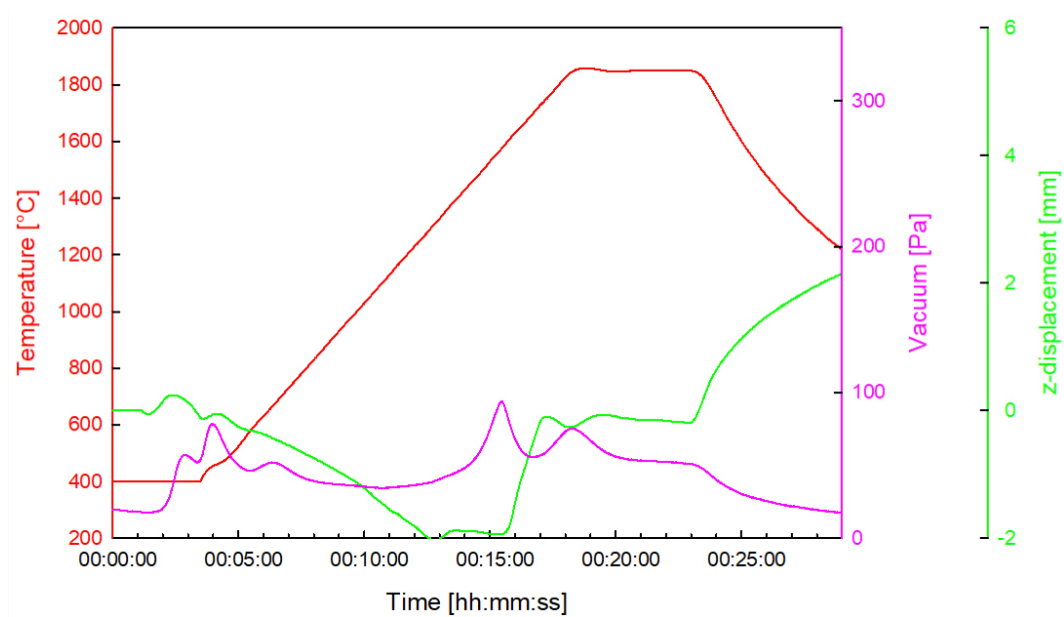
Figure B.0.3: Sintering curves for SiCRe using 3.3MPa. Heating rate was 100 °C.

Figure B.0.4: Sintering curves for SiCSt using 3.3MPa. Heating rate was 100 °C.

Figure B.0.5: Sintering curves for SiCSu using 3.3MPa. Heating rate was 100 °C.

Figure B.0.6 and Figure B.0.7 show the vacuum curve during sintering for sintering pressures of 50MPa and 3.3MPa respectively, here with time on the x-axis. In Chapter 4, the graphs are displayed with the temperature on the x-axis. The heating rate here was 200°C per minute.
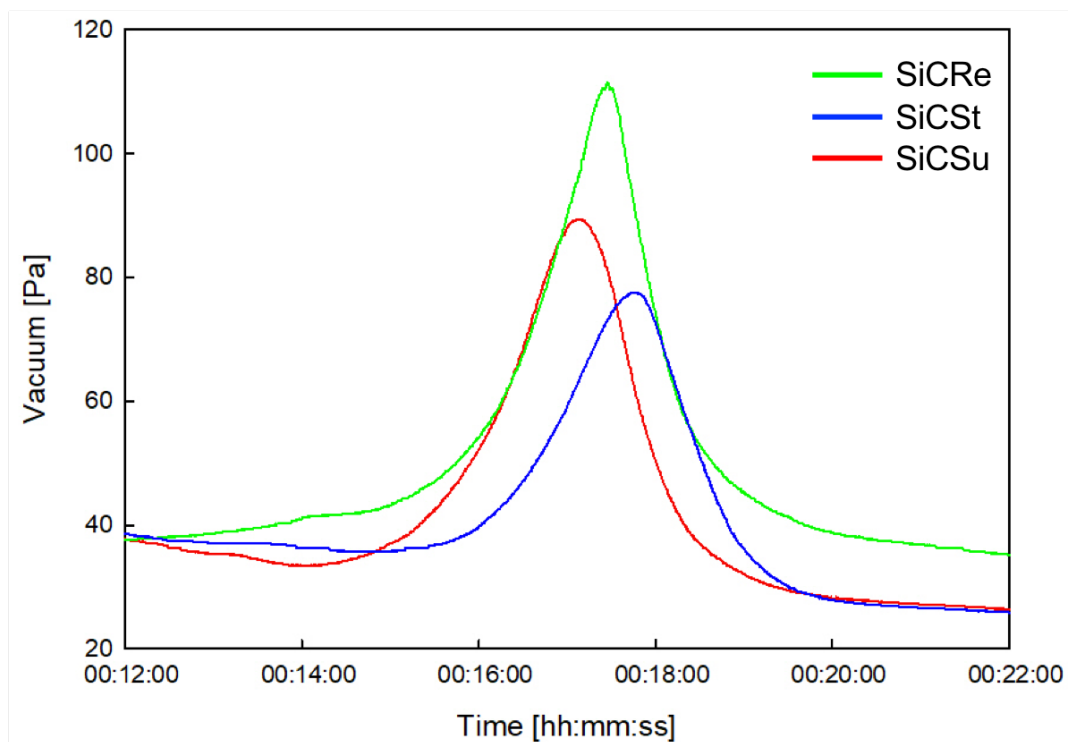
97

Figure B.0.6: Vacuum curve during sintering using a sintering pressure of 50MPa.
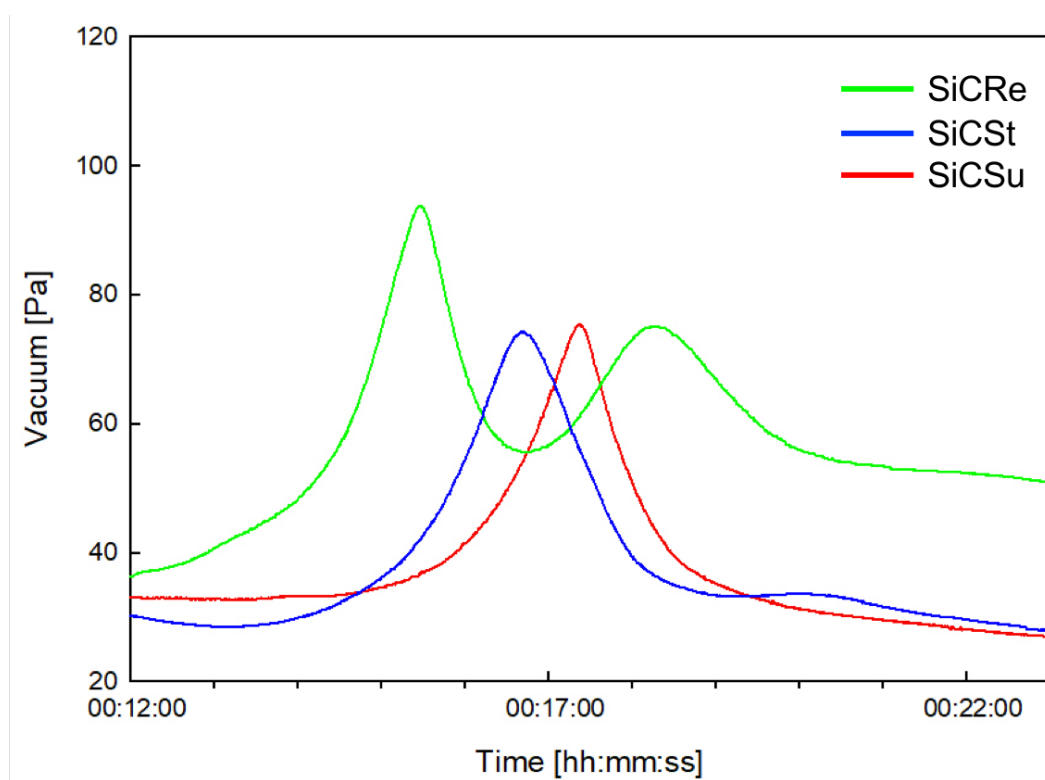

Figure B.0.7: Vacuum curve during sintering using a sintering pressure of 3.3MPa.

Density measurements

In Table B.0.1 a detailed overview of information from the density measurements can be found. Bulk density together with open and closed porosity for all samples are found here. All samples have been sintered using the sintering program presented in Chapter 3.

Table B.0.1: Measured densities using Archmedes' principle. Isopropanol was used as immersion liquid.

Sample	Bulk density $[gcm^{-3}]$	Open porosity [%]	Closed porosity [%]
SiCRe1 50MPa	3.171	0.898	0.392
SiCRe2 50MPa	3.172	0,790	0.400
SiCRe3 50MPa	3.175	0.660	0.418
SiCRe4 50MPa	3.180	0.565	0.364
SiCRe 3.3MPa	2.991	0.669	6.141
SiCSt1 50MPa	3.158	0.797	0.823
SiCSt2 50MPa	3.159	0.760	0.845
SiCSt3 50MPa	3.169	0.424	0.847
SiCSt4 50MPa	3.163	0.691	0.776
SiCSt 3.3MPa	2.976	2.219	5.077
SiCSu1 50MPa	3.146	0.984	1.019
SiCSu2 50MPa	3.152	0.808	1.008
SiCSu3 50MPa	3.155	0.745	0.965
SiCSu4 50MPa	3.151	0.899	0.932
SiCSu 3.3MPa	2.555	19.698	0.698

Raman spectroscopy

Results from Raman spectroscopy of the pyrolysed carbon sources are found in Table B.0.2. Raman spectroscopy results for sintered and polished samples are found in Table B.0.3 and Table B.0.4. Table B.0.3 displays the carbon properties with the D and G peak. Table B.0.4 show the silicon carbide contribution in terms of the position of the longitudinal optic mode (LO) of silicon carbide and the transverse optical mode (TO) of silicon carbide.

Table B.0.2: Features of the residual carbon after pyrolysis using Raman spectroscopy.

Parameter	Sample			
	Resin	Starch	Sucrose	Carbon Black
Position D peak $[cm^{-1}]$	1344	1343	1338	1338
Position G peak $[cm^{-1}]$	1594	1590	1578	1586
Area D peak	360537	258746	44299	20036
Area G peak	170661	109868	20593	20231
A_D/A_G ratio	2.11	2.36	2.15	0.99
FWHM D peak	83.3	116.2	111.1	95.9
FWHM G peak	70.9	71.0	73.5	80.9

Table B.0.3: Result from deconvolution in Fityk sofware. The best fit was found using Lorenztian curves for the G peak and D peak with one Gauss curve to take away any noise like fluorescence. Raman is here performed on sintered samples that were then polished to see the bulk properties and to get a surface with as little topography as possible.

Parameter	Sample		
	SiCRe	SiCSt	SiCSu
Position D peak $[cm^{-1}]$	1363	1363	1365
Position G peak $[cm^{-1}]$	1592	1587	1592
Area D peak	37149	49008	62639
Area G peak	57456	65202	92741
A_D/A_G ratio	0.65	0.75	0.68
FWHM D peak	47.8	55.4	50.4
FWHM G peak	46.5	53.8	44.0

Table B.0.4: Positions of the peaks generated by silicon carbide (TO and LO mode). Spectroscopy was also here performed on polished samples to ensure bulk preperties. TO is the transverse optical mode of silicon carbide and LO denotes the longitudinal optical mode of silicon carbide.

Peak position $[cm^{-1}]$	Sample		
	SiCRe	SiCSt	SiCSu
SiC TO	790	795	790
SiC LO	971	971	975